41540R05

KINETICS OF SLURRY PHASE FISCHER-TROPSCH SYNTHESIS

Final Report

Reporting Period Start Date: 10/01/2002

Reporting Period End Date: 12/31/2006

Report prepared by:

Dr. Dragomir B. Bukur (Professor, PI)

Contributors:
Dr. Gilbert F. Froment (Research Professor, Co-PI)

Tomasz Olewski (Research Technician)

Dr. Lech Nowicki (Post doctoral fellow)
Madhav Nayapati (Graduate Student)

Department of Chemical Engineering
Texas A&M University
College Station, TX 77843-3122

Date Report was issued: April 9, 2007
Grant No. DE-FG26-02NT41540

Texas A&M University
1260 TAMU
College Station, TX 77843-1260

Prepared for

U.S. Department of Energy
University Coal Research Program
National Energy Technology Laboratory
Project Officer: Robert M. Kornosky

Disclaimer

Abstract

The overall objective of this project is to develop a comprehensive kinetic model for slurry-phase Fischer-Tropsch synthesis (FTS) employing iron-based catalysts. This model will be validated with experimental data obtained in a stirred-tank slurry reactor (STSR) over a wide range of process conditions.

Three STSR tests of the Ruhrchemie LP 33/81 catalyst were conducted to collect data on catalyst activity and selectivity under 25 different sets of process conditions. The observed decrease in 1-olefin content and increase in 2-olefin and n-paraffin contents with the increase in conversion are consistent with a concept that 1-olefins participate in secondary reactions (e.g. 1-olefin hydrogenation, isomerization and readsorption), whereas 2-olefins and n-paraffins are formed in these reactions. Carbon number product distribution showed an increase in chain growth probability with increase in chain length.

Vapor-liquid equilibrium calculations were made to check validity of the assumption that the gas and liquid phases are in equilibrium during FTS in the STSR. Calculated vapor phase compositions were in excellent agreement with experimental values from the STSR under reaction conditions. Discrepancies between the calculated and experimental values for the liquid-phase composition (for some of the experimental data) are ascribed to experimental errors in the amount of wax collected from the reactor, and the relative amounts of hydrocarbon wax and Durasyn 164 oil (start-up fluid) in the liquid samples.

Kinetic parameters of four kinetic models (Lox and Froment, 1993b; Yang et al., 2003; Van der Laan and Beenackers, 1998, 1999; and an extended kinetic model of Van der Laan and Beenackers) were estimated from experimental data in the STSR tests. Two of these kinetic models (Lox and Froment, 1993b; Yang et al., 2003) can predict a complete product distribution (inorganic species and hydrocarbons), whereas the kinetic model of Van der Laan and Beenackers (1998, 1999) can be used only to fit product distribution of total olefins and n-paraffins. The kinetic model of Van der Laan and Beenackers was extended to account separately for formation of 1- and 2-olefins, as well as n-paraffins.

A simplified form of the kinetic model of Lox and Froment (1993b) has only five parameters at isothermal conditions. Because of its relative simplicity, this model is well suited for initial studies where the main goal is to learn techniques for parameter estimation and statistical analysis of estimated values of model parameters. The same techniques and computer codes were used in the analysis of other kinetic models. The Levenberg-Marquardt (LM) method was employed for minimization of the objective function and kinetic parameter estimation. Predicted reaction rates of inorganic and hydrocarbon species were not in good agreement with experimental data.

All reaction rate constants and activation energies (24 parameters) of the Yang et al. (2003) model were found to be positive, but the corresponding 95% confidence intervals were large. Agreement between predicted and experimental reaction rates has been fair to good. Light hydrocarbons were predicted fairly accurately, whereas the model predictions of higher molecular weight hydrocarbons values were lower than the experimental ones.

The Van der Laan and Beenackers kinetic model (known as olefin readsorption product distribution model = ORPDM) provided a very good fit of the experimental data for hydrocarbons (total olefins and n-paraffins) up to about C_{20} (with the exception of experimental data that showed higher paraffin formation rates in C_{12}-C_{25} region, due to hydrocracking or other secondary reactions). Estimated values of all model parameters (true and pseudo-kinetic parameters) had high statistical significance after combining parameters related to olefin termination and readsorption into one (total of 7 model parameters). The original ORPDM was extended to account separately for formation of 1- and 2-olefins, and successfully employed to fit experimental data of three major groups of hydrocarbon products (n-paraffins, 1-olefins and 2-olefins). This model is referred to as an extended ORPDM (8 model parameters in its final form). In general, all three groups of products were fitted well, and the estimated model parameters were all positive and the corresponding 95% confidence intervals were small. Even though the extended ORPDM provided a very good fit of experimental data, it can not be used for the prediction of product distributions for a given set of process conditions. This model has several pseudo-kinetic parameters whose values vary with process conditions. Additional work is needed to expand capabilities of the model to predict molar flow rates of all inorganic species and major hydrocarbon products in terms of true kinetic (temperature dependent) constants.

The overall project goals have been achieved, but the two comprehensive kinetic models did not provide accurate predictions for hydrocarbon products over the entire range of carbon numbers. The predictions for light hydrocarbons (up to about C_{10}) were found to be in good agreement with experimental data, however larger errors were obtained for high molecular weight hydrocarbons (Yang et al. model). It is not clear whether this is due to deficiencies in the kinetic model itself, or due to experimental errors, and/or due to their combined effect. Further studies are recommended to develop improved kinetic models and to validate them with experimental data from the STSR and/or other types of reactors (e.g. spinning basket).

TABLE OF CONTENTS **Page**

Introduction

The overall objective of this project is to develop a comprehensive kinetic model for slurry-phase Fischer-Tropsch synthesis (FTS) employing iron-based catalysts. This model will be validated with experimental data obtained in a stirred-tank slurry reactor (STSR) over a wide range of process conditions. This model will be able to predict concentrations of all reactants and major product species (water (H_2O), carbon dioxide (CO_2), linear 1- and 2-olefins, and linear paraffins) as a function of reaction conditions in the STSR. The kinetic model will be useful for preliminary reactor design and process economics studies. The overall program is divided into four tasks. A brief description for each task is provided in the following:

Task 1. Development of Kinetic Models

Kinetic models will be formulated utilizing the current state-of-the-art understanding of reaction mechanisms for the formation of reaction intermediates and hydrocarbon products. Models will be based on adsorption/desorption phenomena for reactants and product species. These models will be continually updated on the basis of experimental data obtained in Task 3, and subsequent data analysis conducted in Task 4.

Task 2. Catalyst Synthesis

A precipitated iron (Fe) catalyst with nominal composition 100 Fe/3 Cu/4 K/16 SiO_2 (in parts per weight; Cu = copper; K = potassium; SiO_2 = silica) will be synthesized utilizing equipment and procedures developed in the laboratory at Texas A&M University (TAMU). As an alternative, a robust commercially available catalyst with similar performance characteristics to the TAMU catalyst may be utilized.

Task 3. Experiments in a Stirred Tank Slurry Reactor

Experiments will be conducted in a 1 dm^3 (1 dm^3 = 1 liter = 1 L) STSR over a wide range of process conditions of industrial significance. Synthesis gas (syngas) feed with hydrogen (H_2) to carbon monoxide (CO) molar ratio ranging from 0.67 (typical of coal-derived syngas) to 2 (typical of natural gas-derived syngas) will be employed. Baseline conditions will be repeated periodically to assess the extent of catalyst deactivation.

Task 4. Model Discrimination and Parameter Estimation

The Langmuir-Hinshelwood-Hougen-Watson (LHHW) approach and the concept of rate limiting step results in a large number of competing kinetic models. Discrimination between the rival models will be based upon the quality of fit, supplemented with statistical tests on parameter values and the physicochemical meaningfulness of the estimated parameter values.

Experimental

Three tests (Runs SB-21903, SB-26203 and SB-28603) were conducted in a 1 dm^3 stirred-tank slurry reactor (Autoclave Engineers). A schematic of the experimental apparatus is shown in Figure 1. The feed gas flow rate was adjusted with a mass flow controller and passed through a series of oxygen removal, alumina, and activated charcoal traps to remove trace impurities. After leaving the reactor, the exit gas passed through a series of high and low (ambient) pressure traps to condense the liquid products. High molecular weight hydrocarbons (wax), withdrawn from a slurry reactor through a porous cylindrical sintered metal filter, and liquid products, collected in the high and low pressure traps, were analyzed by capillary gas chromatography (Varian 3400 gas chromatograph). Liquid products collected in the high and atmospheric pressure traps were first separated into an organic phase and an aqueous phase and then analyzed using different columns and temperature programmed methods (Varian 3400 gas chromatograph). The reactants and noncondensible products leaving the ice traps were analyzed with an on-line gas chromatograph (Carle AGC 400) with multiple columns using both flame ionization and thermal conductivity detectors. A schematic of the product analysis procedure is shown in Figure 2. Further details on the experimental set up, operating procedures, and product quantification can be found elsewhere (Bukur *et al*., 1990; Zimmerman and Bukur, 1990; Bukur *et al*., 1994; Bukur *et al*., 1996).

Instead of synthesizing a new batch of TAMU's precipitated catalyst 100 Fe/3 Cu/4 K/16 SiO_2 (in parts by weight) it was decided to use a precipitated iron catalyst prepared by Ruhrchemie AG (Oberhausen-Holten, Germany). This catalyst (LP 33/81), having a nominal composition 100 Fe/4.3 Cu/4.1 K/25 SiO_2 (in parts by weight), was used initially in fixed-bed reactors at Sasol in South Africa. It has been tested extensively at TAMU (Bukur *et al*., 1990; Zimmerman and Bukur, 1990; Zimmerman *et al.,* 1992; Bukur *et al*., 1995), and was used in a

previous study of the kinetics of FTS by Lox and Froment (Lox and Froment, 1993a, 1993b). The LP 33/81 catalyst is robust and has a selectivity that is similar to the TAMU catalyst.

The Ruhrchemie catalyst (15 g in Run SB-21903, 11.2 g in Run SB-26203, and 25 g in Run SB-28603) was calcined in air at 300°C and a sample with a size fraction between 140-325 mesh was loaded into the reactor filled with 300-320 g of Durasyn 164 oil (a hydrogenated 1-decene homopolymer, ~ C_{30}). The catalyst was pretreated in CO at 280°C, 0.8 MPa (100 psig), and 3 NL/g-cat/h (where, NL/h, denotes volumetric gas flow rate at 0°C and 1 bar) for 12 hours. After the pretreatment, the catalyst was tested initially at 260°C, 1.5 MPa (200 psig), 4 NL/g-Fe/h using CO-rich synthesis gas (H_2/CO molar feed ratio of 2/3). After reaching a stable steady-state value (~60 h on stream), the catalyst was tested at different process conditions. The minimum length of time between changes in process conditions was 20 h.

Results and Discussion

Results from STSR Tests

Three tests (Runs SB-21903, SB-26203 and SB-28603) with the Ruhrchemie catalyst were conducted in a 1 dm^3 stirred-tank slurry reactor (Autoclave Engineers) over a wide range of process conditions. The reaction temperature was 220, 240 or 260°C, the pressure varied from 0.8 to 2.5 MPa, the synthesis gas feed H_2/CO molar ratio was either 2/3 or 2, and the gas space velocity (SV) varied from 0.52 to 23.5 NL/g-Fe/h to obtain wide range of conversions. Process conditions are summarized in Table 1. Definitions of conversions and selectivities used in this report are as follows:

$$H_2 \text{ conversion } (\%) = 100 \times ((\text{Moles of } H_2)_{in} - (\text{Moles of } H_2)_{out})/(\text{Moles of } H_2)_{in} \quad (1)$$

$$\text{CO conversion } (\%) = 100 \times ((\text{Moles of CO})_{in} - (\text{Moles of CO})_{out}))/(\text{Moles CO})_{in} \quad (2)$$

$$(H_2+CO) \text{ conversion } (\%) = 100 \times ((\text{Moles of } H_2+CO)_{in} - (\text{Moles of } H_2+CO)_{out}))/(\text{Moles of } H_2+ CO)_{in} \quad (3)$$

$$\text{Usage ratio (UR (-))} = (\text{Moles of } H_2 \text{ consumed})/(\text{Moles of CO consumed}) \quad (4)$$

$$CO_2 \text{ selectivity } (\%) = 100 \times \frac{(n_{CO_2})_{out}}{(n_{CO})_{in} - (n_{CO})_{out}} \quad (5)$$

Hydrocarbon selectivity on carbon atom basis is calculated from:

$$S_{ij}(\%) = \frac{100 \times (in_{ij})}{(n_{CO})_{in} - (n_{CO})_{out} - (n_{CO_2})_{out}} \quad (6)$$

where: S_{ij} is the selectivity of hydrocarbon species j containing i carbon atoms, n_{ij} is molar flow of compound j in the gas phase, $(n_{CO})_{in}$ and $(n_{CO})_{out}$ are molar flow rates of CO in and out of the reactor, and $(n_{CO_2})_{out}$ is the molar flow rate of carbon dioxide out of the reactor. The above formulas assume that there is no carbon dioxide in the feed, and neglect the formation of oxygenates.

Olefin and paraffin selectivities (contents), based on molar flow rates of the corresponding hydrocarbons of the same carbon number, are calculated as:

1-olefin content (%) = 100 x (1-olefin)/(1-olefin + 2-olefin + n-paraffin) (7)

2-olefin content (%) = 100 x (2-olefin)/ (1-olefin + 2-olefin + n-paraffin) (8)

n-paraffin content (%) = 100 x (n-paraffin)/ (1-olefin + 2-olefin + n-paraffin) (9)

Total olefin to paraffin ratio = Total olefin rate/Total n-paraffin rate (10)

Reproducibility of Results and Catalyst Deactivation

In Runs SB-21903 and SB-26203 after the CO pretreatment, the catalyst was tested initially at the baseline conditions (260°C, 1.5 MPa, 4 NL/g-Fe/h, $H_2/CO = 2/3$), whereas in Run SB-28603 the catalyst was tested initially (up to 46 h on stream) at 220°C (the other process conditions were the same as the baseline conditions) and then the temperature was increased to

260°C (baseline conditions from 50-73 h on stream). Results from all three tests at the baseline conditions are shown in Figures 3 and 4.

Syngas conversion (Fig. 3a) and methane and C_5^+ hydrocarbon selectivities on a carbon atom basis (Fig. 3b) during the first 80 h of testing were remarkably similar in all three tests, indicating that the CO activation procedure was reproducible and that the use of different amounts of catalyst (11.2-25 g) did not have any impact on the initial catalyst activity and selectivity. Activity (syngas conversion) increased with time reaching a constant value at about 50 h on stream.

After testing at the baseline conditions the catalyst was evaluated at different process conditions (see Table 1). In order to assess the extent of catalyst deactivation the baseline conditions were repeated throughout the test (Run SB-21903) or at the end of the test (Runs SB-26203 and SB-28603). These results are shown in Figure 4.

Catalyst activity (measured by syngas conversion) decreased in all three tests (Fig. 4a). Average deactivation rate (expressed in terms of loss of conversion per hour) ranged from 0.018 %/h in run SB-21903 to 0.054 %/h in run SB-26203. Methane selectivity increased whereas C_5^+ selectivity decreased slightly with time in runs SB-21903 and SB-26203. The opposite trend (decrease in methane selectivity and increase in C_5^+ selectivity) was observed in run SB-28603.

Effect of time on stream (i.e. catalyst deactivation) on olefin selectivities (obtained from complete analysis of all products) in run SB-21903 is shown in Figure 5. As can be seen, the olefin selectivity did not change much with time, which is consistent with results shown in Figure 4b (methane and C_5^+ selectivities).

Effects of Process Conditions and Conversion on Water-Gas-Shift Reaction and Hydrocarbon Product Distribution

The catalyst was tested under 25 sets of different process conditions. The following values (or ranges) of process conditions were utilized in these three STSR tests:

Reaction temperature (T):	220, 240 and 260°C
Reaction pressure (P):	8, 15 and 25 (22.5) bar
Feed composition (H_2/CO ratio):	2/3 or 2/1
Gas space velocity (NL/g-Fe/h):	0.5 – 23.5

Effects of temperature, pressure, feed composition and gas space velocity (i.e. limiting reactant conversion) on the extent of water-gas-shift (WGS) reaction (in terms of usage ratio – UR and CO_2 selectivity), and hydrocarbon selectivity (CH_4 and C_5^+) are shown in Figures 6-14.

The effect of temperature and conversion of the limiting reactant (H_2 for H_2/CO = 2/3 feed gas, CO for H_2/CO = 2/1 feed gas) is shown in Figures 6-8. As shown in Figure 6 the usage ratio (UR) decreases whereas the CO_2 selectivity increases with an increase in conversion (at constant temperature) or with an increase in temperature (at constant conversion of the limiting reactant). This trend is the same regardless of feed composition (H_2/CO = 2/3 in Fig. 6a, or H_2/CO = 2/1 in Fig. 6b). The effect of conversion is consistent with the concept that the WGS reaction is a consecutive reaction according to the following stoichiometric equations.

Hydrocarbon formation (FTS) reaction

$$n\,CO + 2\,n\,H_2 = C_nH_{2n} + n\,H_2O;\ (UR = 2) \quad (11)$$

Water-Gas-Shift (WGS) reaction

$$CO + H_2O = CO_2 + H_2 \quad (12)$$

Overall reaction (high WGS activity)

$$2\,n\,CO + n\,H_2 = C_nH_{2n} + n\,CO_2;\ (UR = 0.5,\ CO_2\ \text{selectivity} = 50\%) \quad (13)$$

In the absence of the WGS reaction, the usage ratio is 2 (Equation 10), whereas if all water produced by FTS is consumed by the WGS reaction, the usage ratio is 0.5 and the CO_2 selectivity is 50% (assuming that CO is not consumed in any other reactions). From the above stoichiometry it is expected that the extent of WGS reaction (secondary or consecutive reaction) will increase with increase in conversion, which is manifested in decrease of the usage ratio and increase in CO_2 selectivity. The increase in WGS activity (higher CO_2 selectivity and lower UR) with increase in temperature (at constant conversion) is a kinetic effect (Fig. 6).

As shown in Figures 7 and 8, methane selectivity increases whereas the selectivity of high molecular weight hydrocarbons (C_5^+) decreases with an increase in temperature. Experimental data at 220°C and 240°C in Figure 7 (H_2/CO = 2/3, P =15 bar) do not follow this trend, possibly due to experimental errors. At a given temperature, methane selectivity increases

with an increase in conversion (H_2/CO = 2/3 feed in Fig. 7a) whereas C_5^+ selectivity decreases. However, this trend was not observed with a feed gas having a H_2/CO ratio of 2 (Fig. 8a) at 220°C and 240°C.

The effect of reaction pressure and conversion of the limiting reactant is shown in Figures 9-11. The extent of the WGS reaction increases (lower UR and higher CO_2 selectivity) with an increase in conversion or with a decrease in total pressure (Fig. 9). Conversion effect on the extent of WGS reaction was discussed previously (Fig. 6) whereas the effect of pressure is the kinetic effect. Methane selectivity decreases with an increase in pressure (Figures 10a and 11a), whereas pressure does not have significant effect on C_5^+ selectivity (Figures 10b and 11b). Methane selectivity increases with conversion at constant pressure (Fig. 11a with H_2/CO = 2, and at 15 bar with H_2/CO = 2/3 in Fig. 10a).

The extent of the WGS reaction is higher with the CO rich feed gas (H_2/CO = 2/3) relative to syngas derived from natural gas (H_2/CO = 2) as illustrated in Figure 12. Methane selectivity is lower, and C_5^+ selectivity higher with the CO rich feed gas (Figures 13 and 14). This is related to partial pressures of H_2 and CO. Methane selectivity increases and C_5^+ selectivity decreases with increase in partial pressure of H_2, i.e. with increase in H_2/CO ratio inside the reactor.

Effects of Conversion (gas space velocity) and Carbon Number on Olefin and Paraffin Selectivities

As shown in Figures 15-17, 1-olefin content decreases, whereas 2-olefin content and n-paraffin content increase with increase in conversion of the limiting reactant. This trend is less pronounced for the CO-rich feed gas at conversions of 40-65%, but is clear at higher conversions (Figures 16 and 17). This indicates that 1-olefins are consumed in secondary reactions, whereas n-paraffins and 2-olefins are formed in part in secondary reactions.

Carbon number dependences of selectivities (at constant conversion) show the following trend: 1-olefin selectivity passes through a maximum and n-paraffin selectivity passes through a minimum at C_3, whereas 2-olefin selectivity increases with carbon number. It is well known that ethylene is more reactive than other 1-olefins and it can initiate chain growth or be incorporated into the growing chains, and thus its selectivity is lower than that of 1-propene and other low molecular weight (MW) 1-olefins (Novak et al., 1981, 1982; Iglesia et al., 1991; Komaya and

Bell, 1994; Kuipers et al., 1995). Described carbon number effects have been ascribed to secondary reactions of 1-olefins (1-olefin readsorption, hydrogenation and/or isomerization) and increase in residence time with increase in molecular weight (Schulz et al., 1982, 1988; Dictor and Bell, 1986; Iglesia et al., 1993; Madon and Iglesia, 1993).

Carbon Number Product Distribution

Typical carbon number product distributions at different process conditions are shown in form of Anderson-Schulz-Flory (ASF) plots (Figures 18 and 19). Carbon number distributions could not be described by uniform value of the chain growth probability factor α, which would result in a straight line ($\ln x_n$ vs C_n). Experimental data were fitted using a three-parameter model of Huff and Satterfield (1984):

$$x_n = \beta (1-\alpha_1) \alpha_1^{n-1} + (1 - \beta) (1 - \alpha_2) \alpha_2^{n-1} \qquad (14)$$

where: x_n = mole fraction of products containing n carbon atoms (hydrocarbons and oxygenates), β = fraction of type 1 sites, α_1 = chain growth probability on type 1 sites, and α_2 = chain growth probability on type 2 sites.

Experimental data are reasonably well represented by this type of model. The model parameters were estimated using a nonlinear regression.

Vapor-Liquid Equilibrium Calculations

In the analysis of the experimental data it is assumed that the STSR behaves as a perfectly mixed flow reactor, and that the gas-liquid interphase mass transfer resistance is negligible, i.e. the gas and the liquid phase are in thermodynamic equilibrium. Also, reaction rates can be expressed in terms of fugacities, instead of liquid phase concentrations and/or vapor phase partial pressures. Vapor-liquid equilibrium (VLE) calculations are needed to calculate fugacities, and to check whether the assumption of thermodynamic equilibrium between the gas and the liquid phase is valid under the FTS reaction conditions in the STSR.

Basic concepts and definitions

Vapor and liquid phases are in equilibrium at the same temperature and pressure, when the fugacity of each constituent species is the same in all phases

$$\hat{f}_i^v = \hat{f}_i^l \tag{15}$$

Both the vapor and liquid fugacities can be calculated using the corresponding fugacity coefficients, $\hat{\phi}_i$, from Equation (16) as follows:

$$y_i \cdot \hat{\phi}_i^v \cdot P = x_i \cdot \hat{\phi}_i^L \cdot P \tag{16}$$

where x_i is a mole fraction of species *i* in the liquid and y_i is a mole fraction of species *i* in the gas. This expression of the vapor-liquid equilibrium is very convenient and relationship between gas and liquid composition can be expressed in terms of so called *K-value*

$$K_i = \frac{y_i}{x_i} = \frac{\hat{\phi}_i^L}{\hat{\phi}_i^v} \tag{17}$$

The fugacity coefficients $\hat{\phi}_i$ are calculated from an equation of state (EOS). Several equations of state have been used for this purpose. The following EOS have been used for the VLE calculations in Fischer-Tropsch synthesis: Peng-Robinson (PR) equation of state (Marano and Holder, 1997; Breman and Beenackers, 1996; Li and Froment, 1996), Redlich-Kwong (RK) EOS (Zimmerman, 1990) and Soave-Redlich-Kwong (SRK) EOS (Ahón *et al*., 2005). In this work the modified Peng-Robinson equation of state has been selected for VLE calculations. According to the PR EOS the fugacity coefficient can be expressed as:

$$\ln\hat{\phi}_i = \frac{b_i}{b}(Z-1) - \ln(Z-B) + \frac{A}{2\sqrt{2}B}\left(\frac{b_i}{b} - \frac{2\sum_j z_j a_{ij}}{a}\right)\ln\left(\frac{Z+\left(1+\sqrt{2}\right)B}{Z+\left(1-\sqrt{2}\right)B}\right) \tag{18}$$

where z is a mole fraction of species in the liquid phase, x, or in the gas phase, y. Definitions of other symbols (*A*, *B*, *Z*, *a*, a_{ij}, *b* and b_i) and additional explanations can be found in Appendix A.

In order to get good agreement between the PR EOS predictions and experimental data for inorganic species (H_2, CO, CO_2, H_2O) in higher molecular weight hydrocarbons two modifications of the PR EOS were made. The first modification deals with changes in the acentric factor function, $f_i(\varpi)$, from the original formulation (Equation A.9 in Appendix A) to the extended form (Equation A.10) proposed by Li and Froment (1996). The binary interaction factors k_{ij} (Appendix A, Equation A.3) were estimated utilizing experimental data from literature on solubility of inorganic species in various hydrocarbons. Critical properties (the critical temperature and pressure) and acentric factor ω of inorganic species and linear paraffins and olefins (up to C_{20}) were taken from Poling *et al*. (2001) and Nikitin *et al*. (1997). For higher molecular weight hydrocarbons (> C_{20}) the equations of Gao *et al.* (2001) were used. The critical temperature and pressure of the start-up fluid (Durasyn) were estimated from Joback's group contribution methods (Joback, 1984; Joback and Reid, 1987), whereas the acentric factor was estimated from Lee and Kessler (1975). Details of calculation procedure for estimation of properties of Durasyn are given in Appendix B.

VLE Calculations for Binary Systems

The binary interaction factors k_{ij} for inorganic species (H_2, CO, CO_2, H_2O) in hydrocarbons were estimated from experimental VLE data in binary systems from the literature (Peter and Weinert, 1955; Calderbank *et al*., 1963; Gasem and Robinson, 1985; Nettelhoff *et al*. 1985; Chao and Lin, 1988; Miller and Ekstrom, 1990; Breman *et al*., 1994; Park *et al*., 1995; Gao *et al*., 1999). Experimental conditions employed in these studies are summarized in Table 2.

The interaction factors were optimized to obtain the best agreement with reported experimental K_i values ($K_i = y_i/x_i$). Comparisons of calculated (from the PR EOS with optimized k_{ij} values) and experimental K values for different binary systems and different conditions (P and T) are shown in Figures 20-26. It can be seen that there is excellent agreement between calculated K values and the experimental ones for permanent gases (H_2, CO, CO_2) in different solvents over a wide range of pressures and temperatures (Figures 20-25). Discrepancies between calculated and experimental values for water (Figure 26) are caused by large differences in reported experimental K values by different authors. In several Figures (20-22, 24 and 26) predictions based on Nettelhoff et al. (1985) correlation for Henry's law constant have also been included. This correlation was obtained from authors' experimental data with H_2 and CO in

Vestowax (hydrocarbon wax) and Peter and Weinert's (1955) data in hydrocarbon wax (molecular weight = 345). The Nettelhoff et al. (1985) correlation for Henry's law constant does not account for the effects of pressure and molecular weight of solvent, and the predicted K values are usually lower than the experimental ones. The use of PR EOS with adjustable interaction factors provides a much better fit of the experimental data over a wide range of conditions.

The optimized values of interaction factors vary with molecular weight of solvent, but are weak functions of temperature (200-300 °C) and pressure (10-30 bar). Average values of the interaction coefficients k_{ij} in different hydrocarbons are summarized in Table 3, and their variation with carbon number is shown graphically in Figure 27. In subsequent VLE calculations the data from Figure 27 were used to obtain interaction factors of the inorganic species in hydrocarbons with carbon numbers between 20 and 36 by linear interpolation.

VLE Calculations for FTS in the STSR

The PR EOS was used with the above-mentioned modifications (acentric factor function and the binary interaction coefficients for inorganic components with hydrocarbons having more than 20 carbon atoms) to perform VLE calculations for the experiments in the STSR (Table 1).

The following species were taken into account in the VLE calculations: inorganic species (H_2, CO, CO_2, H_2O), n-paraffins (C_1-C_{20}), 1-olefins (C_2-C_{15}), Durasyn (C_{30}) and two pseudo-components: C_{21}^+ paraffins and unanalyzed wax (with critical properties and acentric factor of C_{30} n-paraffin). Thus, the VLE calculations were done for a two-phase mixture of 41 components (species). Interaction factors (k_{ij}) were used for each combination of inorganic species with one of the following high molecular weight hydrocarbons: C_{20} paraffin, C_{21}^+ paraffins (represented by a component having the average molecular weight of the mixture), unanalyzed wax (C_{30} n-paraffin) and Durasyn. Thus, for each inorganic species there are four non-zero interaction factors. The interaction factors for all other species were set to zero. Detailed explanations, equations and the computational algorithm for the VLE calculations are given in the Appendix C.

The VLE calculations were made for all 27 sets of process conditions (mass balances) shown in Table 1. Representative results (four mass balances) are shown in Figures 28 and 29. In each of these figures calculated mole fractions of hydrocarbon species (C_1-C_{20} n-paraffins, and

C_2-C_{15} 1-olefins) in the liquid (x_i) and vapor (y_i) phase are shown together with the corresponding experimental values. In all cases (including the ones not shown in these two figures) there is a very good agreement between the calculated and experimental values for the vapor phase composition, whereas the agreement between the calculated and experimental values of mole fractions in the liquid phase ranges from fairly good (Figure 28) to poor (Figure 29). The reason for larger discrepancies (calculated vs. experimental) for the liquid phase components is that the amounts of Durasyn and wax (as well as their ratio) withdrawn from the reactor are not measured accurately.

It should be noted that lower molecular weight hydrocarbons (C_1-C_9) and inorganic species are not detected experimentally in the liquid phase, and thus their experimental values are not shown in Figures 28 and 29. To account for the absence of lighter components in the liquid phase one can use the normalized calculated mole fractions (xnorm in Figures 28 and 29) for comparison with the experimental mole fractions (for the liquid phase only). The normalized values of the calculated liquid phase mole fractions were calculated from the following equation:

$$x_i^{norm} = \frac{x_i^{calc}}{\sum_{i \in \Delta} x_i^{calc}} \tag{19}$$

where Δ means components, which were measured experimentally in the liquid phase. As can be seen in Figures 28 and 29, the normalization does not have significant effect on results because the measured components account for more than 90% of the total liquid phase.

It can be concluded that the VLE calculations show that the vapor and liquid phase are in thermodynamic equilibrium during Fischer-Tropsch synthesis in the STSR. The discrepancies between calculated and experimental liquid phase compositions are attributed to experimental errors.

Kinetic Modeling and Parameter Estimation

Kinetic parameters were estimated from experimental data in the STSR (Table 1). Three kinetic models from the literature have been adopted to analyze the experimental data from the STSR. Two kinetic models (Lox and Froment, 1993b; Yang et al., 2003) provide a complete product distribution (inorganic species and hydrocarbons) whereas the kinetic model of Van der

Laan and Beenackers (1998, 1999) can be used to predict hydrocarbon product distribution only. Also we extended the kinetic model of Van der Laan and Beenackers to include 2-olefin formation.

Kinetic Model of Lox and Froment

The model reported as the best by Lox and Froment (marked by symbol ALII in Lox and Froment, 1993b) for their operating conditions (high H_2/CO feed ratio of 3) has been selected for the initial estimation of kinetic parameters from the experimental data in the STSR. It accounts for formation of carbon dioxide, water, paraffins, and total olefins (it does not distinguish between 1- and 2-olefins) as well as consumption of hydrogen and water. This model predicts a constant value for the chain growth probability factor, α, however TAMU experimental data show that α is not constant (i.e. it varies with carbon number). A simplified form of this model contains only five parameters at isothermal conditions. Because of its relative simplicity, this model is well suited for initial studies where the main goal is to learn techniques for parameter estimation and statistical analysis of estimated values of model parameters. The same techniques and computer codes were used in the analysis of other kinetic models.

The ALII model utilizes the LHHW approach and the concept of rate-determining steps (RDS). The elementary steps (reactions) for FTS and WGS reaction are shown in Tables D.1 and D.2, respectively. Reactant molecules are adsorbed on two types of active sites, one for FTS and the second for WGS reaction, where the surface reactions take place. The model assumes the following two RDS in each path of formation of paraffins and olefins in the Fischer-Tropsch reaction:

- adsorption of carbon monoxide (HC1) and desorption of the paraffin (HC5) in the reaction path leading to the paraffins,
- adsorption of carbon monoxide (HC1) and desorption of the olefin (HC6) in the reaction path leading to the olefins,

and the following RDS for the WGS reaction path:

- reaction of an adsorbed carbon monoxide with adsorbed hydroxyl group (WGS2; Table D.2).

All relevant equations are given in Appendix D of this report.

Parameter Estimation Methodology

A simplified ALII model of Lox and Froment (1993b) has five kinetic parameters, three for the FTS reaction:

- adsorption of carbon monoxide, $k_{\mathrm{CO,HC}}$,

- desorption of a paraffin, $k_{\mathrm{t,p}}$,

- desorption of an olefin, $k_{\mathrm{t,o}}$,

and two parameters for the WGS reaction:

- constant containing the WGS rate constant $k_{\nu}^{'}$.

- ratio of adsorption constants K_{ν}.

In equations (D.1) to (D.4) the unknowns are five kinetic constants, whereas partial pressures of hydrogen, carbon monoxide, carbon dioxide, and water are known from the VLE calculations ($p_i = y_i \cdot P$).

Parameters are estimated by minimizing an objective function, S. An objective function that minimizes the sum of squares of residuals of reaction rates was used:

$$S = \sum_{h=1}^{v} \sigma_{h,h} \cdot \sum_{i=1}^{n} \left(\hat{R}_{i,h} - R_{i,h} \right)^2 \tag{20}$$

where $\hat{R}$ means experimental, R represents calculated reaction rate, and $\sigma_{h,h}$ are diagonal elements of the inverse of the error covariance matrix. If the weighting factors are not used in Equation (20) then the σ matrix is the identity matrix, i.e. $\sigma_{\mathrm{h,h}} = 1$.

When replicate experiments are available the weighting factors can be calculated (Froment and Bischoff, 1990) as:

$$\sigma_{h,h} = \left(\frac{\sum_{i=1}^{n_e} \left(\hat{R}_{i,h} - \overline{R}_h \right)^2}{n_e - 1} \right)^{-1} \tag{21}$$

where $\overline{R}_h$ represents the average value of response h over n_e replicate experiments (n_e is equal to 3 in our case), n is a number of experiments at constant temperature, and v is a number of components (in this case: CO, CO_2, H_2, H_2O, twenty n-paraffins $C_{1\text{-}20}$, fourteen 1-olefins $C_{2\text{-}14}$

and pseudo-component C_{21-50}). The reaction rate of pseudo-component C_{21}^{+} is calculated as follows:

$$R_{21+} = \sum_{i=21}^{50} R_i \tag{22}$$

When there is insufficient information about the nature of errors in experimental measurements, another weighting factor can be used. In such cases, the simplest form of the weighting factor is the inverse of squared mean response of the j^{th} variable (Englezos and Kalogerakis, 2001):

$$\sigma_{j,j} = \left(\frac{1}{n} \cdot \sum_{i=1}^{n} \hat{R}_{ij} \right)^{-2} \tag{23}$$

Minimization of the objective function was done by the Levenberg-Marquardt (LM) method (Marquardt, 1963) which is an improved form of the Newton-Gauss optimization technique. The minimization procedure consists of the following steps:

An initial guess of unknown parameters k^0 is made. The corresponding reaction rates are calculated using the assumed values of kinetic parameters and the objective function is evaluated.

1. New (improved) values of kinetic parameters k^i are found by the LM method.
2. New values of reaction rates and the objective function are obtained.
3. If the current (new) value of the objective function is smaller or equal to the previous (old) one then go to Step 4. If not, go to Step 2 and keep iterating until a criterion for minimization is satisfied, i.e.:

$$S\left(k^{i+1}\right) \leq S\left(k^{i}\right)$$

4. Stop iterations when the difference between the current and the previous value of the objective function is smaller than the desired convergence criterion, ε_p.

$$\left| S\left(k^{i+i}\right) - S\left(k^{i}\right) \right| \leq \varepsilon_p$$

If the convergence is not achieved, go back to Step 2 and iterate until the convergence criterion is achieved. The numerical value of ε_p is set at 10^{-6}.

Results from Parameter Estimation

Estimated values of kinetic parameters obtained using the objective function (Equation (20)) with weighting factors equal to one and with weighting factors calculated using Equation (23) are shown in Table 4. As can be seen from this table, the rate constant for olefin formation, $k_{t,0}$, estimated assuming that all weighting factors are equal to one, is negative for data at 220°C and 260°C. Therefore, this approach ($\sigma_{h,h} = 1$ in Equation (20)) yields unsatisfactory results. The use of weighting factors calculated from Equation (23) results in positive values for all five rate constants at all three temperatures (Table 4).

Statistical parameters associated with calculated rate constants are shown in Table 5. Approximate 95% confidence intervals for the WGS kinetic parameters $k_{\nu}^{'}$ and K_{ν} show that these parameters are not significantly different from zero (lower 95% confidence interval gives negative values), whereas the mean values of the three kinetic parameters for the FTS are statistically reliable.

Representative parity plots, for a reaction temperature of 260°C, are shown in Figures 30 and 31. These figures show a comparison of calculated and experimental reaction rates. Calculated and experimental rates for inorganic species (H_2, CO, CO_2, and H_2O) are shown in Figure 30, whereas the results for hydrocarbons are shown in Figure 31. In the case of H_2 and CO, the absolute rates are shown in Figure 30. If the model fits the data, experimental points would lie on a straight line with a slope of 45°. However, almost all of the calculated reaction rates are smaller then the experimental values (Figures 30 and 31). Results for various hydrocarbon species (Figure 31) are shown with two different scales. As can be seen in this figure, the Lox and Froment's (1993b) ALII model does not predict accurately the formation rates of various hydrocarbons (individual species as well as lumped species). Detailed comparison of predicted and experimental formation rates of individual species (C_1-C_{20} n-paraffins, and C_2-C_{15} olefins) is shown in Figure 32. Experimental values are represented by points, whereas solid lines are model predictions. Model predictions are represented by straight lines on a semi-logarithmic plot (log Rate vs. Carbon number) whereas experimental points have curvatures. It can be seen that the model does not predict accurately the observed reaction rates of individual hydrocarbons.

Figure 33 shows carbon number distribution of hydrocarbon products on a semi-logarithmic scale (logarithm of reaction rate of hydrocarbons containing n carbon atoms vs. carbon number). The model yields a straight line, whereas experimental data show nonlinear dependence on carbon number. The model predictions reflect the ideal Anderson-Schulz-Flory distribution characterized by a constant value of the chain growth probability factor α, whereas experimental data show that α varies with carbon number.

Predicted and experimental values of olefin to n-paraffin reaction rates (Olefin to paraffin ratio) as a function of carbon number are shown in Figure 34. The model predictions are represented by a horizontal line, whereas experimental values are carbon number dependent. Clearly the model fails to predict the observed experimental trends both qualitatively and quantitatively.

Activation Energies

From estimated values of kinetic parameters at three reaction temperatures (Table 4, with weighting factors from Equation (23)), the corresponding activation energies and frequency factors have been calculated. The adsorption constant for carbon monoxide adsorption $k_{\mathrm{CO,HC}}$, the desorption rate constant of n-paraffins $k_{\mathrm{t,p}}$, the desorption rate constant of olefin $k_{\mathrm{t,o}}$, and the WGS reaction rate constant $k_{\nu}^{'}$ satisfy the Arrhenius equation:

$$k = A_0 \cdot e^{\frac{-E_a}{RT}} \tag{24}$$

where A_0 is a frequency factor, E_a is an activation energy, R is universal gas constant equal to *8.3144 kJ/mol*, and T is temperature measured in *Kelvin*.

Numerical values of activation energies (E_a) are shown in Table 6. Statistical parameters in this table are calculated for one degree of freedom ($n - p$, where n is number of independent values, data at temperatures: 220, 240 and 260°C, whereas p is a number of parameters, A_0 and E_a) and for probability of 0.95. Approximate 95% confidence intervals are large, due to the fact that there is only one degree of freedom in the estimation. However, the approximate confidence intervals indicate that estimated values of activation energies for carbon monoxide adsorption $E_{\mathrm{CO,HC}}$, n-paraffin formation $E_{\mathrm{t,p}}$, and olefin formation $E_{\mathrm{t,o}}$ are reliable, because they are all non-negative. The approximate confidence intervals for the WGS activation energy

E_v range from -585 to 1003. This means that the estimated value for E_v (209 kJ/mol) is not significantly different from zero, and it has a small impact on the model result. The relatively small standard error value and high t-value imply that estimated parameter value is obtained with good accuracy. As can be seen, these conditions are satisfied for activation energies: $E_{\mathrm{CO,HC}}$, $E_{\mathrm{t,p}}$ and $E_{\mathrm{t,o}}$.

Activation energies for the formation of paraffins ($E_{\mathrm{t,p}}$) and olefins ($E_{\mathrm{t,o}}$) can be compared with the corresponding values reported in the literature (Table 7). Reported values of the activation energy for the paraffin formation are between *70* and *112 kJ/mol*, and those for the olefin formation are *97 – 132 kJ/mol*. Activation energies from the TAMU data with the ALII kinetic model of Lox and Froment (1993b) are *121 kJ/mol* for paraffin formation, and *54 kJ/mol* for the olefin formation. The former is slightly higher than the upper bound from the literature, whereas the olefin formation activation energy value is about 50% lower than a typical value from the literature. The estimated activation energy for the WGS reaction (*209 kJ/mol*) is too high when compared to the corresponding values in the literature (*28-137 KJ/mol*), and is not reliable as discussed previously (lower 95% confidence interval gives negative value).

Multi-Response Objective Functions

The following objective functions have been used in all subsequent estimations of kinetic parameters. The objective function S_1 utilizes reaction rates R_i and the weighting factor σ.

$$S_1 = \sum_{h=1}^{N_{resp}} \sigma_{h,h}^{-1} \cdot \sum_{i=1}^{N_{\exp}} \left(\hat{R}_{i,h} - R_{i,h}\right)^2 \tag{25}$$

where h is a response that represents a component: CO, CO_2, H_2, H_2O, twenty paraffins $C_{1\text{-}20}$, nineteen olefins $C_{2\text{-}20}$, and lumped-component $C_{21\text{-}50}$, which gives 40 responses (components); N_{exp} is a number of experiments, and $\sigma_{h,h}^{-1}$ are diagonal elements of the inverse of the error covariance matrix.

The objective function, S_2, utilizes molar flow rates of individual components

$$S_2 = \sum_{j=1}^{N_{resp}} \sum_{i=1}^{N_{\exp}} W_i \cdot \left(\frac{m_{i,j,\exp} - m_{i,j,cal}}{m_{i,j,\exp}} \right)^2 \tag{26}$$

where $m_{i,j}$ is molar flow rate of jth component in ith experiment, and W_i is the weighting factor.

The accuracy of the fitted model relative to the experimental data was obtained from the mean absolute relative residual (MARR) function:

$$MARR = \frac{1}{N_{resp} N_{\exp}} \sum_{i=1} \sum_{j=1} \left| \frac{\hat{R}_{i,j} - R_{i,j}}{R_{i,j}} \right| \tag{27}$$

A statistical test for the kinetic model is measured either by the F-value or by correlation coefficient. The statistics for the estimated parameters are expressed by either t-value or the 95% confidence interval.

An analysis of residuals of estimates has been done utilizing the relative residual (RR) which is defined as follows:

$$RR_{i,j} = 100 \cdot \frac{\hat{R}_{i,j} - R_{i,j}}{R_{i,j}} \tag{28}$$

where i represents the component, j represents the experiment, and R and $\hat{R}$ are the experimental and calculated reaction rates, respectively.

Kinetic Model of Yang et al.

This model was proposed by Dr. Li's group at the Institute of Coal Chemistry of Chinese Academic of Science in Taiyuan, PR China (Yang et al., 2003). The main features of this model are as follows:

- olefin readsorption is included,
- separate reaction rate constant is used for methane,
- solution of hydrocarbon formation reaction rates requires the numerical solution of a set of two non-linear algebraic equations,
- the model predicts that olefin to paraffin ratio is a function of carbon number.

Elementary reactions and final equations for this model are given in Appendix E. The total number of parameters that need to be estimated is 24 (20 parameters for hydrocarbon formation, and 4 parameters for the WGS reaction). Kinetic parameters for the WGS reaction and FTS synthesis were estimated first separately, and then simultaneously.

Estimation of Parameters for WGS Reaction

The WGS reaction model is described as one equation for carbon dioxide formation (Equation E.12). This model contains four parameters (two for the reaction rate constant k_V and two for the adsorption equilibrium constant K_V). It can be noted that the constant K_V is a ratio of adsorption constants (Equation E.13). Kinetic parameters were estimated using a trust-region reflective Newton large-scale (LS) method (Coleman and Li, 1994, 1996). Results are given in Table 8. The grey-colored cells in Table 8 represent results obtained with the objective function S_1 whereas the results in cells without color were obtained using the objective function S_2. The objective function S_2 (relative objective function) gives a better fit, measured by MARR (~20% vs. 26% using S_1). Obtained activation energy values for CO_2 formation are in range 60 – 95 kJ/mol whereas values for enthalpy change, which represents the difference of two enthalpy change values (therefore it can be negative), are between -46 and – 80 (kJ/mol).

Although fitting of the model gives good statistical values in all cases (F-value ~30 – 60 and correlation coefficient ~0.64 – 0.91), the estimated parameters have large confidence intervals ranging from negative to large positive values. A parity plot, calculated vs. experimental reaction rate of carbon dioxide formation, is shown in Figure 35. It can be seen that the calculated values are nearly constant for a particular temperature (4 low points are at 220^{o}C, 8 points in the middle are for 240^{o}C, and 15 upper points are for 260^{o}C). This shows that the model predicts that the WGS reaction rate is proportional to the reaction rate constant (R_{CO2} ~ k_V).

In order to check if these results represent a global minimum, a genetic algorithm (GA) has been incorporated into the estimation procedure (Goldberg, 1989, Conn et al., 1997). A hybrid method: GA first, followed by the Levenberg-Marquardt (LM) or LS method was employed. The GA method finds a good initial guess close to the global minima, and LM or LS provides more precise values. Results are shown in Table 9. The grey-colored cells in the table represent results from the GA method whereas cells that are not colored are results from either LM or LS method. The GA method has found two global minima (grey cells, rows W17 and W20), which have different values of parameters. These values were used as initial guesses for the LM and LS methods. The activation energy obtained is between 128 and 143 kJ/mol whereas the difference of enthalpy change varies from 6 to -12. It can be seen that applying a hybrid method gives similar statistics for fitting of the model (~33, 20 and 0.65 for F-value, MARR and

correlation coefficient, respectively), but it gives a narrow confidence interval for the activation energy (lower 95% confidence interval limit is positive). For case W18 in Table 9, the activation energy is 143 kJ/mol and its confidence interval is 95 – 192 kJ/mol. It can be noted that both the LM and LS methods give the same result (Table 9, W18 and W19, respectively), but the LM method converges much faster (only 26 iterations, compared to 131 for the LS). It seems that a combination of the GA method followed by the LM method is better, and very effective for estimation of kinetic parameters. This confirms that the LM is a good searching method provided it has a good starting point.

The parity plot for carbon dioxide (Figure 36) shows better agreement between model predictions (GA method followed by the LM method) and experimental data, than that obtained using the LM or LS method directly. Estimated values for the WGS activation energy by the GA method followed by the LM or the LS method (128-143 kJ/mol) are comparable to some of the previously reported values for the WGS reaction (Table 7).

Estimation of Parameters for FTS Reaction

The Fischer-Tropsch synthesis reaction model (hydrocarbons rate formation) contains 20 unknown parameters. Calculation of rates for every set of parameters (i.e. for every iteration) requires numerical solution of two non-linear algebraic equations (Equations E.4 and E.11). Parameters were estimated using the objective function S_2 (with W_i = 1) and a trust-region reflective Newton large-scale method (LS). Results are shown in Table 10.

From the F-test a significant value for the model was obtained (about 15). In addition, a relatively narrow 95% confidence interval for all activation energies was obtained. However, the degree of agreement between experimental and calculated responses, measured by MARR, is relatively large (~65%) and the correlation coefficient is small (~0.15). A parity plot for methane, ethane, and ethene is shown in Figure 37, whereas the results for hydrocarbon groups $C_{3\text{-}10}$ and $C_{11\text{-}20}$ are shown in Figure 38. It can be seen that the model provides good fit for light paraffins and all olefins, whereas the calculated $C_{11\text{-}20}$ paraffins are significantly smaller than the corresponding experimental values. Paraffin and olefin rates as a function of carbon number are shown in Figures 39 and 40 (for all mass balances). Again, good agreement was obtained between calculated and experimental values for light paraffins and olefins for most mass balances.

Simultaneous Estimation of Kinetic Parameters for WGS and FTS Reactions

This is a multi-response estimation of all species: carbon dioxide (WGS), hydrocarbons (FTS), and inorganic species (hydrogen, carbon monoxide, and water). Rates for carbon monoxide, hydrogen and water were calculated based on stoichiometry (Equations D.6, D.7 and D.8, respectively). This approach considers 24 parameters. The results from WGS and FTS estimations were used as initial guesses in this estimation.

The use of a multi-response estimation did not result in the improvement of model parameters. Both minimization methods, LM and LS, lead to minor changes in values of pre-exponential factors (mostly for WGS) and do not result in improvement of other parameters. Figure 41 is a parity plot for inorganic components: carbon monoxide, hydrogen, carbon dioxide, and water. Almost all calculated rates are smaller than experimental ones. Predicted rates for carbon dioxide formation are not as good as those obtained from the WGS estimation alone (Figures 35 and 36 vs. Figure 41).

Hydrocarbon selectivity Model of Van der Laan and Beenackers

Van der Laan and Beenackers (1998, 1999) developed so-called olefin readsorption product distribution model (ORPDM) for formation of hydrocarbons in FTS. Reaction network of hydrocarbon formation for this model is presented in Appendix F (Figure F.1). Chain growth initiates by hydrogenation of an adsorbed monomer ($^{*}CH_2$) to an adsorbed methyl group ($^{*}CH_3$). Chain propagation occurs via insertion of an adsorbed monomer into an adsorbed alkyl species ($^{*}C_nH_{2n+1}$), which can terminate to either n-paraffin (C_nH_{2n+2}) by hydrogenation or to olefin (C_nH_{2n}) by dehydrogenation (i.e. hydrogen abstraction). According to this reaction network olefin readsorption leads to adsorbed alkyl species, which can either propagate or terminate. Elementary reactions for this model are shown in Table F.1, and detailed derivation of kinetic equations is given in Appendix F.

Parameters were estimated from experimental data at constant temperature. There are three sets of experimental data at temperatures 220, 240 and 260°C, which include 4, 8 and 15 mass balances, respectively.

Parameters were estimated using objective function S_1, defined by Equation (25) and the LM method. Total number of experiments, $N_{\exp}$, is 4, 8, or 15 at 220, 240 and 260°C,

respectively, whereas number of responses, N_{resp}, is 40 ($C_{1\text{-}20}$ paraffins, $C_{2\text{-}20}$ olefins, and pseudo-component $C_{21\text{-}50}$). Degrees of freedom for all of these three cases are high and equal to 137, 277, and 522 for temperatures of 220, 240, and 260°C.

Van der Laan and Beenackers model (1998, 1999) has 8 parameters (for every set of process conditions). These parameters are related to the following steps: initiation (κ_1), propagation (κ_p), methane formation ($\kappa_{t,p}^{(1)}$), ethane formation ($\kappa_{t,p}^{(2)}$), olefin formation ($\kappa_{t,o}$), ethylene readsorption ($\kappa_{r,o}^{(2)}$), readsorption of C_3^+ olefins ($\kappa_{r,o}$), and solubility/physiosorption dependence of olefin with carbon number (c). The pseudo-kinetic parameters are related to the true kinetic parameters and surface coverages of the reaction intermediates as follows:

$$\kappa_1 = k_{p1} \cdot \theta_{CH_2,s_1} \cdot \theta_{H,s_1}$$

$$\kappa_p = \frac{k_p \cdot \theta_{CH_2,s_1}}{k_{t,p} \cdot \theta_{H,s_1}}$$

$$\kappa_{t,p}^{(1)} = \frac{k_{t,p}^{(1)}}{k_{t,p}}$$

$$\kappa_{t,p}^{(2)} = \frac{k_{t,p}^{(2)}}{k_{t,p}} \qquad (29)$$

$$\kappa_{t,o} = \frac{k_{t,o} \cdot \theta_{s_1}}{k_{t,p} \cdot \theta_{H,s_1}}$$

$$\kappa_{r,o}^{(2)} = k_{r,o}^{(2)} \cdot \theta_{s_1} \cdot \theta_{H,s_1} \cdot \frac{R_g \cdot T}{SV}$$

$$\kappa_{r,o} = k_{r,o} \cdot \theta_{s_1} \cdot \theta_{H,s_1} \cdot \frac{R_g \cdot T}{SV}$$

where θ is the surface coverage of species (or sites).

Van der Laan and Beenackers (1998, 1999) found that parameters $\kappa_{t,p}^{(1)}$, $\kappa_{t,p}^{(2)}$, $\kappa_{r,o}^{(2)}$, and c are constant at a given temperature (250°C). From the above definitions and Appendix F, one can see that only two parameters, $\kappa_{t,p}^{(1)}$ and $\kappa_{t,p}^{(2)}$, represent ratios of two true kinetic constants and thus are expected to be dependent on temperature only. Also, parameter c can be constant at a given temperature. This parameter is related to non-intrinsic effects on reaction rates, such as

intraparticle diffusion, physisorption and/or solubility. However, it must be noted that $\kappa_{r,o}^{(2)}$ parameter is expected to be a function of process conditions (gas space velocity, and surface concentrations of intermediates, which in turn are expected to vary with P, T, SV, and/or H_2/CO feed ratio). Two types of estimation for $\kappa_{r,o}^{(2)}$ parameter: (a) temperature dependent only; and (b) dependent on all conditions (i.e. its numerical value is different for each mass balance conducted at different process conditions) were performed.

The first estimation, with $\kappa_{r,o}^{(2)}$ dependent on temperature only (Van der Laan and Beenackers approach) is shown in Table 11. In addition parameters $\kappa_{t,p}^{(1)}$, $\kappa_{t,p}^{(2)}$, and c were also assumed to be dependent on temperature only, whereas the remaining 4 model parameters κ_1, κ_p, $\kappa_{t,0,}$ and $\kappa_{r,0}$ were estimated for each set of conditions. As can be seen from Table 11, this assumption leads to negative values of some parameters (highlighted cells). Thus, this approach is not valid for the TAMU experimental data.

Results from the second procedure, $\kappa_{r,o}^{(2)}$ estimated for each set of conditions, are shown in Table 12. The statistics for estimated parameters, t-values, corresponding to this case are shown in Table 13. All parameters, except $\kappa_{t,o}$, $\kappa_{r,o}^{(2)}$, and $\kappa_{r,o}$, are significantly different than zero, and their t-values are greater than two. Moreover most of t-values are quite high (greater then 10), which means that the parameters have a quite narrow 95% confidence interval. However most of parameters related to termination and readsorption of olefins ($\kappa_{t,o}$, $\kappa_{r,o}^{(2)}$, and $\kappa_{r,o}$) are statistically insignificant (their t-values are smaller then 1 – highlighted cells in Table 13).

Comparison of predicted and experimental reaction rates of n-paraffins and olefins for selected mass balances (6 cases) is shown in Figure 42. In general a good fit has been obtained for paraffins and olefins up to C_{20}. Average mean absolute relative residuals (MARR) values for C_1-C_{20} hydrocarbons are generally smaller then 30%. As shown in Figure 42, the TAMU experimental data often show high paraffin reaction rates in C_{12}-C_{25} carbon number range (a "hump" in experimental data) which may be due to secondary reactions (e.g. hydrocracking). These deviations are not accounted by the present model and result in higher MARR values. The agreement between predicted and experimental values for a pseudo-component (paraffin C_{21}^{+}) is

generally worse than that for paraffins and olefins up to C_{20}. In some cases MARR values for C_{21}^{+} showed a very good overall fit, whereas the fit was not so good for individual paraffins (C_{21} to C_{50}).

Van der Laan and Beenackers (1999) noted that a strong correlation between parameters $\kappa_{t,o}$ and $\kappa_{r,o}$ occurs at a high olefin readsorption rate ($\kappa_{r,o} \cdot \exp(c \cdot n) >> 1$). In such a case, these parameters should not be estimated separately, and the $\kappa_{t,o} / \kappa_{r,o}$ ratio should be estimated as one parameter. Correlation between these two parameters results in their non-significant statistical values as mentioned previously for the TAMU experimental data (results shown in Table 13). By combining these two parameters into one, the kinetic model of Van der Lann and Beenackers has 7 parameters (see Appendix F for details). Three of these parameters are temperature dependent only ($\kappa_{t,p}^{(1)}$, $\kappa_{t,p}^{(2)}$ and c) whereas others (κ_1, κ_p, $K_o^{(2)}$, K_o) have different values at different process conditions. Estimated parameter values are given in Table 14, and the corresponding t-values in Table 15. Parameter estimation by this method gives much better statistics (t-values) for parameters related to olefin readsorption and termination ($K_o^{(2)}$, K_o) while at the same time does not change statistical significance of other model parameters.

The best, median, and worse fitting results for total product distribution, expressed by MARR, are shown in Figure 43. The largest MARR values were obtained for the pseudo-component C_{21}^{+}. It should be noted that high MARR values are caused by errors in experimental data, and existence of the "hump' in paraffin production rates in C_{12}-C_{25} carbon number range.

Extended Model of Van der Laan and Beenackers

The original ORPDM of Van der Laan and Beenackers (1998, 1999) has been extended to account for formation of 2-olefins. The original model considers only the total olefin formation, whereas the extended model accounts separately for 1- and 2-olefins. Reaction network of hydrocarbon formation for this model is presented in Appendix G (Figure G.1). Elementary reactions for this model are shown in Table G.1, and they are the same as for the original ORPDM except that step HC6 (2-olefin formation) is added.

After reparametrizations the extended model contains eight parameters (one more than the original ORPDM) which are given by:

$$\kappa_1 = k_i \cdot \theta_{CH_2,s_1} \cdot \theta_{H,s_1},$$

$$\kappa_p = \frac{k_p \cdot \theta_{CH_2,s_1}}{k_{t,p} \cdot \theta_{H,s_1}},$$

$$\kappa_{t,p}^{(1)} = \frac{k_{t,p}^{(1)}}{k_{t,p}},$$

$$\kappa_{t,p}^{(2)} = \frac{k_{t,p}^{(2)}}{k_{t,p}}, \qquad (30)$$

$$\kappa_{t,2o} = \frac{k_{t,2o} \cdot \theta_{s_1}}{k_{t,p} \cdot \theta_{H,s_1}},$$

$$K_{1o}^{(2)} = \frac{k_{t,p}^{(1)}}{k_{t,p}^2} \cdot \frac{k_{t,1o} \cdot He_0 \cdot SV}{k_{r,1o}^{(2)} \cdot \theta_{H,s_1}^2 \cdot R_g \cdot T}$$

$$K_{1o} = \frac{1}{k_{t,p}} \cdot \frac{k_{t,1o} \cdot He_0 \cdot SV}{k_{r,1o} \cdot \theta_{H,s_1}^2 \cdot R_g \cdot T}$$

plus the solubility/physiosorption dependence of olefin surface concentration with carbon number (c parameter). Two of these parameters $\kappa_{t,p}^{(1)}$ and $\kappa_{t,p}^{(2)}$ depend on temperature only whereas the remaining ones depend on all reaction conditions.

Estimated values of model parameters are given in Table 16, and the corresponding t-values in Table 17. All parameters are positive, and the overall MARR values range from 22 to 36% (Table 16). Most of t-values are large (>10) implying that the parameters have a narrow 95% confidence interval.

Comparisons of predicted and experimental product distributions for n-paraffins, 1- and 2-olefins are shown in Figures 44 and 45 for four representative mass balances. In general, very good agreement is obtained for hydrocarbons up to about C_{15}. In some cases experimental data show large deviations from predicted values but these are largely caused by experimental errors. For hydrocarbons up to C_{20}, these deviations occur generally in two carbon number ranges C_4-C_{11} and C_{15}-C_{20}. Experimental errors in C_4-C_{11} carbon number range are caused by inaccuracies arising from combining three gas chromatographic analyses (Figure 2) for components in this

range: light hydrocarbons (C_1-C_5) from Carle analysis, other gases (Varian) up to C_{10}, and organic phase (C_5-C_{11}). Deviations in the second range (C_{15-20}) for 2-olefins, and in some cases for 1-olefins as well, are caused by difficulties in separation of olefins in this range.

In addition, even greater deviations between the predicted and experimental values were observed in some cases for heavier paraffins (C_{15}^+). These can be related to experimental difficulties in quantification of these components. The first and the most significant difficulty is caused by wax withdrawal from the reactor through a filter element. The amount of wax withdrawn from the reactor is subject to errors. The second difficulty is related to errors in analysis of wax due to incomplete solubilization of the wax in carbon disulfide and loss of separation for high molecular weight paraffins. Also, in some experiments (e.g. Figure 45b) higher reaction rates were observed for paraffins in C_{12-25} range, and lower rates for heavier paraffins C_{25}^+. The cause of this deviation has not been determined, but hydrocracking of heavier paraffins could account for this type of behavior.

Comparison of experimental and predicted values for total olefin to paraffin ratio and 2-olefin selectivity is shown in Figures 46 and 47. As can be seen the extended model captures the observed experimental trends quite accurately.

Some groups of products are of particular interest from commercial point of view, and it is important to compare the model predictions with experimental data for these groups of products. Products formed during FTS are divided into five groups: methane, light gases (C_{1-4}), gasoline (C_{5-12}), diesel oil (C_{13-20}) and wax (C_{21}^+). Comparisons are provided in Figures 48 and 49, and in Table 18. Very good agreement can be seen for methane, light gases, gasoline and diesel oil for which MARR values are smaller then 21% (Table 18). A large discrepancy is observed for wax only (MARR ~ 60%) which is related to experimental difficulties in accurate quantification of products in this range. It should be noted here that total amount of wax is relatively small in comparison to other products (less than 5% in total weight).

Plots of relative residuals, defined by Equation (28), as a function number for all three groups of hydrocarbons considered in the present model are shown in Figures 50 to 52. Large deviations can be seen for hydrocarbons in certain hydrocarbon ranges, as discussed above in conjunction with Figures 44 and 45. However, the relative residuals do not show definite trends with carbon number, which means that the applied kinetic model is appropriate to describe experimental data.

Conclusions

Three STSR tests of the Ruhrchemie LP 33/81 catalyst were conducted to collect data on catalyst activity and selectivity under 25 different sets of process conditions. These data were used to test validity of four kinetic models (Lox and Froment, 1993b; Yang et al., 2003; Van der Laan and Beenackers, 1998, 1999; and the extended kinetic model of Van der Laan and Beenackers). The main qualitative findings from experimental data are as follows.

Catalyst deactivation was moderate in Run SB-21903 (694 h on stream) but more severe in the other two STSR tests (terminated after approximately 340 h on stream). Deactivation did not have significant effect on hydrocarbon selectivity in Runs SB-21903 and SB-26203. However, lower methane and higher C_5^+ selectivity (C-atom basis) were obtained in Run SB-28603 at 340 h in comparison to results at 70 h on stream.

The extent of WGS reaction increased with the increase in conversion of the limiting reactant, which is consistent with the concept that the WGS is a consecutive reaction with respect to water that is formed in FTS reaction. An increase in the extent of WGS reaction with an increase in temperature, decrease in total pressure, or a decrease in H_2/CO feed ratio (i.e. decrease in CO partial pressure) is attributed to kinetic effects.

A decrease in 1-olefin content and an increase in 2-olefin and n-paraffin contents with an increase in conversion are consistent with the concept that 1-olefins participate in secondary reactions (e.g. 1-olefin hydrogenation, isomerization and readsorption), whereas 2-olefins and n-paraffins are formed in these reactions. Secondary hydrogenation and isomerization reactions increased with increase in partial pressure of hydrogen. Gas residence time had a pronounced effect on selectivity of ethylene and gaseous 1-olefins, but it was less pronounced for higher molecular weight (MW) olefins (C_{10}^+). The residence time of high MW hydrocarbons is much longer than that of gaseous hydrocarbons and is determined by the rate of liquid (wax) removal from the reactor.

Carbon number product distribution showed an increase in chain growth probability with an increase in chain length (i.e. MW). The total olefin to paraffin ratio decreased with an increase in chain length (for C_3^+ hydrocarbons), whereas ethylene to ethane ratio was low due to increased reactivity of ethylene relative to other low MW 1-olefins.

A method for calculation of VLE based on modified Peng-Robinson equation of state was successfully implemented. First, the binary interaction factors k_{ij} were estimated for

inorganic species (H_2, CO, CO_2 and H_2O) in high molecular weight hydrocarbons from an extensive set of experimental data from the literature, which cover the range of experimental conditions for FTS used in our study (220 – 260 °C, 8 – 25 bar). An excellent fit of available experimental data for binary systems was obtained: H_2, CO or CO_2 in a hydrocarbon, whereas the experimental data for water in hydrocarbons are more sparse and scattered. Utilizing the modified PR EOS VLE calculations for FTS reaction in the STSR were performed, and compared to calculated vapor phase and liquid phase compositions with the corresponding experimental values. Excellent agreement was obtained for the vapor phase composition, whereas differences between the calculated and experimental liquid phase compositions were observed for some mass balances. Experimental values of the liquid phase composition are not measured accurately, due to difficulties in accurate quantification of the total amount of liquid withdrawn from the reactor and relative amounts of hydrocarbon wax and the start-up fluid (Durasyn). Overall, the calculations indicate that the vapor and liquid phase are in thermodynamic equilibrium during FTS in the STSR.

Three kinetic models from the literature have been adopted for analysis of experimental data from the STSR. Two of these kinetic models (Lox and Froment, 1993b; Yang et al., 2003) can predict a complete product distribution (inorganic species and hydrocarbons), whereas the kinetic model of Van der Laan and Beenackers (designated as ORPDM) can be used only to fit product distribution of total olefins and n-paraffins. The ORPDM of Van der Laan and Beenackers was extended to include 2-olefin formation. This extended model was used to fit n-paraffin, 1-olefin and 2-olefin product distributions, and is referred to as extended ORPDM.

The model reported as the best by Lox and Froment (designated as ALII in Lox and Froment, 1993b) for their operating conditions (high H_2/CO feed ratio of 3) has been selected for the initial estimation of kinetic parameters from the experimental data in the STSR. This model predicts the chain growth parameter (α) and olefin to paraffin ratio are independent of carbon number, whereas TAMU experimental data show that they vary with the carbon number

A simplified form of this model has only five parameters at isothermal conditions. Because of its relative simplicity, this model is well suited for initial studies where the main goal is to learn techniques for parameter estimation and statistical analysis of estimated values of model parameters. The same techniques and computer codes were used in the analysis of other kinetic models. The Levenberg-Marquardt (LM) method was employed for minimization of the

objective function and kinetic parameter estimation. With a judicious choice of weighting factors in the objective function, non-negative values for all five model parameters were obtained. Statistical analysis of estimated values of model parameters revealed that kinetic parameters for FTS (3 parameters), as well as their corresponding activation energies, are statistically significant, whereas two parameters for the WGS reaction were not statistically significant. Predicted reaction rates of inorganic and hydrocarbon species were not in good agreement with experimental data.

The kinetic model of Yang et al. (2003) has 24 parameters (20 parameters for hydrocarbon formation, and 4 parameters for the WGS reaction). Kinetic parameters for the WGS reaction and FTS were estimated first separately, and then simultaneously. To accomplish this, the LM method and a trust-region reflective Newton large-scale method were employed. A genetic algorithm was incorporated into the estimation of parameters for the FTS reaction to provide initial estimates of model parameters. These values were subsequently used as initial guesses for the LM and/or the LS methods to obtain improved values of model parameters.

All reaction rate constants and activation energies were found to be positive, but the 95% confidence intervals were large. The agreement between predicted and experimental reaction rates has been fair to good. Light hydrocarbons were predicted fairly accurately, whereas the model underpredicted values of higher molecular weight hydrocarbons. Also, the model does not predict that the chain growth parameter increases with increase in molecular weight.

The ORPDM of Van der Laan and Beenackers provided a very good fit of the experimental data for hydrocarbons up to about C_{20} (with the exception of experimental data that showed higher paraffin formation rates in C_{12}-C_{25} region, due to hydrocracking or other secondary reactions). Estimated values of all model parameters (true and pseudo-kinetic parameters) had high statistical significance after combining parameters related to olefin termination and readsorption into one (total of 7 model parameters). The model was found to capture the observed experimental trends of decreasing olefin to paraffin ratio and increasing α (chain growth length) with increase in chain length well.

The extended ORPDM was successfully employed to fit experimental data of three major groups of hydrocarbon products (n-paraffins, 1-olefins and 2-olefins). After reparametrization and combining parameters related to olefin termination and readsorption the total number of parameters for this model is eight (i.e. one more than in the original ORPDM). In general, all

three groups of products were fitted well, and the estimated parameters were all positive and the corresponding 95% confidence intervals were small.

Even though the extended ORPDM provides a very good fit of experimental data, it can not be used for prediction of product distributions for a given set of process conditions. This model has several pseudo-kinetic parameters whose values vary with process conditions. This model needs to be further developed to include predictions of inorganic species and hydrocarbon products in terms of true kinetic constants (temperature dependent constants).

The overall project goals have been achieved, but the two comprehensive kinetic models did not provide accurate predictions for hydrocarbon products over the entire range of carbon numbers. The predicted values for light hydrocarbons (up to about C_{10}) were found to be in good agreement with experimental data, however larger errors were obtained for high MW hydrocarbons (Yang et al. model). It is not clear whether this is due to deficiencies in the kinetic model itself, or due to experimental errors, and/or due to their combined effect.

As discussed previously the amount of wax produced during each mass balance is subject to relatively large experimental errors. Also, the experimental rates for C_{12}-C_{25} hydrocarbons were often significantly higher than the model predictions, and this may have been caused by cracking of higher molecular weight hydrocarbons. The kinetic model of Yang et al. (2003) does not account for these types of reactions. Also, catalyst deactivation was observed in all three STSR tests, and this was not accounted for in the kinetic models employed in this study.

The existing kinetic model of Yang and co-workers, coupled with VLE calculations for slurry-phase operation, is not accurate enough for process economics studies and preliminary reactor design calculations. Further studies are recommended to develop improved kinetic models and to validate them with experimental data from the STSR and/or other types of reactors (e.g. spinning basket).

Acknowledgements

This work was supported by the U.S. Department of Energy (University Copal Research Program) under Grant No. DE-FG26-02NT41540. We are grateful to Mr. Mirko Stijepovic and Mrs. Alia Fakhr for their assistance with preparation of this report, and to Mr. Robert M. Kornosky of NETL (TPO for this project) for his interest and valuable comments.

References

Ahon, V.R., E F. Costa Jr., J.E.P. Monteagudo, C.E. Fontes, E.C. Biscaia Jr., P.L.C. Lage, *Chemical Engineering Science*, 60, 677 (2005)

Ambrose, D., *"Correlation and Estimation of Vapor-Liquid Critical Properties. I. Critical Temperatures of Organic Compounds"*, National Physical Laboratory, Teddington, *NPL Rep. Chem*., 98 (1979)

Ambrose, D. and J. Walton, *Pure & Appl. Chem*., 61, 1395 (1989)

Ambrose, D. and C. Tsonopoulos, *J. Chem. Eng. Data*, 40, 531-546 (1995)

Breman, B. B., A. A. C. M. Beenackers, E. W. J. Rietjens and R. J. H., J. Stege, *Chem. Eng. Data*, 39, 647 (1994)

Breman, B. B. and A. A. Beenackers, *Ind. Eng. Chem. Res*., 35 (10), 3763 (1996)

Bukur D.B., G.F. Froment, L. Nowicki, M. Nyapathi and X. Wang, *"Kinetics of Slurry Phase Fischer-Tropsch Synthesis"*, Second Annual Technical Progress Report for DOE, Contract No. DE-FG26-02NT41540, Texas A&M University, College Station, TX, January 2005.

Bukur D.B., G.F. Froment and T. Olewski, *"Kinetics of Slurry Phase Fischer-Tropsch Synthesis"*, Third Annual Technical Progress Report for DOE, Contract No. DE-FG26-02NT41540, Texas A&M University, College Station, TX, January 2006.

Bukur, D.B., S.A. Patel and X. Lang, *Appl. Catal.*, 61, 329 (1990)

Bukur, D. B., L. Nowicki and X.Lang, , *Chem. Eng. Sci*., 49, 4615 (1994)

Bukur, D. B., L. Nowicki, R. K. Manne and X. Lang, *J. Catal*., 155, 366 (1995)

Bukur, D. B., L. Nowicki and S. A. Patel, *Can. J. Chem. Eng*., 74, 399 (1996)

Calderbank, P.H., F. Evans, R. Farley, G. Jepson and A. Poll, *Catalysis in Practice*, *IChemE*, 66 (1963)

Chao, K.C. and M. Lin, "*Synthesis gas solubility in Fischer-Tropsch slurry: Final report"*, Final Report for DOE Contract No. DE-AC22-84PC70024, DOE/PC/70024-T9, Purdue University, West Lafayette, IN, 1988

Coleman, T.F. and Y. Li, *Mathematical Programming,* Volume 67, Number 2, 189 (1994)

Coleman, T.F. and Y. Li, *SIAM Journal on Optimization,* Volume 6, 418 (1996)

Conn, A. R., N. I. M. Gould, and Ph. L. Toint, *Mathematics of Computation,* Volume 66, Number 217, 261 (1997)

Deckwer W.-D., R. Kokuun, E. Sanders and S. Ledakowicz, *Ind. Eng. Chem. Process Des. Dev.*, 25, 643 (1986)

Dictor R.A. and A.T. Bell, *J. Catal*., 97:121–36 (1986)

Donnelly, T. J. and Satterfield, C. N., *Appl. Catal.*, 52, 93 (1989).

Dry, M. E., T. Shingles, L. J. Boshoff and J. Oosthuizen, *J. Catal.*, 25, 99-104 (1972)

Edmister, W.C., *Pet. Refin*., 37, 173 (1958)

Englezos, P. and N. Kalogerakis, (2001) *"Applied parameter estimation for Chemical Engineers"*, New York: Mercel Dekker, Inc.
Feimer J.L., P.L. Silveston and RT. Huggins, *Ind. Eng. Chem. Prod. Res. Dev.*, 20, 609 (1981)
Froment G.F. and Bischoff K.B., (1990) *"Chemical Reactor Analysis And Design"*, Second Edition, New York: John Wiley & Sons, Inc.
Gao W., R.L. Robinson Jr. and K.A.M. Gasem, *J.Chem.Eng.Data*, 44, 130 (1999)
Gao W., R.L. Robinson, Jr. and K.A.M. Gasem, *Fluid Phase Equilibria*, 179, 207–216 (2001)
Gasem, K.A.M. and R.L. Robinson, Jr., *J.Chem.Eng.Data*, 30, 53 (1985)
Goldberg, David E., Genetic Algorithms in Search, Optimization & Machine Learning, Addison-Wesley, 1989.
Huff, G. A. and Satterfield, C. N., *J. Catal.*, 85, 370 (1984).
Iglesia, E.; Reyes, S. C.; Madon, R. J.and Soled, S. L., *J. Catal.*, 129, 238 (1991).
Iglesia, E.; Reyes, S. C.and Madon, R. J., *Adv. Catal.*, 39**,** 221 (1993).
Joback, K. G., *M.S. Thesis*, Massachusetts Institute of Technology, Cambridge, MA, June, 1984
Joback K.G. and R.C. Reid, *Chem. Eng. Comm*., 57, 233 (1987)
Klincewicz, K.M. and R.C. Reid, *AIChE*, 30 (1), 137 (1984)
Komaya, T. and Bell, A. T., *J. Catal.*, 146, 237 (1994).
Kuipers, E. W., Vinkenburg, I. H. and Osterbeck, H., *J. Catal*., 152, 137 (1995).
Lee, B.I. and M.G. Kesler, *AIChE*, 21 (3), 510-527 (1975)
Li, Y.W. and Froment, G.F., *"ARSOFTS: Advanced Reactor Simulation of Fischer-Tropsch Synthesis"*, Unpublished work, Laboratorium voor Petrochemische Techniek, Rijksuniversiteit, Gent, Belgium, May, 1996
Lox, E. S. and G. F. Froment, *Ind. Eng. Chem. Res.*, 32, 61 (1993a)
Lox, E. S. and G. F. Froment, *Ind. Eng. Chem. Res.*, 32, 71 (1993b)
Lydersen, A.L., *"Estimation of Critical Properties of Organic Compounds"*, *Univ. Wisconsin Coll. Eng., Eng. Exp. Stn. rept. 3*, Madison, WI, April, 1955
Madon, R. J. and Iglesia, E. *J. Catal.*, 139, 576.(1993).
Marano, J.J. and G.D. Holder, *Fluid Phase Equilibrium*, 138, 1-21 (1997)
Marquardt, D.W., *J. Soc. Industr. Appl. Math.*, 11, 431 (1963)
Miller, S.A., and A. Ekstrom, *J. Chem. Eng. Data*, 35, 125 (1990)
Nettelhoff, H., R. Kokuun, S. Ledakowicz and W.D. Decker, *Ger. Chem. Eng.*, 8, 177 (1985)
Nikitin E.D., P.A. Pavlov and A.P. Popov, *Fluid Phase Equilib.*, 141, 155 (1997)
Novak, S., Madon, R. J. and Suhl, H., *J. Catal*., 77, 141 (1982)
Novak, S., Madon, R. J. and Suhl, H., *J. Chem. Phys.*, 74, 6083 (1981)
Park, J., and R.L. Robinson, Jr. and K.A.M. Gasem, *J.Chem.Eng.Data*, 40, 241 (1995)
Passut, C.A. and R.P. Danner, *Ind. Eng. Chem. Process Des. Develop.*, 12 (3) (1973)
Peng, D. Y. and D.B. Robinson, *Ind. Eng. Chem. Fundam.*, 15 (1), 59 (1976)
Peter, S. and M. Weinert, Z. Phys. Chem., (Neue Folge) 5, 114 (1955)
Poling, B.E., J.M. Prausnitz and J.P. O'Connell, (2001) *"The Properties of Gases and Liquids*", Fifth Edition, New York: McGraw-Hill
Reid, R.C., J.M. Prausnitz and T.K. Sherwood, (1977) *"The properties of gases and liquids*", Third Edition, New York: McGraw-Hill
Schulz, H.; Rosch, S.and Gokcebay, H. Selectivity of the Fischer-Tropsch CO-hydrogenation, in Coal: Phoenix of '80s, Proc. 64th CIC. Coal Symp. Vol. 2, pp. 486-493, Ottawa (1982)
Schulz, H., Beck, K. and Erich, E., *Fuel Proc. Technol.*, 18, 293 (1988).
Van der Laan, G. P. and A. A. C. M. Beenackers, *Stud. Surf. Sci. Catal.*, 119, 179 (1998)

Van der Laan, G. P. and A. A. C. M. Beenackers, *Ind. Eng. Chem. Res.*, 38, 1277 (1999)
Wang Y.-N., W.P. Ma, Y.J. Lua, J. Yang, Y.Y. Xu, H.W. Xiang, Y.W. Li, Y.L. Zhao and B.J. Zhang, *Fuel*, 82, 195-213 (2003)
Yang J., L. Ying, J. Chang, Y.N. Wang, L. Bai, Y.Y. Xu, H.W. Xiang, Y.W. Li and B. Zhong, *Ind. Eng. Chem. Res.*, 42, 21 (2003)
Zimmerman, W. H. and D. B. Bukur, *Can. J. Chem. Eng.*, 68, 292 (1990)
Zimmerman, W. H., *"Kinetic Modeling of the Fischer-Tropsch Synthesis"*, Ph.D. dissertation, Texas A&M University, College Station, TX, 1990
Zimmerman, W., D.B. Bukur and S. Ledakowicz, *Chem. Eng. Sci.*, 47, 2707 (1992)

Table 1. Process conditions for tests in the STSR

	MB#	TOS	T	P	H_2/CO	SV
		h	°C	bar	(-)	NL/g-Fe/h
SB-21903	I/1	71-78	260	15	0.67	4.0
	I/2	94-101	260	15	0.67	1.7
	I/3	119-126	260	15	0.67	9.2
	I/4	152-164	240	15	0.67	2.0
	I/5	193-215	240	15	0.67	1.0
	I/6	225-238	240	15	0.67	5.5
	I/7	263-270	260	15	0.67	4.0
	I/8	298-310	240	15	2	4.2
	I/10	364-368	240	15	2	10.8
	I/13	489-505	260	15	0.67	4.0
	I/14	600-606	260	22.5	0.67	6.1
	I/15	647-654	260	22.5	0.67	1.0
SB-26203	II/1	86-92	260	15	2	7.1
	II/2	118-122	260	15	2	10.1
	II/3	142-146	260	15	2	23.5
	II/4	175-191	240	15	2	5.8
	II/5	224-240	260	25	0.67	6.7
	II/6	264-268	260	25	0.67	17.1
	II/7	297-313	260	25	0.67	2.0
SB-28603	III/1	94-101	220	15	0.67	4.1
	III/2	128-143	220	15	0.67	0.5
	III/3	166-170	220	15	2	9.5
	III/4	192-198	220	15	2	0.6
	III/5	224-238	260	8	2	1.5
	III/6	262-268	260	8	2	9.0
	III/7	287-292	240	8	0.67	5.5
	III/8	313-318	240	8	0.67	0.7

Table 2. Solubility data for inorganic species in hydrocarbons

Authors	Solute	Solvent			T	P
		Name	CN	MW		
				g/mol	°C	bar
Chao and Lin, 1988	Hydrogen, Carbon Monoxide, Carbon Dioxide, Syngas	n-Eicosane	20	282	100 – 300	10 – 50
		n-Octacosane	28	394		
		n-Hexatriacontane	36	506		
		Mobil Wax	?	?		
		Sasol Wax	?	?		
Breman *et al*., 1994	Hydrogen,	n-Hexadecane, n-Octacosane	28	394	150 - 250	40 - 50
	Carbon Monoxide					30 - 38
	Carbon Dioxide					20 - 25
	Water					1.5 - 2.5
Peter and Weinert, 1955	Hydrogen*, Carbon Monoxide, Carbon Dioxide, Water	Wax 250	~18	250	106 - 300	1 – 100
		Wax 345	~24.5	345		
Gasem and Robinson, 1985; Park *et al*., 1995; Gao *et al*., 1999	Hydrogen, Carbon Dioxide	n-Decane	10	142	100, 150	10 - 50
		n-Eicosane	20	282		
		n-Octacosane	28	394		
		n-Hexatriacontane	36	506		
	Carbon Monoxide	n-Dodecane	12	170		
	Carbon Dioxide	n-Tetratetracontane	44	619		
Calderbank *et al*., 1963	Hydrogen	Krupp Wax			107 - 300	1
Nettelhoff *et al*., 1985	Hydrogen, Carbon Monoxide	Vestowax	28	394	200 – 240	4 - 12
Miller and Ekstrom, 1990	Hydrogen, Carbon Monoxide	n-Octacosane,	28	394	~250	?
		Gulf,	?	?		
		FT-heavy,	?	?		
		Mobil FT	?	?		

? – No information provided by authors.

Table 3. Estimated values of binary interaction coefficients k_{ij} in Peng-Robinson EOS

Solvent		**Solute**			
CN	**Name**	**Hydrogen**	**Carbon Monoxide**	**Carbon Dioxide**	**Water**
10	n-Decane	0.2852	-	-	-
16	n-Hexadecane	-	-	-	0.3008
20	n-Eicosane	0.3233	0.2108	0.0878	-
~25	wax 345 g/mol	-	-	-	0.2098
28	n-Octacosane	0.4071	0.1878	0.0477	0.0542
36	n-Hexatriacontane	1.0496	0.4976	0.0679	-

Table 4. Estimated values of kinetic parameters (ALII Model of Lox and Froment)

Parameter	**units**	**220°C**	**240°C**	**260°C**
(a) Weighting factors equal to 1				
$k_{CO,HC}$	mmol/kg/s/bar	0.277	1.46	4.02
$k_{t,p}$	mmol/kg/s/bar	0.151	0.0352	0.131
$k_{t,o}$	mmol/kg/s	-0.618	0.00644	-0.166
k_v'	mmol/kg/s/bar^1.5	8.04	0.817	25.2
K_v	bar^-0.5	23.6	0.7	9.35
(b) Weighting factors from Equation (23)				
$k_{CO,HC}$	mmol/kg/s/bar	0.0709	0.39	1.55
$k_{t,p}$	mmol/kg/s/bar	0.00463	0.016	0.0434
$k_{t,o}$	mmol/kg/s	0.0194	0.031	0.051
k_v'	mmol/kg/s/bar^1.5	0.194	0.53	9.08
K_v	bar^-0.5	1.31	0.533	7.05

Table 5. Confidence intervals for kinetic parameters (ALII Model of Lox and Froment)

T = 220 °C	***units***	***Parameter estimate***	***95%-confidence limit***	
			lower	***upper***
$k_{CO,HC}$	mmol/kg/s/bar	0.0709	0.0561	0.0856
$k_{t,p}$	mmol/kg/s/bar	0.00463	0.00365	0.00562
$k_{t,o}$	mmol/kg/s	0.0194	0.0143	0.0245
k_v'	mmol/kg/s/bar^1.5	0.194	-0.401	0.79
K_v	bar^-0.5	1.31	-4.34	6.97

T = 240 °C	***units***	***Parameter estimate***	***95%-confidence limit***	
			lower	***upper***
$k_{CO,HC}$	mmol/kg/s/bar	0.391	0.324	0.459
$k_{t,p}$	mmol/kg/s/bar	0.016	0.0138	0.0182
$k_{t,o}$	mmol/kg/s	0.0305	0.023	0.038
k_v'	mmol/kg/s/bar^1.5	0.531	-1.06	2.12
K_v	bar^-0.5	0.533	-4.2	5.27

T = 260 °C	***units***	***Parameter estimate***	***95%-confidence limit***	
			lower	***upper***
$k_{CO,HC}$	mmol/kg/s/bar	1.55	1.28	1.81
$k_{t,p}$	mmol/kg/s/bar	0.0434	0.0384	0.0484
$k_{t,o}$	mmol/kg/s	0.051	0.0286	0.0733
k_v'	mmol/kg/s/bar^1.5	9.08	-43.8	62
K_v	bar^-0.5	7.05	-20.1	34.2

Table 6. Activation energies and statistical parameters for the FTS and WGS reactions

		Standard Error	*t Stat*	*Lower 95%*	*Upper 95%*
$E_{\mathrm{CO,HC}}$	168.73	6.62	25.49	84.62	252.85
$E_{\mathrm{t,p}}$	122.41	4.89	25.05	60.33	184.50
$E_{\mathrm{t,o}}$	52.75	3.13	16.84	12.96	92.55
E_{v}	208.78	62.51	3.34	-585.46	1003.02

Table 7. Activation energies for the FTS and WGS reactions from the literature (in kJ/mol)

Author(s), Year	Reactor	Catalyst	Paraffin formation	Olefin formation	WGS	Overall FT
Yang *et al*., 2003	Fixed bed	Fe/Mn	97 – methane 111 – C_2^+	97	58	
Wang *et al*., 2003	Fixed bed	Fe/Cu/K	93 – methane 87 – C_2^+	111	45	
Lox and Froment, 1993	Fixed bed	Fe	94	132	28	
Zimmerman and Bukur, 1990	Slurry	Fe/Cu/K			132 – 137	86
Deckwer *et al*., 1986	Slurry	Fe/K			63 – 105	
Dictor and Bell, 1986	Slurry	Reduced and Unreduced Fe and Fe/K	80 – 90*	100 – 110*		105 (Fe/K), 109 (Fe)
Feimer *et al*., 1981	Fixed bed	$Fe/Cu/K_2O$	92 – CH_4 84 – C_2H_6 78 (C_2 – C_5 HC)		124	
Dry *et al*., 1972	Fixed bed differential	$Fe/K_2O/Al_2O_3/SiO_2$	70 (C_2 – C_5 HC **)			70

*as reported by Yang *et al*., 2003
**as reported by Feimer *et al*., 1981

Table 8. Kinetic parameters for WGS results obtained by the LM and LS methods (Yang et al. Model)

ID		units	initial guess	estimates	st. dev.	| t-value |	95% confidence interval low	high			
	$k_{v,0}$	mol g^{-1} s^{-1} $bar^{-1.5}$	0.1	22.86	393.7	0.05808	-791.5	837.2	**F-value**	**Corr. Coeff.**	**Iteration No.**
W04	E_v	kJ mol^{-1}	1	**61.15**	69.54	0.8793	-82.71	205	49.11	0.6377	255
	$K_{v,0}$	$bar^{-0.5}$	0.1	8.73E-08	1.80E-06	0.04847	-3.64E-06	3.81E-06	**MARR**	**SSQ**	**exitflag**
	ΔH_v	kJ mol^{-1}	1	**-80.87**	71.47	1.132	-228.7	66.97	20.72	1.52	1
	$k_{v,0}$	mol g^{-1} s^{-1} $bar^{-1.5}$	39800	39810	7586000	0.005248	-15650000	15730000	**F-value**	**Corr. Coeff.**	**Iteration No.**
W07	E_v	kJ mol^{-1}	90.7	**90.55**	844.5	0.1072	-1656	1838	59.17	0.9115	131
	$K_{v,0}$	$bar^{-0.5}$	0.0022	0.0001878	0.03676	0.005109	-0.07585	0.07623	**MARR**	**SSQ**	**exitflag**
	ΔH_v	kJ mol^{-1}	-39	**-49.9**	867.5	0.05752	-1844	1745	26.32	216.05	1
	$k_{v,0}$	mol g^{-1} s^{-1} $bar^{-1.5}$	39800	3.98E+04	1.15E+06	0.03473	-2.33E+06	2.41E+06	**F-value**	**Corr. Coeff.**	**Iteration No.**
W08	E_v	kJ mol^{-1}	90.7	**94.38**	127.2	0.7422	-168.7	357.4	32.2	0.6433	51
	$K_{v,0}$	$bar^{-0.5}$	0.0022	0.0002082	0.006362	0.03272	-0.01295	0.01337	**MARR**	**SSQ**	**exitflag**
	ΔH_v	kJ mol^{-1}	-39	**-46.21**	135	0.3424	-325.4	233	20.17	1.51	1

Table 9. Kinetic parameters for the WGS reaction obtained using the genetic algorithm followed by the LM or LS method

ID		units	initial guess	estimates	st. dev.	| t-value |	95% confidence interval low	high			
	$k_{v,0}$	mol g^{-1} s^{-1} $bar^{-1.5}$		2.6E+09					**F-value**	**Corr. Coeff.**	
W17	E_v	kJ mol^{-1}		144.5							**GA**
	$K_{v,0}$	$bar^{-0.5}$		5.38					**MARR**	**SSQ**	
	ΔH_v	kJ mol^{-1}		0.0276					19.92		
	$k_{v,0}$	mol g^{-1} s^{-1} $bar^{-1.5}$	2.6E+09	2.64E+09	4.91E+09	0.5366	-7.52E+09	1.28E+10	**F-value**	**Corr. Coeff.**	
W18	E_v	kJ mol^{-1}	144.5	**143.5**	23.22	6.183	**95.52**	**191.6**	33.02	0.6509	**LM**
	$K_{v,0}$	$bar^{-0.5}$	5.38	3.32E+01	8.89E+02	0.03731	-1805	1872	**MARR**	**SSQ**	
	ΔH_v	kJ mol^{-1}	0.0276	**6.876**	120.3	0.05715	-242	255.8	20.089	276.5	
	$k_{v,0}$	mol g^{-1} s^{-1} $bar^{-1.5}$	2.6E+09	2.64E+09	2.38E+08	11.06	2.14E+09	3.13E+09	**F-value**	**Corr. Coeff.**	
W19	E_v	kJ mol^{-1}	144.5	**143.5**	23.21	6.185	**95.52**	**191.5**	33.19	0.6525	**LS**
	$K_{v,0}$	$bar^{-0.5}$	5.38	3.11E+01	8.34E+02	0.03726	-1695	1757	**MARR**	**SSQ**	
	ΔH_v	kJ mol^{-1}	0.0276	**6.58**	121	0.05439	-243.7	256.8	20.06	275.7	
	$k_{v,0}$	mol g^{-1} s^{-1} $bar^{-1.5}$		7.9E+07					**F-value**	**Corr. Coeff.**	
W20	E_v	kJ mol^{-1}		128.6							**GA**
	$K_{v,0}$	$bar^{-0.5}$		0.36					**MARR**	**SSQ**	
	ΔH_v	kJ mol^{-1}		-12.45					19.81		
	$k_{v,0}$	mol g^{-1} s^{-1} $bar^{-1.5}$	7.9E+07	7.92E+07	9.67E+08	0.0819	-1.92E+09	2.08E+09	**F-value**	**Corr. Coeff.**	
W21	E_v	kJ mol^{-1}	128.6	**128.1**	54.48	2.351	**15.36**	**240.8**	32.75	0.6489	**LM**
	$K_{v,0}$	$bar^{-0.5}$	0.36	7.08E-01	2.12E+01	0.03336	-43.22	44.64	**MARR**	**SSQ**	
	ΔH_v	kJ mol^{-1}	-12.45	**-10.12**	130.3	0.07768	-279.6	259.4	20.05	277.8	

Table 10. Kinetic parameters of FTS reaction by the LS method (Yang et al. Model)

							95% confidence interval		
ID		**units**	**initial guess**	**estimates**	**st. dev.**	**| t-value |**	**low**	**high**	**Fitting stat.**
	$k_{5,0}$	mol g^{-1} s^{-1} bar^{-1}	1.23E+04	12300	22750	0.5409	-32340	56940	
Fr02	E_5	kJ mol^{-1}	93.73	**91.97**	7.965	11.55	**76.34**	**107.6**	**F-value**
	$k_{7m,0}$	mol g^{-1} s^{-1} bar^{-1}	2.01E+06	2010000	6305000	0.3188	-10360000	14380000	14.9
	E_{7m}	kJ mol^{-1}	88.83	**108.7**	13.52	8.038	**82.13**	**135.2**	**MARR**
	$k_{7,0}$	mol g^{-1} s^{-1} bar^{-1}	1.10E+06	1100000	3228000	0.3408	-5234000	7434000	65.14
	E_7	kJ mol^{-1}	115.9	**111.4**	12.76	8.737	**86.42**	**136.5**	**SSQ**
	$k_{8}^{+},_0$	mol g^{-1} s^{-1}	0.006231	0.08758	0.08836	0.9911	-0.08581	0.261	29.67
	E_8^+	kJ mol^{-1}	54.7	**54.22**	4.294	12.63	**45.8**	**62.65**	**Corr. Coeff.**
	$k_{8}^{-},_0$	mol g^{-1} s^{-1} bar^{-1}	7.16E-02	0.01459	0.06998	0.2085	-0.1227	0.1519	0.1491
	E_8^-	kJ mol^{-1}	37.98	**44.03**	20.63	2.134	**3.544**	**84.52**	
	$K_{1,0}$	bar^{-1}	2.59	0.1877	0.4341	0.4325	-0.664	1.04	**Note**
	ΔH_1	J mol^{-1}	8.00E-09	157.6	9801	0.01608	-19070	19390	first 9 parameters as well as adsorption constants ($K_{X,0}$) are from Yang 2003
	$K_{2,0}$	bar^{-1}	0.00167	2.22E-02	0.01684	1.319	-0.01083	0.05526	
	ΔH_2	J mol^{-1}	8.00E-09	165.6	6269	0.02642	-12140	12470	
	$K_{3,0}$	-	8.34E-02	1.69E+00	3.247	0.5204	-4.682	8.062	
	ΔH_3	J mol^{-1}	8.00E-09	10.9	10180	0.001071	-19960	19980	
	$K_{4,0}$	bar^{-1}	1.21	0.05296	0.2267	2.34E-01	-0.3919	0.4978	
	ΔH_4	J mol^{-1}	8.00E-09	155.3	17730	8.76E-03	-34630	34940	
	$K_{6,0}$	-	0.1	0.4757	2.051	2.32E-01	-3.549	4.501	
	ΔH_6	J mol^{-1}	8.00E-09	5.576	18020	3.09E-04	-35360	35370	

Table 11. Kinetic parameters of Van der Laan and Beenackers Model ($\kappa_{t,p}^{(1)}$, $\kappa_{t,p}^{(2)}$, $\kappa_{r,o}^{(2)}$ and c treated as constant at a given temperature)

No.	κ_1	κ_p	$\kappa_{t,p}^{(1)}$	$\kappa_{t,p}^{(2)}$	$\kappa_{t,o}$	$\kappa_{r,o}^{(2)}$	$\kappa_{r,o}$	c
Temperature	220	C						
1	0.5531	19.43			30.51		2.215	
2	0.2176	12.02	3.804	0.8671	15.78	3.378	1.015	0.2011
3	0.9924	7.299			9.815		0.9276	
4	0.3314	9.712			6.414		0.777	
				MARR				
				32				
Temperature	240	C						
5	0.7768	8.729			3.073		-0.1939	
6	0.6468	11.81			9.628		0.3722	
7	0.5077	9.594			-0.07769		-0.2594	
8	2.609	9.399	5.151	1.699	5.265	4.819	0.1566	0.2734
9	3.562	9.689			9.245		0.6549	
10	3.58	12.06			6.552		0.3536	
11	0.9152	61.21			26.82		0.8048	
12	0.1449	26.35			-0.465		-0.266	
				MARR				
				41.6				
Temperature	260	C						
13	2.687	22.1			255		21.2	
14	1.899	15.15			62.64		7.077	
15	3.939	25.73			376.4		29.56	
16	2.645	20.72			245.3		21.9	
17	2.599	20.88			223.6		19.17	
18	3.547	26.92			312.8		25.24	
19	1.484	15.69			11.7		1.184	
20	6.479	11.79	7.032	1.921	62.36	120.2	11.91	0.1883
21	8.048	13.53			86.7		13.75	
22	12.04	13.68			155.6		20.71	
23	3.698	23.81			314.3		23.15	
24	6.123	26.89			340.6		23.25	
25	1.716	21.38			181.8		14.32	
26	1.493	7.933			7.244		1.369	
27	3.237	11.52			171.1		19.04	
				MARR				
				21.5				

Table 12. Kinetic parameters of Van der Laan and Beenackers Model ($\kappa_{t,p}^{(1)}$, $\kappa_{t,p}^{(2)}$ and c treated as constant at a given temperature)

No.	κ_1	κ_p	$\kappa_{t,p}^{(1)}$	$\kappa_{t,p}^{(2)}$	$\kappa_{t,o}$	$\kappa_{r,o}^{(2)}$	$\kappa_{r,o}$	c
Temperature	220	C						
1	0.5666	19.81			129.1	17.47	10.26	
2	0.2228	12.23	3.861	0.8901	39.17	10.12	3.024	0.199
3	0.9814	7.325			6.846	2.113	0.5506	
4	0.3451	9.853			19.26	14.58	2.849	
				MARR				
				31.7				
Temperature	240	C						
5	0.9106	21			10.49	2.528	0.4768	
6	0.6581	11.79			39.36	25.96	2.899	
7	1.35	21.02			13.75	2.827	0.7281	
8	2.604	9.284	5.106	1.671	6.311	6.1	0.3143	0.2281
9	3.593	9.634			137.1	91.19	16.8	
10	3.591	11.91			13.02	11.05	1.23	
11	0.7475	45.96			7.27	0.6098	0.2728	
12	0.3304	33.18			33.94	9.369	1.808	
				MARR				
				24.7				
Temperature	260	C						
13	2.679	22.16			39.62	17.45	2.769	
14	1.888	15.12			19.02	33.53	1.768	
15	3.924	25.77			41.52	12.19	2.73	
16	2.629	20.69			32.44	14.73	2.407	
17	2.572	20.73			27.87	13.82	1.947	
18	3.299	24.68			10.27	3.078	0.5611	
19	1.493	15.58			7.056	11.9	0.5615	
20	6.49	11.83	7.013	1.912	19.81	36.61	3.247	0.2009
21	8.073	13.61			26.5	35.26	3.619	
22	12.22	13.9			214.2	163.1	25.89	
23	3.747	24.51			165.9	60.96	10.9	
24	5.835	24.75			14.77	4.422	0.6987	
25	1.66	20.49			16.02	9.465	0.926	
26	1.499	7.945			4.873	27.1	0.7514	
27	3.27	11.66			380.3	263.9	39.32	
				MARR				
				21.1				

Table 13. t-values of parameters obtained with $\kappa_{t,p}^{(1)}$, $\kappa_{t,p}^{(2)}$ and c as constant (Van der Laan and Beenackers Model)

No.	κ_1	κ_p	$\kappa_{t,p}^{(1)}$	$\kappa_{t,p}^{(2)}$	$\kappa_{t,o}$	$\kappa_{r,o}^{(2)}$	$\kappa_{r,o}$	c
Temperature	220	C						
1	19.5	11.6	15	6.15	0.084	0.080	0.079	3.83
2	7.53	5.28			0.20	0.18	0.17	
3	31	20			1.58	1.05	0.76	
4	11.4	10.3			0.26	0.24	0.22	
Temperature	220	C						
5	14.5	9.14	35.7	20.5	1.83	1.32	1.20	10.6
6	9.78	6.89			0.28	0.27	0.25	
7	21.2	13			1.72	1.31	1.17	
8	38.6	27.7			4.51	3.12	1.96	
9	52.1	35.2			0.13	0.13	0.12	
10	52.7	40.1			1.57	1.38	1.10	
11	10.3	4.54			1.84	0.81	1.20	
12	5.07	2.51			0.28	0.26	0.26	
Temperature	220	C						
13	18	11.4	50.9	25.8	0.63	0.60	0.57	17
14	12.4	9.68			0.66	0.56	0.57	
15	26.6	15.1			0.84	0.78	0.74	
16	17.6	11.5			0.69	0.65	0.62	
17	17.3	11.4			0.83	0.77	0.72	
18	23	13.8			2.64	1.97	1.83	
19	10.1	7.95			1.23	0.72	0.92	
20	41.9	34.2			0.83	0.79	0.73	
21	52.2	40.9			0.86	0.82	0.76	
22	78.3	54.5			0.14	0.14	0.14	
23	25.2	14.7			0.22	0.22	0.21	
24	40.2	23.5			3.45	2.75	2.22	
25	11.3	7.56			1.05	0.89	0.83	
26	9.79	7.45			0.73	0.35	0.55	
27	21.2	14.7			0.05	0.05	0.05	

Table 14. Improved values of kinetic parameters for Van der Laan and Beenackers Model

No.	MB#	κ_i	κ_p	$\kappa_{t,p}^{(1)}$	$\kappa_{t,p}^{(2)}$	$K_o^{(2)}$	K_o	c
Temperature 220°C								
1	28603-001	0.53	18.8	3.80	0.85	5.97	9.8	0.171
2	28603-002	0.22	11.9			3.03	9.8	
3	28603-003	0.98	7.2			1.98	6.3	
4	28603-004	0.34	9.7			1.07	5.0	
MARR for 220°C								
31.0								
Temperature 240°C								
5	21903-004	1.02	21.8	4.75	1.66	5.11	11.9	0.194
6	21903-005	0.68	11.5			2.22	10.0	
7	21903-006	1.50	21.2			6.16	11.3	
8	21903-008	2.78	9.3			1.33	8.4	
9	21903-010	3.70	9.5			2.38	6.4	
10	26203-004	3.72	11.7			1.76	6.9	
11	28603-007	0.89	51.9			8.98	13.5	
12	28603-008	0.34	31.7			5.36	12.6	
MARR for 240°C								
24.8								
Temperature 260°C								
13	21903-001	2.89	22.2	6.52	1.91	4.07	11.7	0.186
14	21903-002	1.94	15.0			0.93	8.3	
15	21903-003	4.32	25.9			6.05	12.4	
16	21903-007	2.84	20.8			3.90	10.9	
17	21903-013	2.77	20.9			3.53	11.3	
18	21903-014	3.83	27.0			5.02	12.0	
19	21903-015	1.61	16.3			0.91	8.0	
20	26203-001	6.65	11.7			1.03	5.0	
21	26203-002	8.33	13.5			1.42	6.1	
22	26203-003	12.75	13.7			2.43	7.3	
23	26203-005	4.01	23.9			4.91	13.2	
24	26203-006	6.64	27.0			5.41	14.2	
25	26203-007	1.81	21.4			2.85	12.2	
26	28603-005	1.54	7.9			0.23	4.2	
27	28603-006	3.46	11.7			2.68	8.7	
MARR for 260°C								
21.3								

Table 15. t-values of improved kinetic parameters (Van der Laan and Beenackers Model)

No.	MB #	κ_i	κ_p	$\kappa_{t,p}^{(1)}$	$\kappa_{t,p}^{(2)}$	$K_o^{(2)}$	K_o	c
Temperature 220°C								
1	28603-001	18.9	13.0	14.5	6.2	7.6	7.5	13
2	28603-002	8.0	5.4			2.6	4.1	
3	28603-003	27.0	20.3			10.4	10.9	
4	28603-004	13.3	10.6			1.9	5.8	
Temperature 240°C								
5	21903-004	16.3	10.0	35	20	4.6	8.8	35
6	21903-005	9.8	6.9			2.3	5.1	
7	21903-006	23.3	14.2			7.6	11.4	
8	21903-008	37.8	27.0			7.0	16.9	
9	21903-010	47.7	36.2			14.3	18.2	
10	26203-004	50.4	41.5			10.7	19.0	
11	28603-007	15.1	4.9			3.5	8.2	
12	28603-008	6.1	2.9			1.3	3.6	
Temperature 260°C								
13	21903-001	19.6	13.1	49	26	4.7	11.2	57
14	21903-002	12.8	10.5			1.2	7.8	
15	21903-003	29.3	17.7			8.3	15.7	
16	21903-007	19.2	13.2			4.7	11.0	
17	21903-013	18.7	13.0			4.2	10.8	
18	21903-014	26.8	16.0			6.5	14.9	
19	21903-015	10.9	8.9			0.9	6.9	
20	26203-001	43.3	35.8			5.1	19.3	
21	26203-002	53.1	43.4			7.8	23.6	
22	26203-003	72.2	57.6			17.9	29.1	
23	26203-005	26.7	17.2			7.1	14.6	
24	26203-006	42.9	26.6			11.7	21.5	
25	26203-007	12.2	8.6			2.3	7.4	
26	28603-005	9.8	7.4			0.4	4.0	
27	28603-006	21.6	15.1			5.4	10.1	

Table 16. Kinetic parameters of extended Van der Laan and Beenackers model

Temperature: 220°C

MB#	κ_1	κ_p	$\kappa_{t,p}^{(1)}$	$\kappa_{t,p}^{(2)}$	$\kappa_{t,2o}$	$K_{1o}^{(2)}$	K_{1o}	c
28603-001	0.531	17.9			0.208	6.31	12.8	0.212
28603-002	0.205	10.3	3.56	0.539	0.32	3	10.3	0.194
28603-004	0.298	7.43			0.217	1.09	5.5	0.215
				MARR				
				36				

Temperature: 240°C

Name	κ_1	κ_p	$\kappa_{t,p}^{(1)}$	$\kappa_{t,p}^{(2)}$	$\kappa_{t,2o}$	$K_{1o}^{(2)}$	K_{1o}	c
21903-004	1	24.8			0.443	5.65	12.1	0.23
21903-005	0.695	13.3			0.424	2.57	11.3	0.239
21903-006	1.5	26.1			0.391	7.38	14.5	0.259
21903-008	2.78	11.1	5.53	1.58	0.467	1.52	7	0.194
21903-010	3.91	12			0.258	3.07	10.9	0.311
26203-004	3.94	14.5			0.309	2.05	8.63	0.263
28603-007	0.854	49.1			0.491	8.91	11.9	0.226
28603-008	0.358	40.2			0.393	6.18	14.7	0.234
				MARR				
				32				

Temperature: 260°C

Name	κ_1	κ_p	$\kappa_{t,p}^{(1)}$	$\kappa_{t,p}^{(2)}$	$\kappa_{t,2o}$	$K_{1o}^{(2)}$	K_{1o}	c
21903-001	3.03	28.6			0.525	4.76	13	0.234
21903-002	2.12	17.9			0.668	1.03	6.97	0.219
21903-003	4.47	33.6			0.471	7.15	14.9	0.242
21903-007	2.97	26.8			0.525	4.63	12.2	0.24
21903-013	2.92	26.3			0.55	4.17	12.7	0.243
21903-014	3.94	33.8			0.484	5.73	11.8	0.221
21903-015	1.74	20.3			0.571	1.08	5.76	0.203
26203-001	7.73	17.1	7.84	1.99	0.296	1.22	6.5	0.272
26203-002	9.51	19.1			0.326	1.69	7.95	0.271
26203-003	14.1	19.6			0.321	3.05	10.2	0.261
26203-005	4.22	32.5			0.28	5.92	15.9	0.223
26203-006	6.71	33			0.303	5.91	13.3	0.195
26203-007	1.86	24.7			0.439	3	9.86	0.186
28603-005	1.71	10.8			0.44	0.306	2.45	0.171
28603-006	3.64	15.5			0.472	3.38	12	0.271
				MARR				
				22.5				

Table 17. t-values of estimates for extended kinetic model of Van der Laan and Beenackers

Temperature: 220°C

MB#	κ_1	κ_p	$\kappa_{t,p}^{(1)}$	$\kappa_{t,p}^{(2)}$	$\kappa_{t,2o}$	$K_{1o}^{(2)}$	K_{1o}	c
28603-001	20.4	10.9			7.35	8.26	7.49	14.6
28603-002	8.37	5.44	15.9	4.87	2.65	2.8	2.59	3.27
28603-004	11	8.2			5.89	2.2	3.6	5.51

Temperature: 240°C

MB#	κ_1	κ_p	$\kappa_{t,p}^{(1)}$	$\kappa_{t,p}^{(2)}$	$\kappa_{t,2o}$	$K_{1o}^{(2)}$	K_{1o}	c
21903-004	16.3	9.84			8.92	4.72	4.36	8.56
21903-005	10.9	7.48			3.91	2.45	2.54	3.54
21903-006	23.4	13			12.5	7.64	6.22	12.9
21903-008	37.7	23.4	35.1	17.8	17.3	7.54	9.47	11.1
21903-010	45.9	23.6			20.8	14.1	11.1	18
26203-004	42.9	25.2			29.9	10.7	13.3	22.5
28603-007	13.2	6.4			9.87	3.76	3.54	8.88
28603-008	5.94	2.87			3.4	1.34	1.67	3.99

Temperature: 260°C

MB#	κ_1	κ_p	$\kappa_{t,p}^{(1)}$	$\kappa_{t,p}^{(2)}$	$\kappa_{t,2o}$	$K_{1o}^{(2)}$	K_{1o}	c
21903-001	20.4	12.4			11.3	4.68	5.21	10.3
21903-002	14.1	11.8			9.12	1.17	2.87	4.57
21903-003	29.1	15.6			16	8.23	7.77	16.5
21903-007	19.9	12.6			11.3	4.63	4.86	9.47
21903-013	19.5	12.5			11.1	4.22	4.82	9.25
21903-014	26	14.6			15.8	6.52	6.84	14.5
21903-015	11.8	9.65			8.34	0.969	2.35	4.06
26203-001	39.9	25.4	49.6	23.6	27	4.62	8.12	14.7
26203-002	45.8	27.9			34.3	7.25	11.4	21.2
26203-003	60.1	32.4			41.6	17.7	19.4	35.1
26203-005	28	14.3			9.78	7.07	7.95	16
26203-006	41.8	21.6			16.8	11.6	12.8	24.5
26203-007	12.8	8.41			5.92	2.34	3.34	5.59
28603-005	11.3	9.09			5.81	0.418	1.35	1.61
28603-006	23.5	15.6			9.22	5.32	4.58	7.06

Table 18. MARR values for extended Van der Laan and Beenackers model

	MAAR
Methane	13.2
Light gases C_{1-4}	6.3
Gasoline C_{5-12}	10.9
Diesel oil C_{13-20}	20.7
Wax C_{20}^{+}	59.7

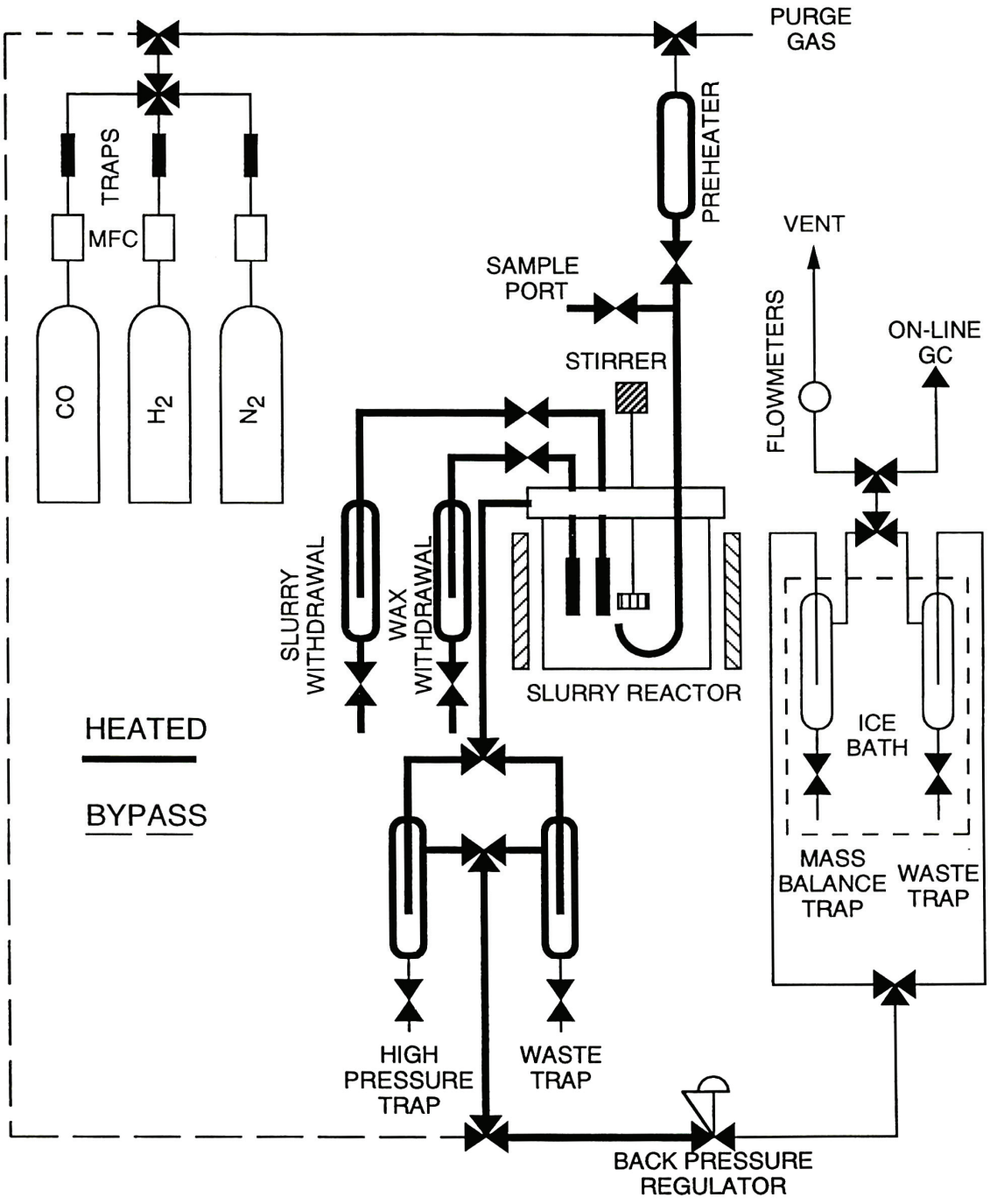

Figure 1. Schematic of stirred tank slurry reactor system.

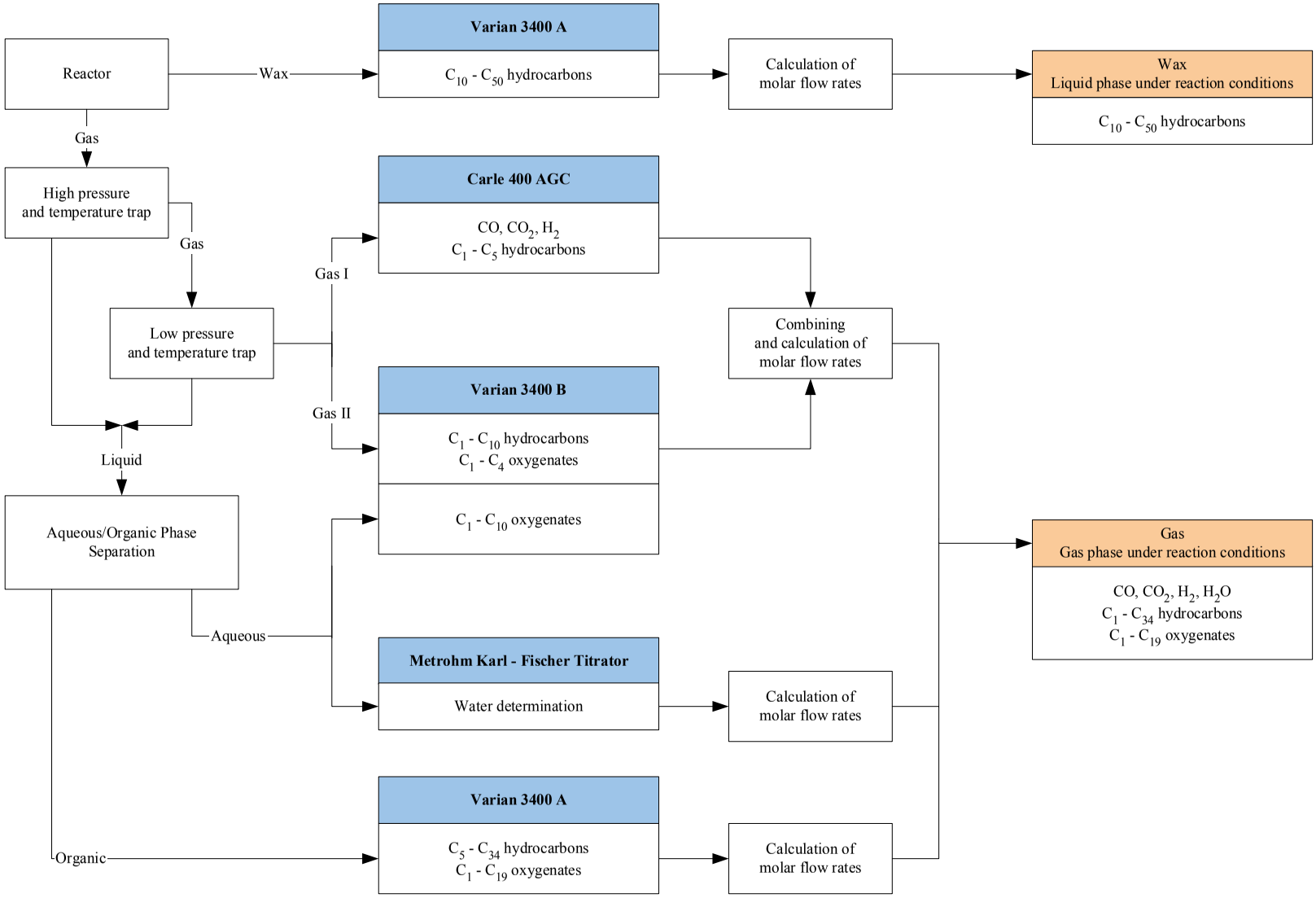

Figure 2. Product analysis schematic.

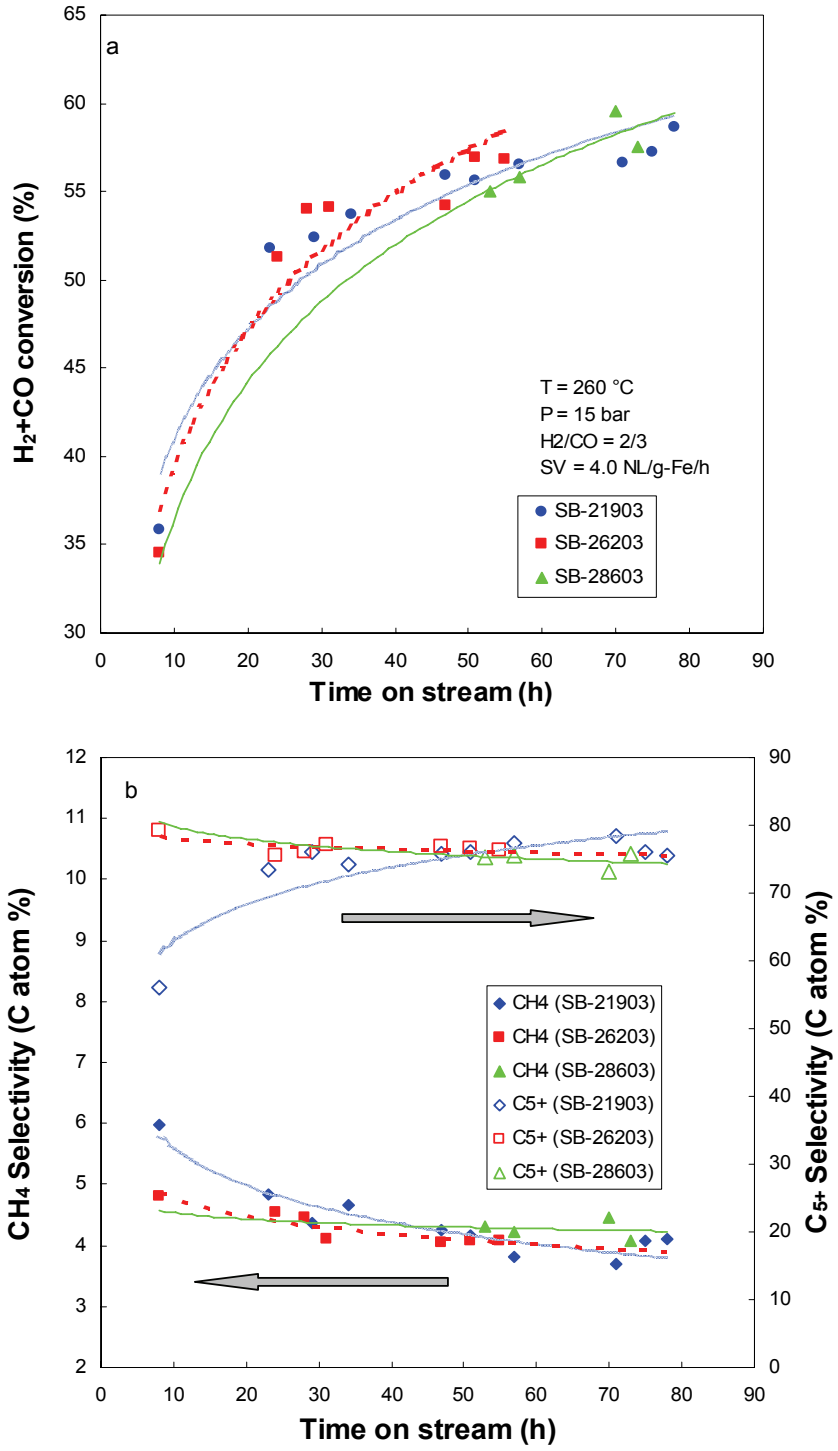

Figure 3. Effect of time at the baseline conditions (initial period). (a) Syngas conversion, (b) Methane and C_5^+ selectivity.

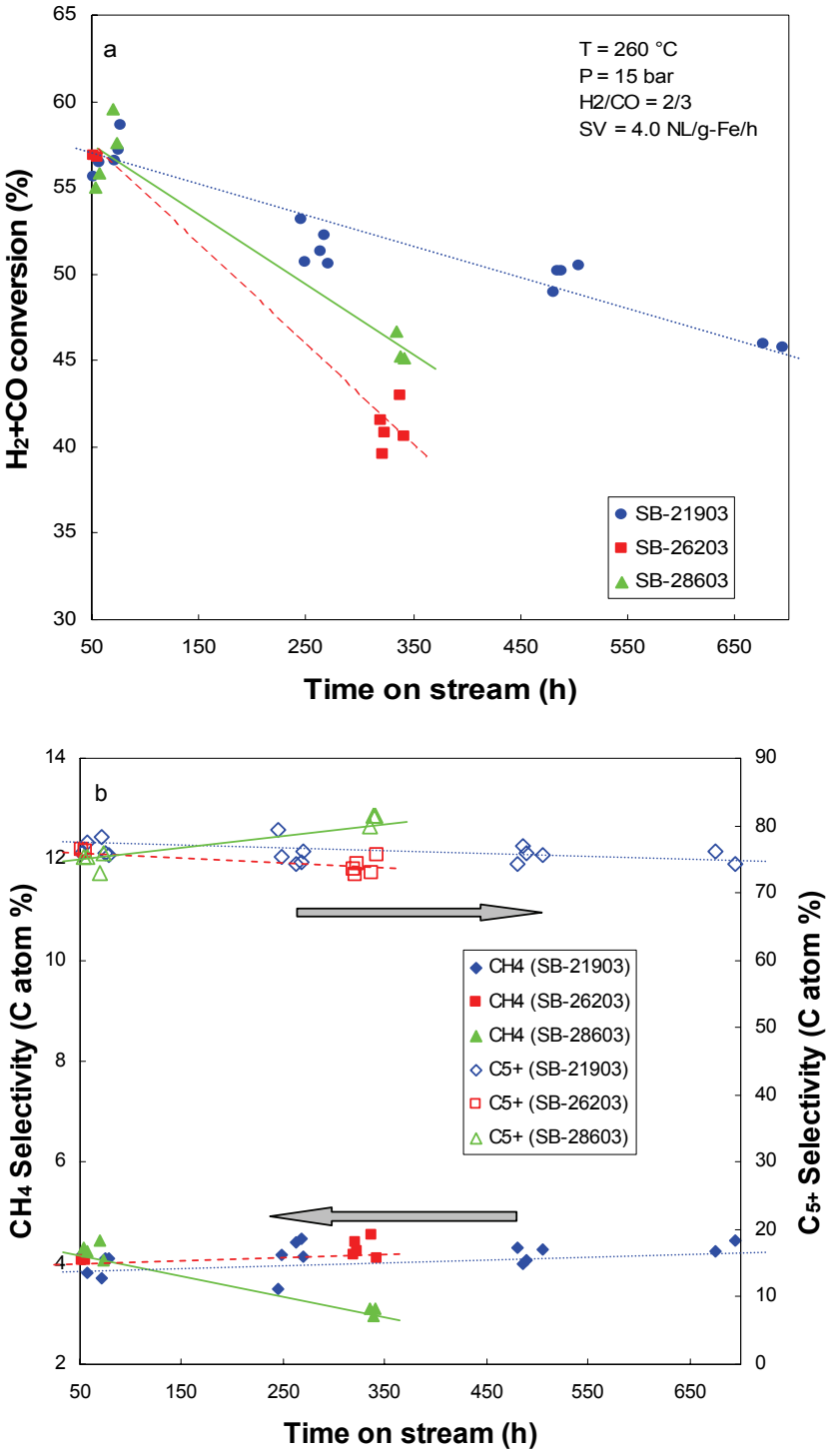

Figure 4. Effect of time on stream at the baseline conditions (a) Syngas conversion, (b) Methane and C_5^+ selectivity.

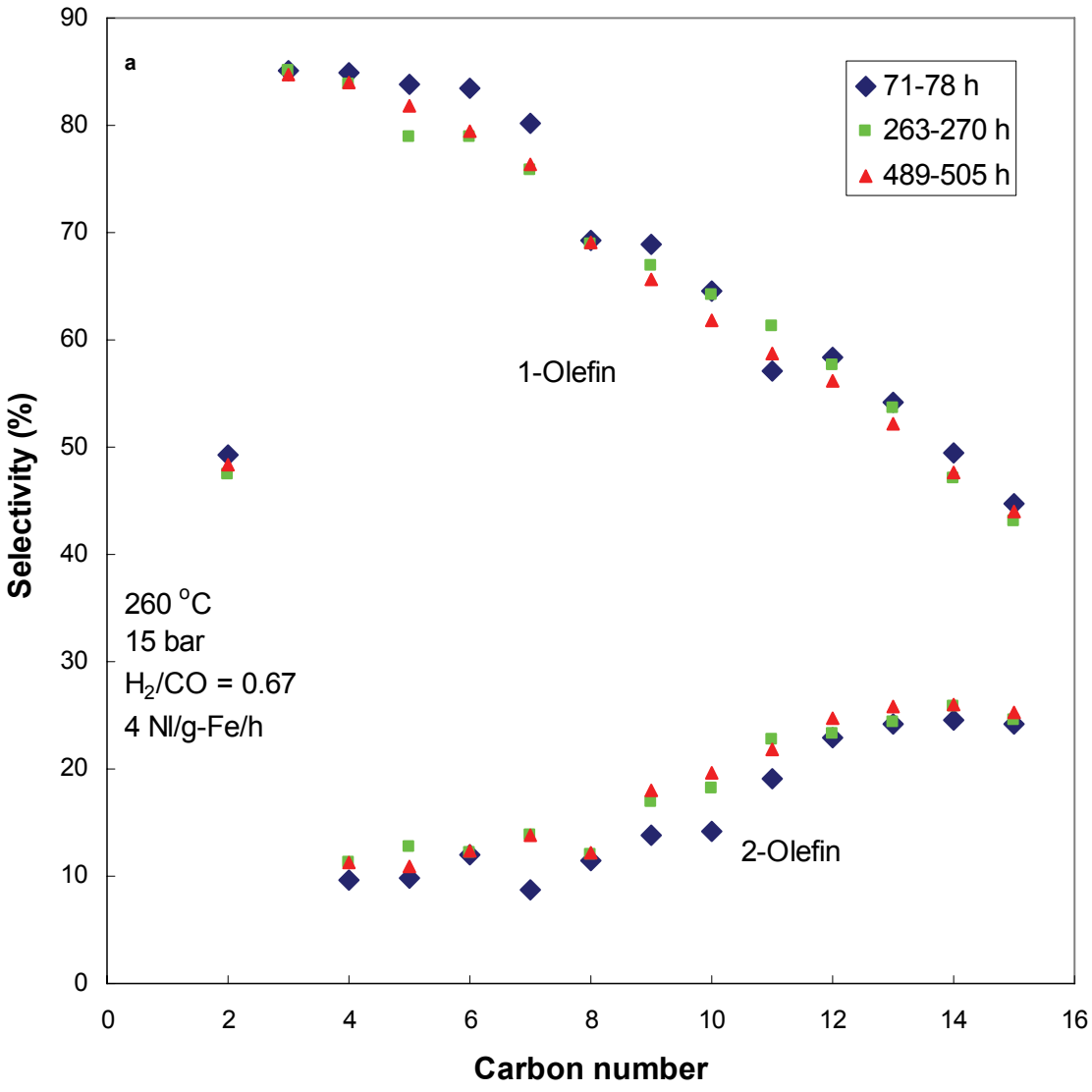

Figure 5. Effect of time-on-stream on olefin selectivities.

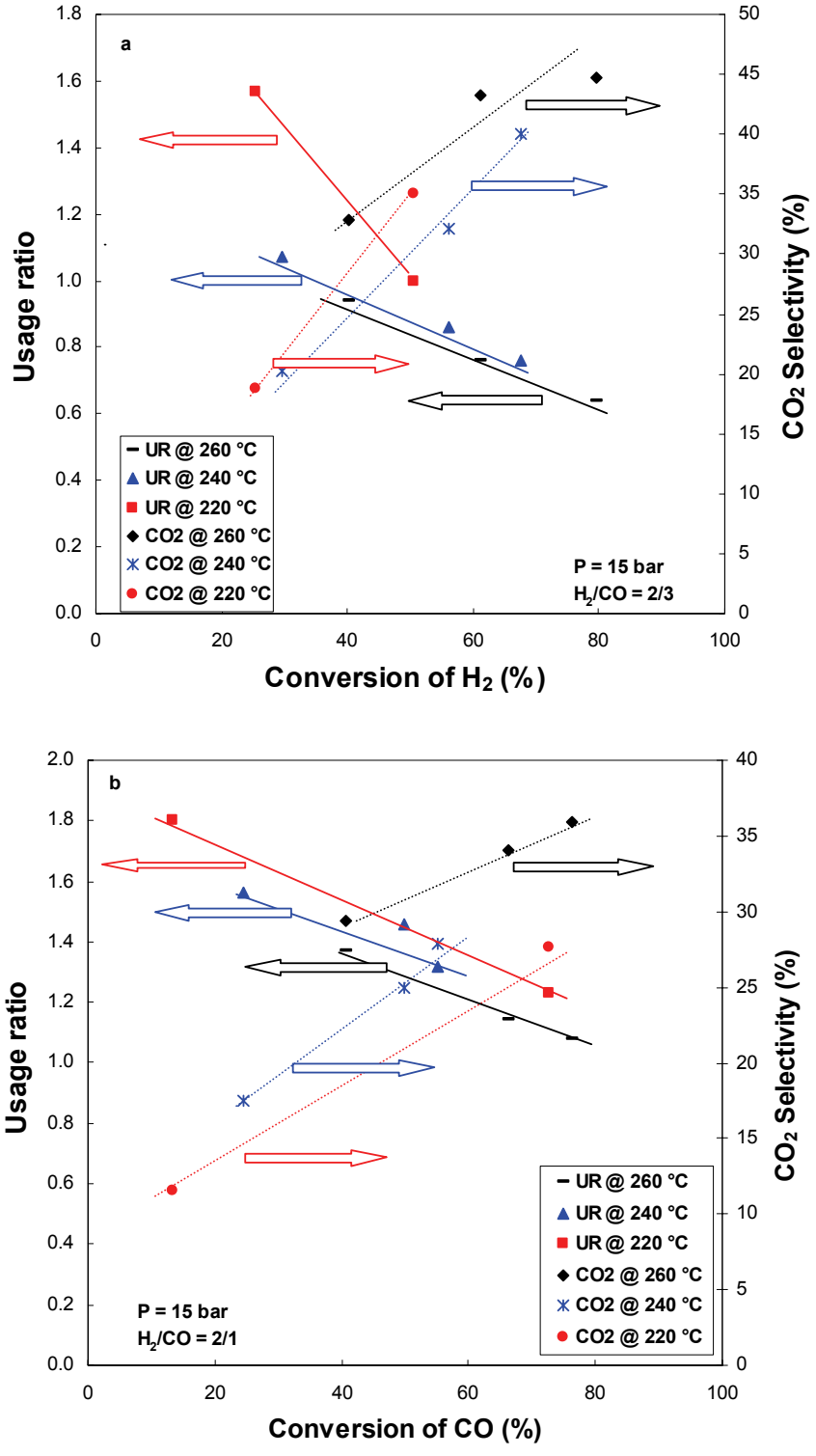

Figure 6. Effect of temperature on WGS reaction (15 bar) (a) feed $H_2/CO = 2/3$, (b) feed $H_2/CO = 2/1$.

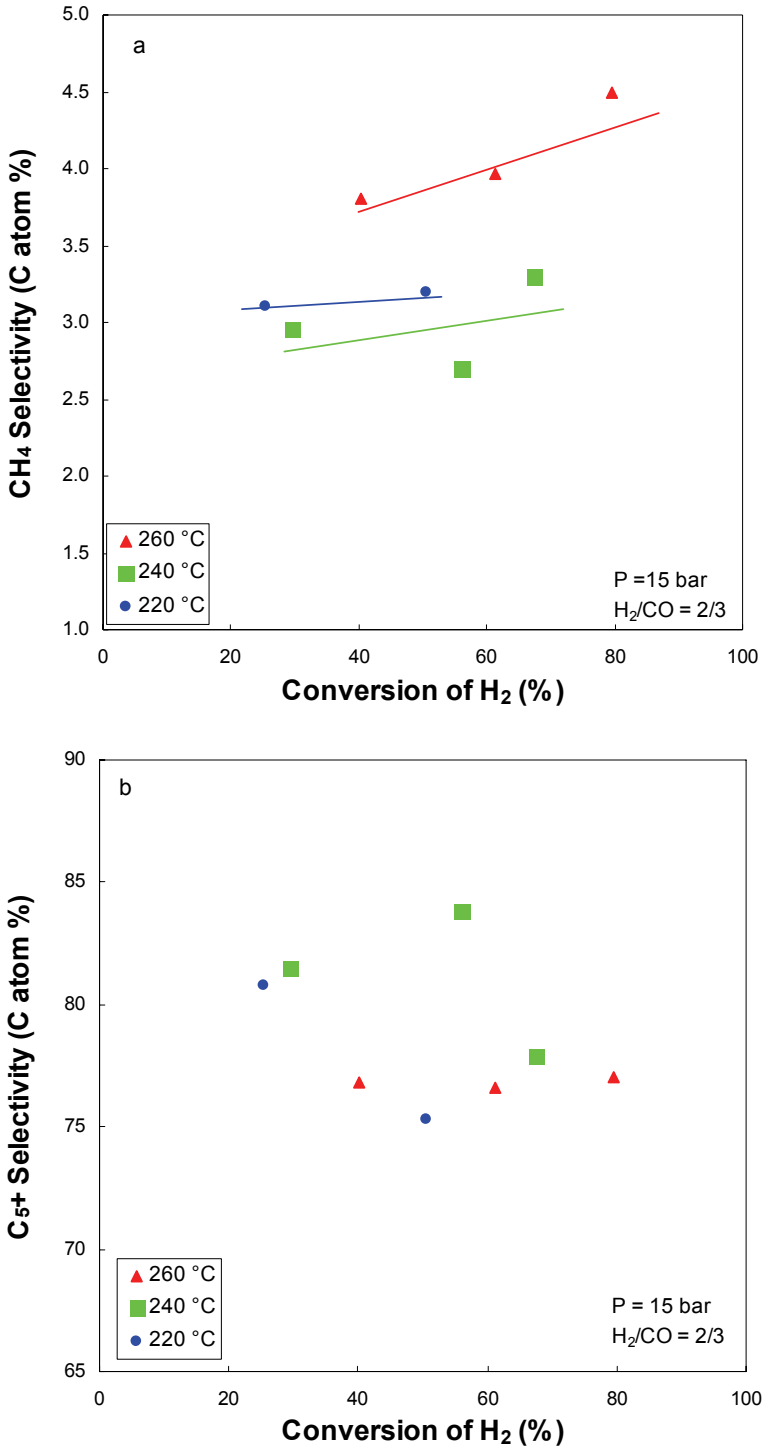

Figure 7. Effect of temperature on hydrocarbon selectivity (15 bar, $H_2/CO = 2/3$) (a) Methane selectivity, (b) C_5^+selectivity.

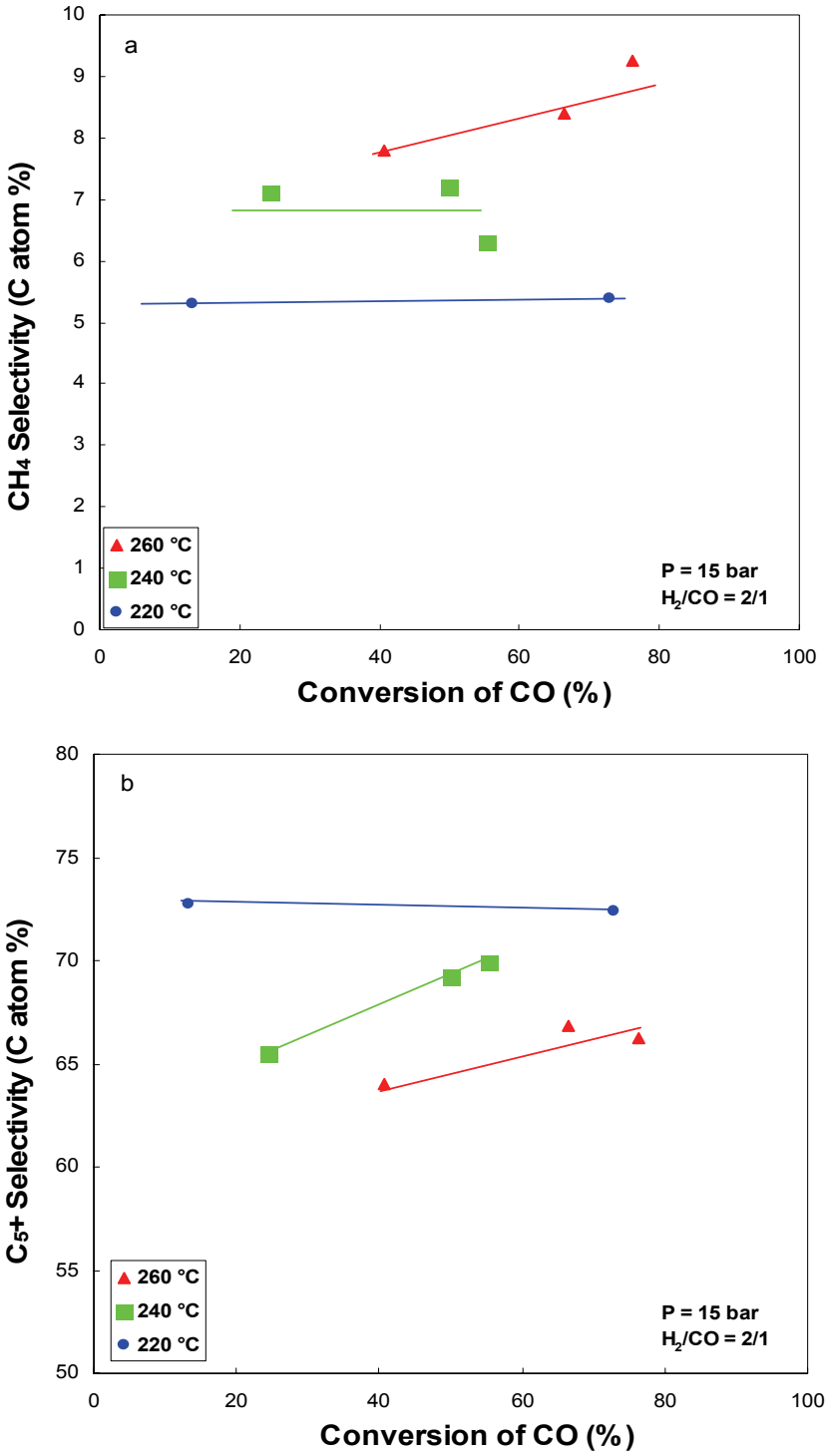

Figure 8. Effect of temperature on hydrocarbon selectivity (15 bar, $H_2/CO = 2/1$) Methane selectivity, (b) C_5^+selectivity.

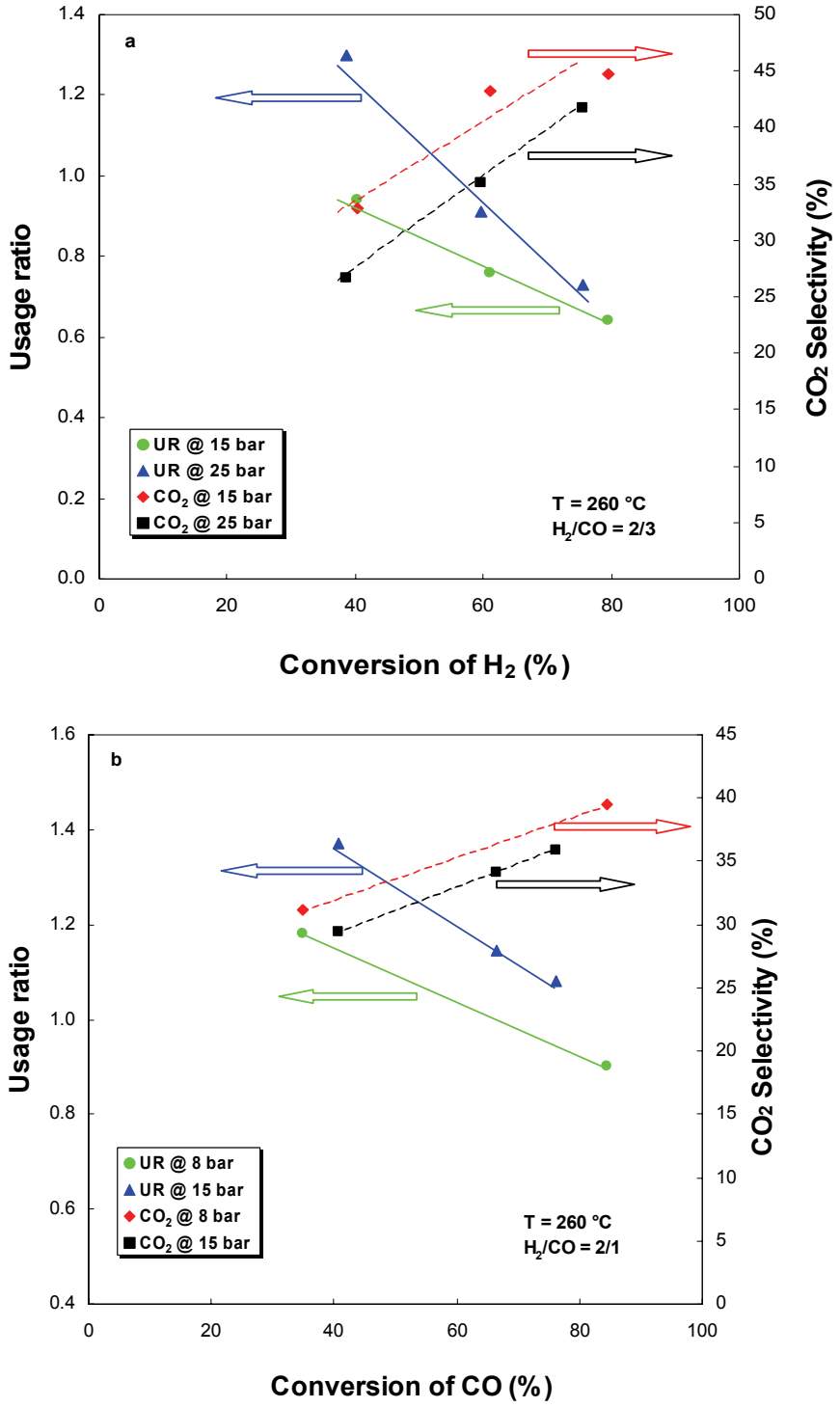

Figure 9. Effect of pressure on WGS reaction (260°C) a) feed H_2/CO = 2/3, (b) feed H_2/CO = 2/1.

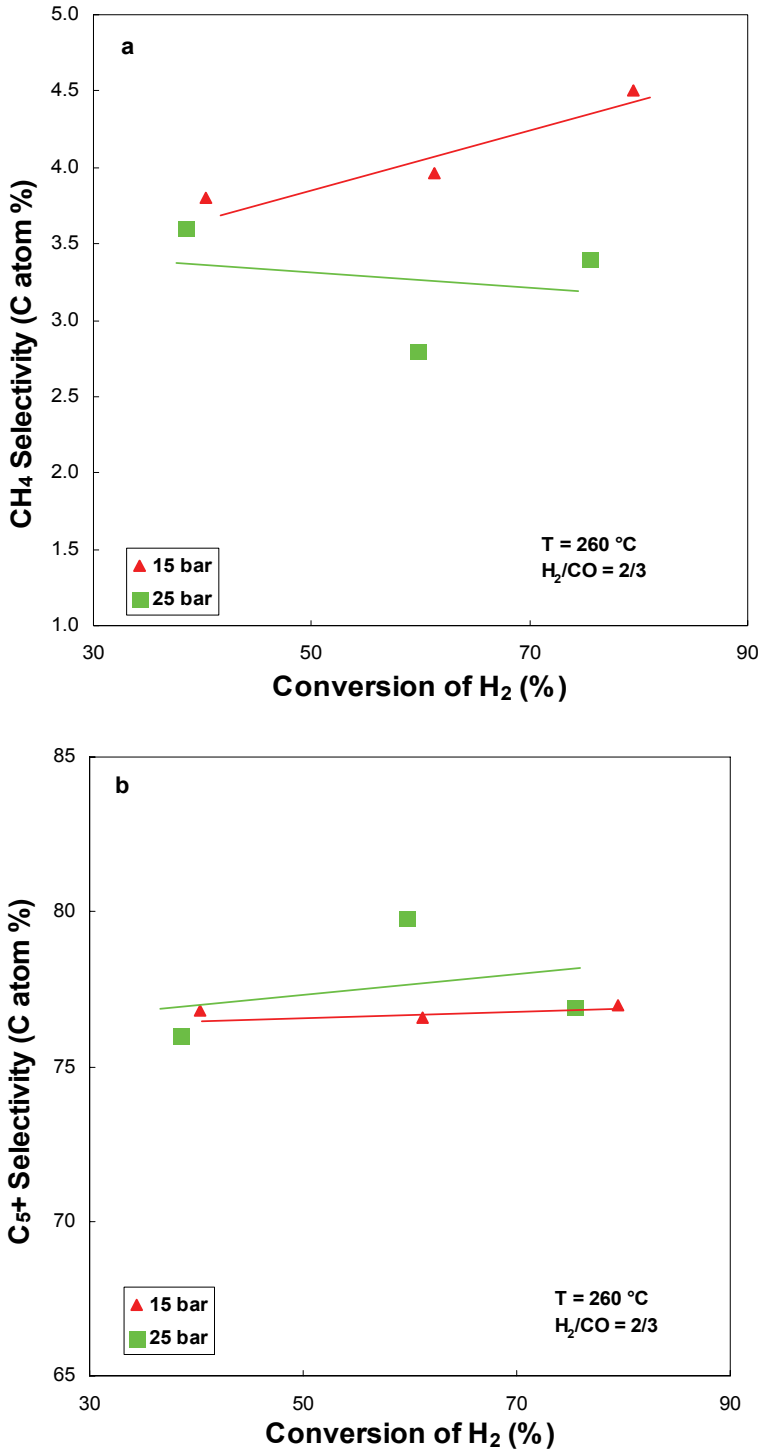

Figure 10. Effect of pressure on hydrocarbon selectivity (260°C, $H_2/CO = 2/3$) (a) Methane selectivity, (b) C_5^+ selectivity.

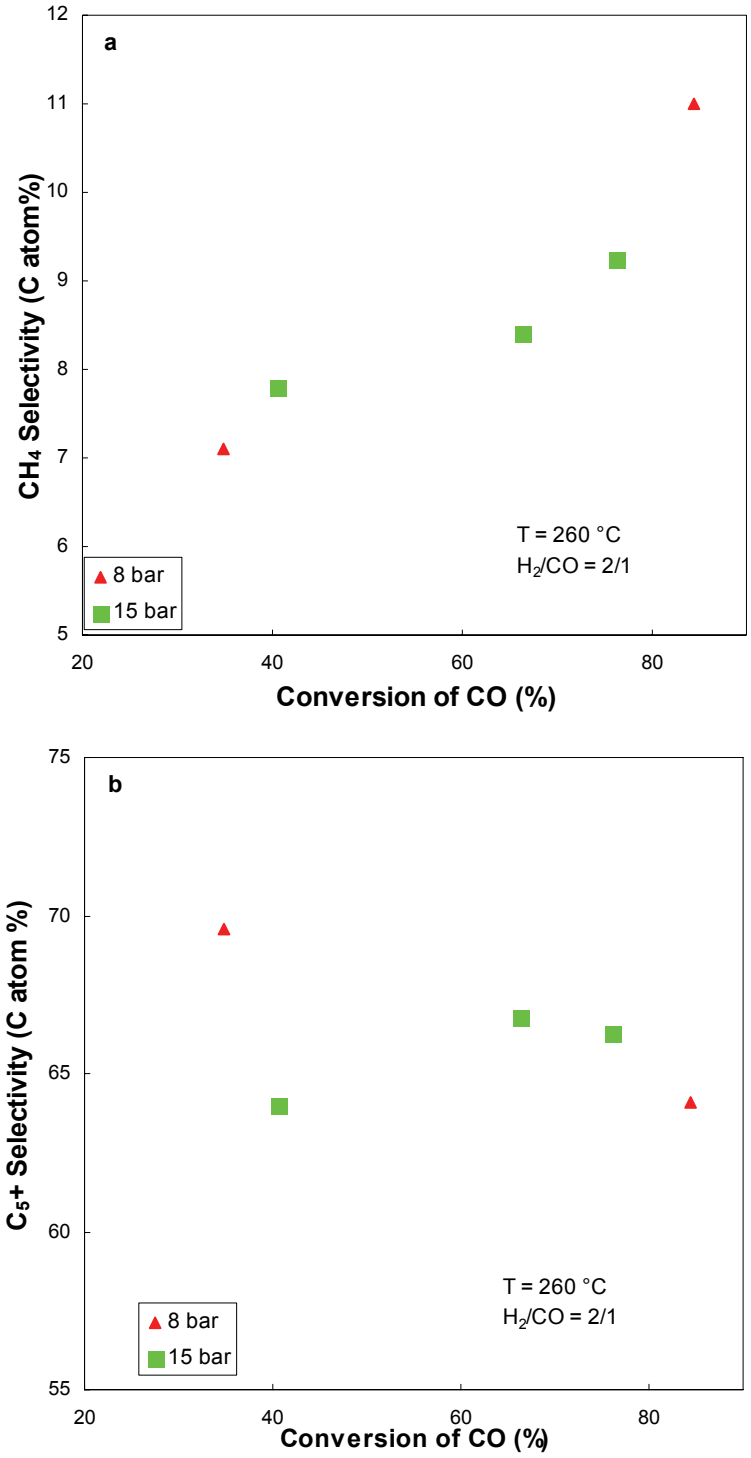

Figure 11. Effect of pressure on hydrocarbon selectivity (260°C, $H_2/CO = 2/1$) (a) Methane selectivity, (b) C_5^+ selectivity.

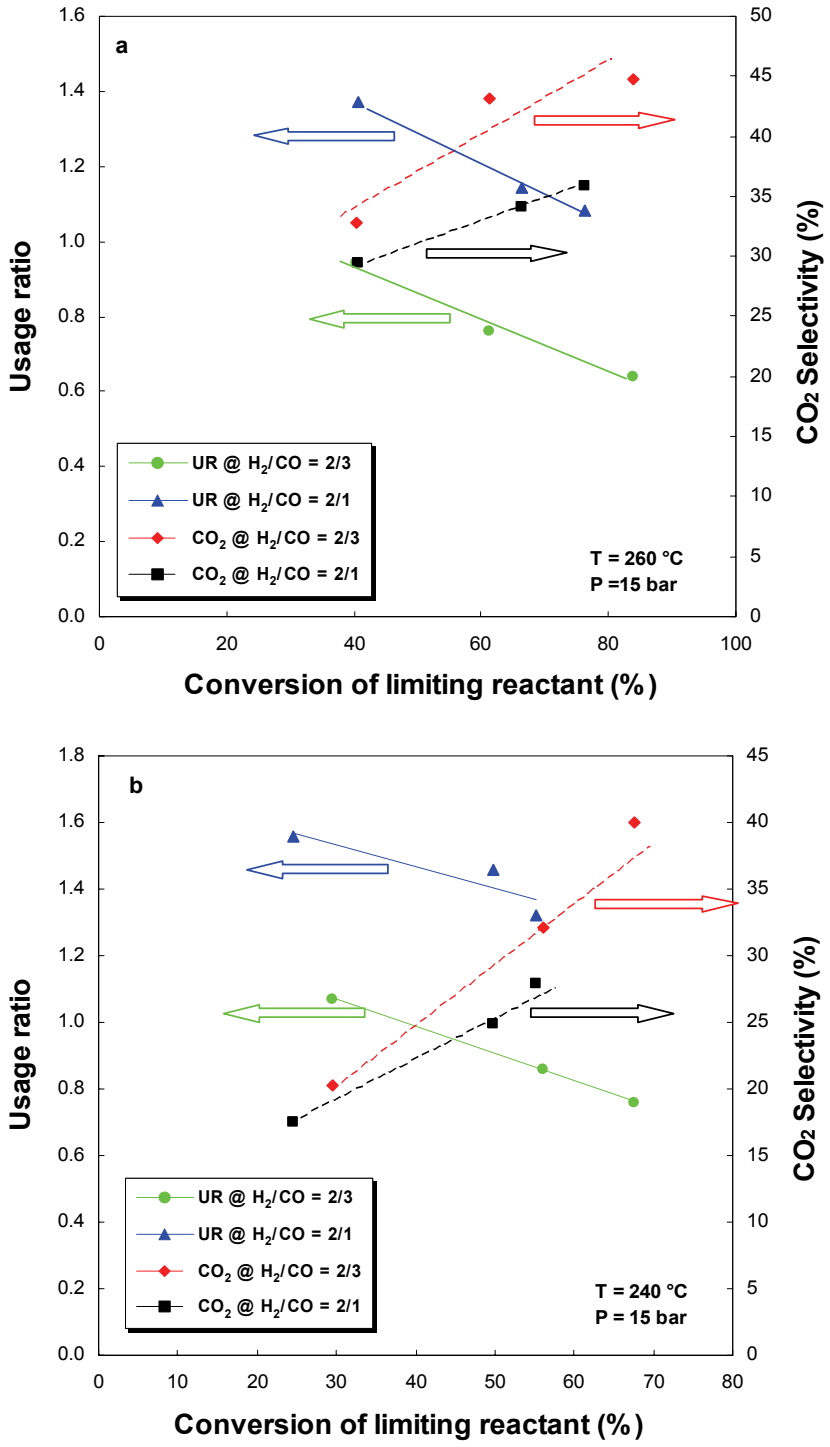

Figure 12. Effect of feed composition on WGS reaction (15 bar)
(a) 260°C, (b) 240°C

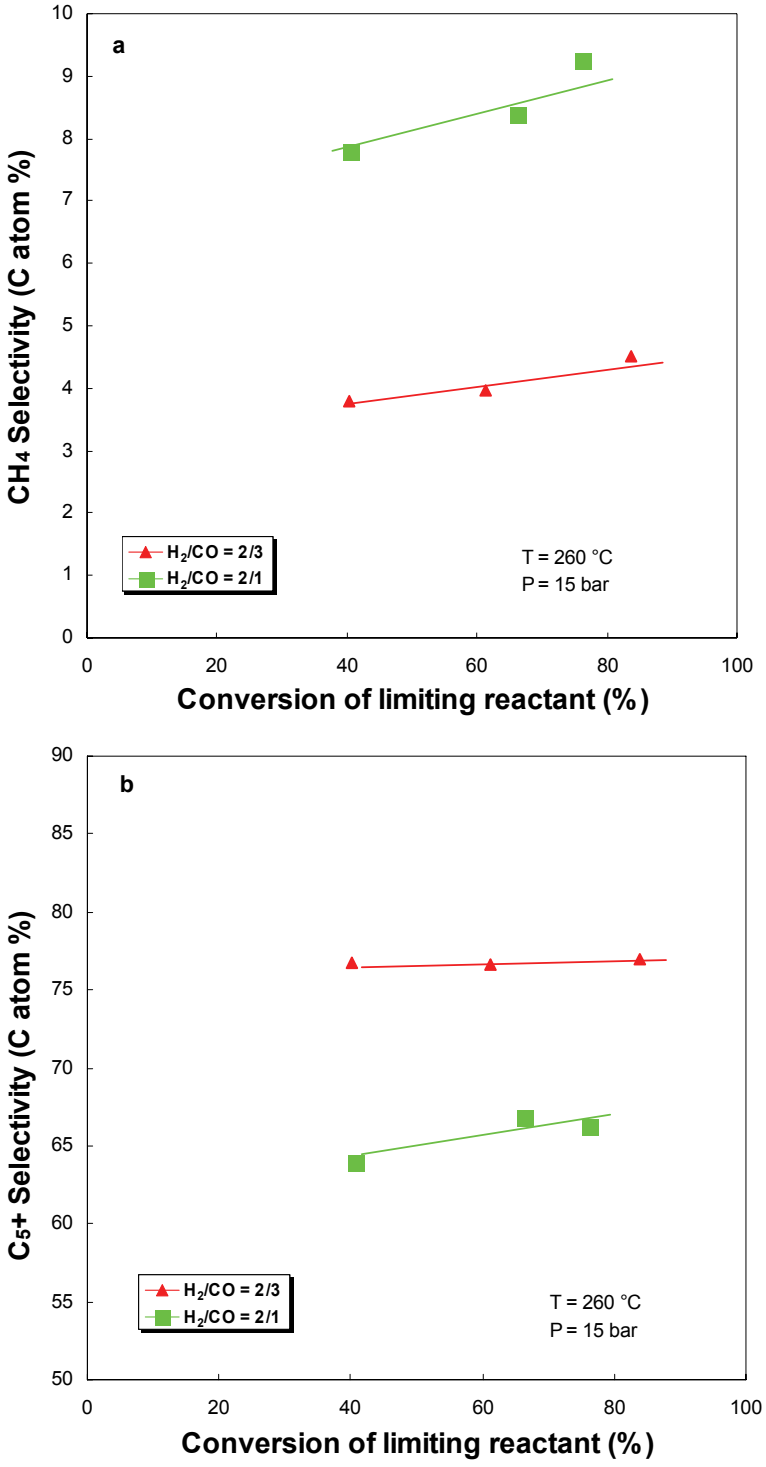

Figure 13. Effect of feed composition on hydrocarbon selectivity (260°C, 15 bar) (a) Methane selectivity, (b) C_5^+ selectivity.

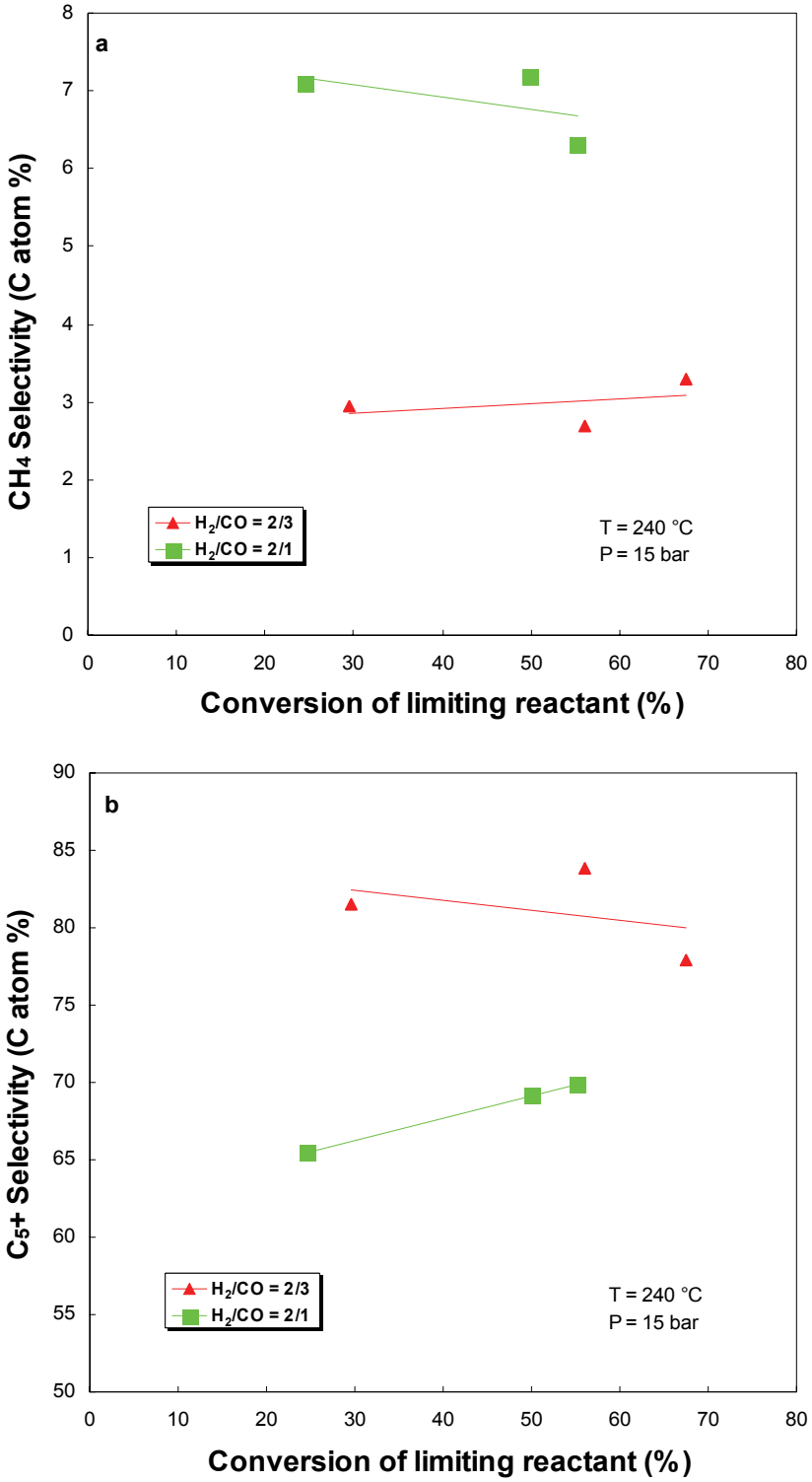

Figure 14. Effect of feed composition on hydrocarbon selectivity (240°C, 15 bar)(a) Methane selectivity, (b) C_5^+ selectivity.

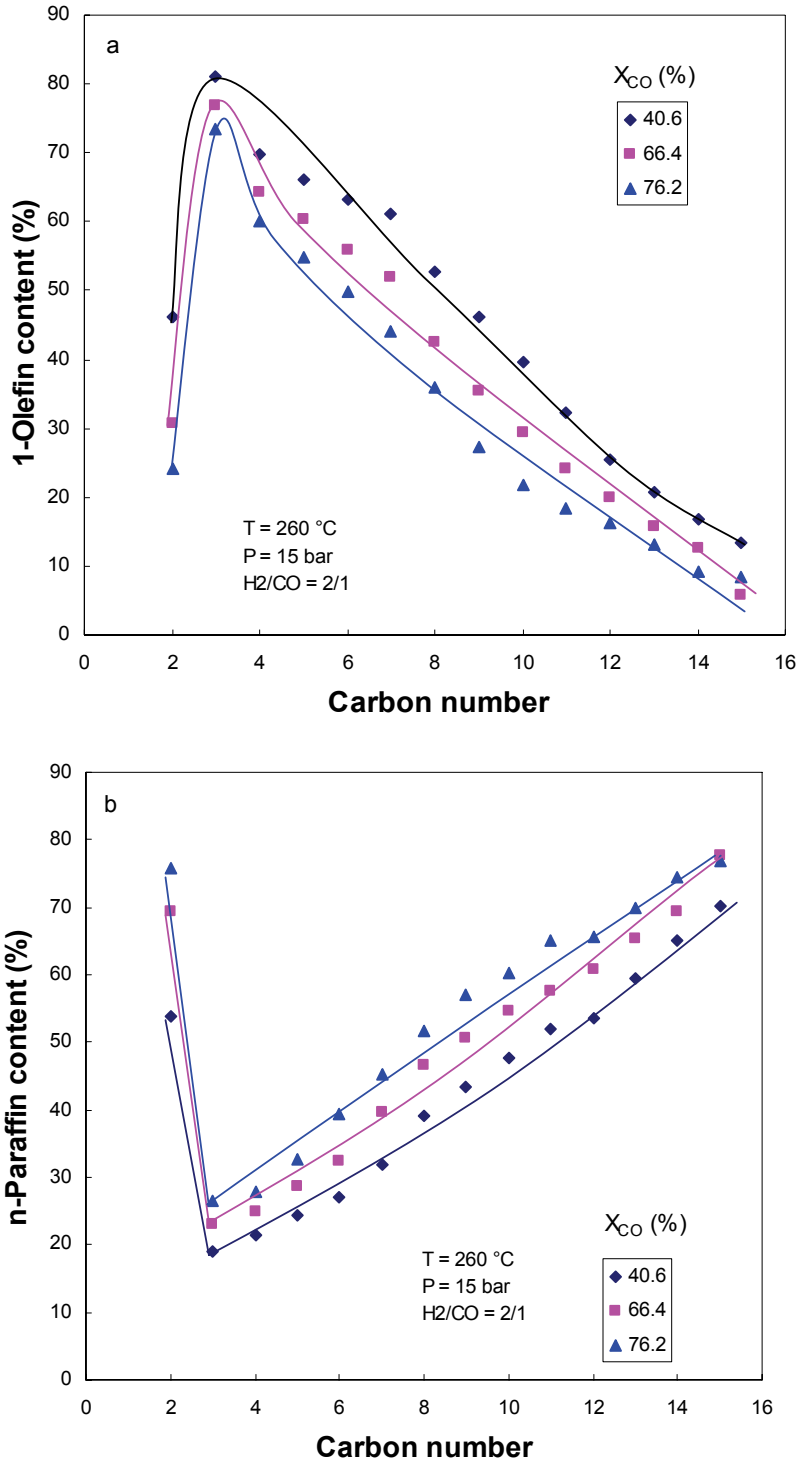

Figure 15. Effect of conversion (260°C, 15 bar, $H_2/CO = 2/1$) on (a) 1-olefin content and (b) n-paraffin content.

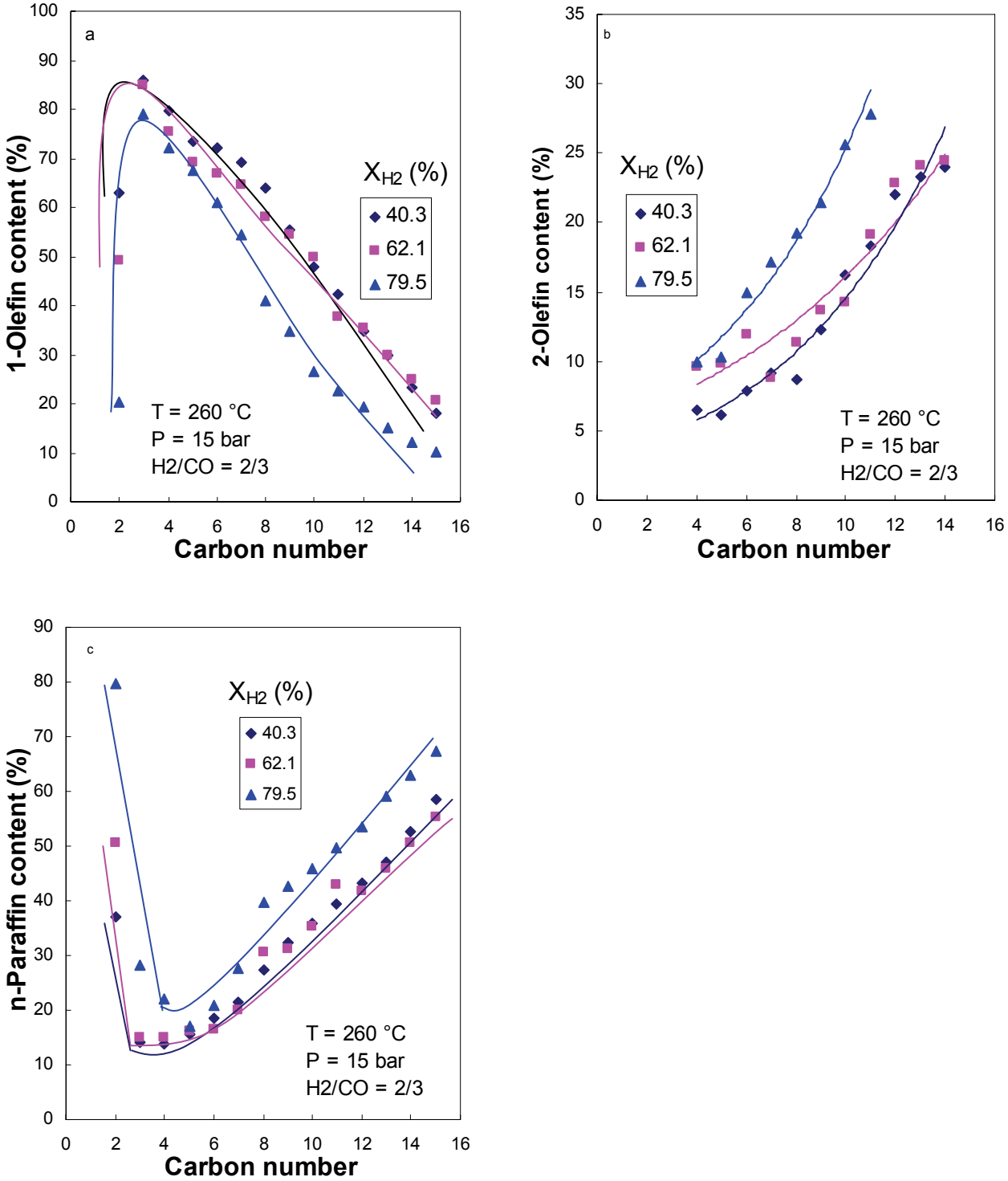

Figure 16. Effect of conversion (260°C, 15 bar, H_2/CO = 2/3) on (a) 1-olefin content, (b) 2-olefin content and (c) n-paraffin content.

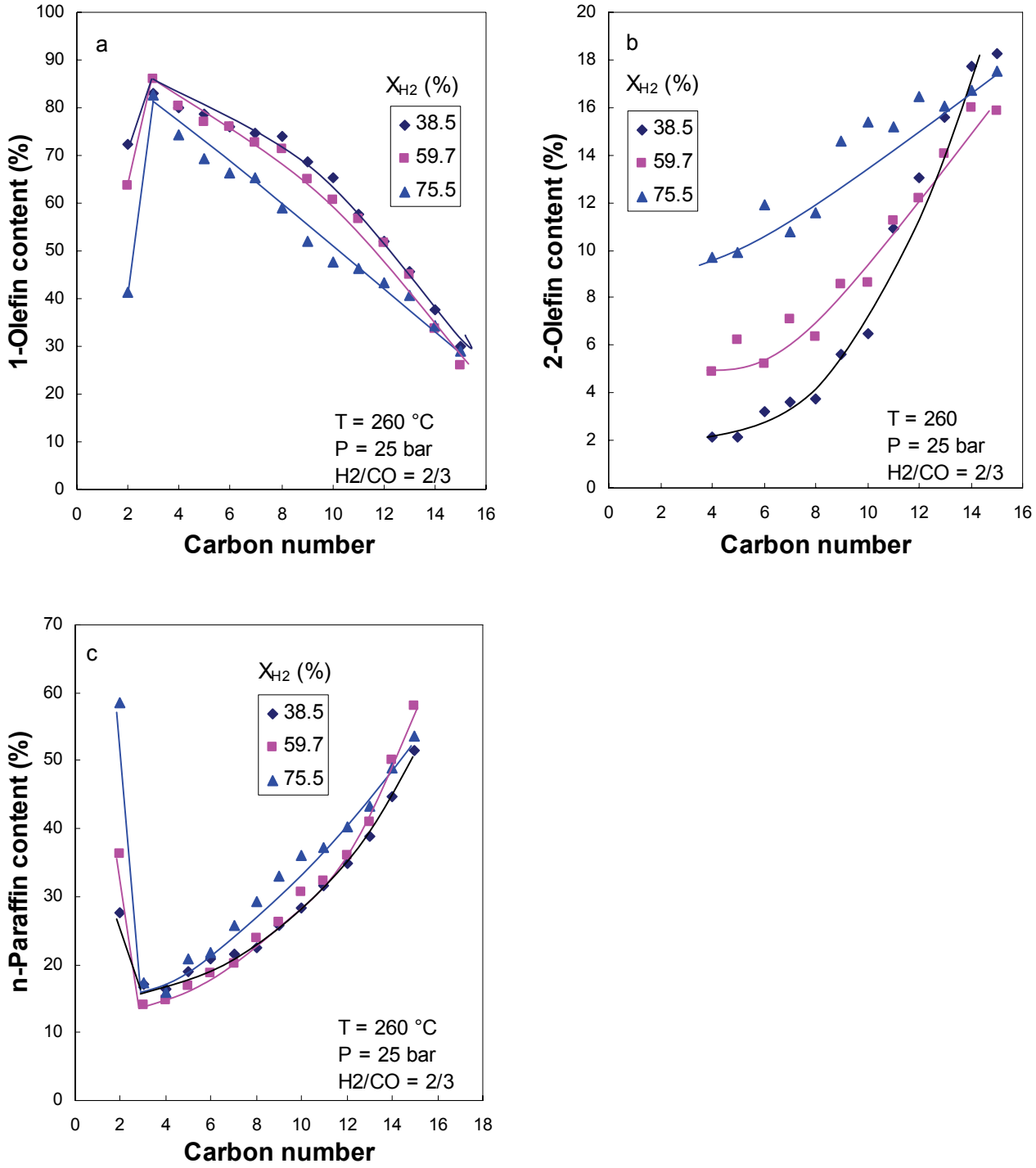

Figure 17. Effect of conversion (260°C, 25 bar, $H_2/CO = 2/3$) on (a) 1-olefin content, (b) 2-olefin content and (c) n-paraffin content.

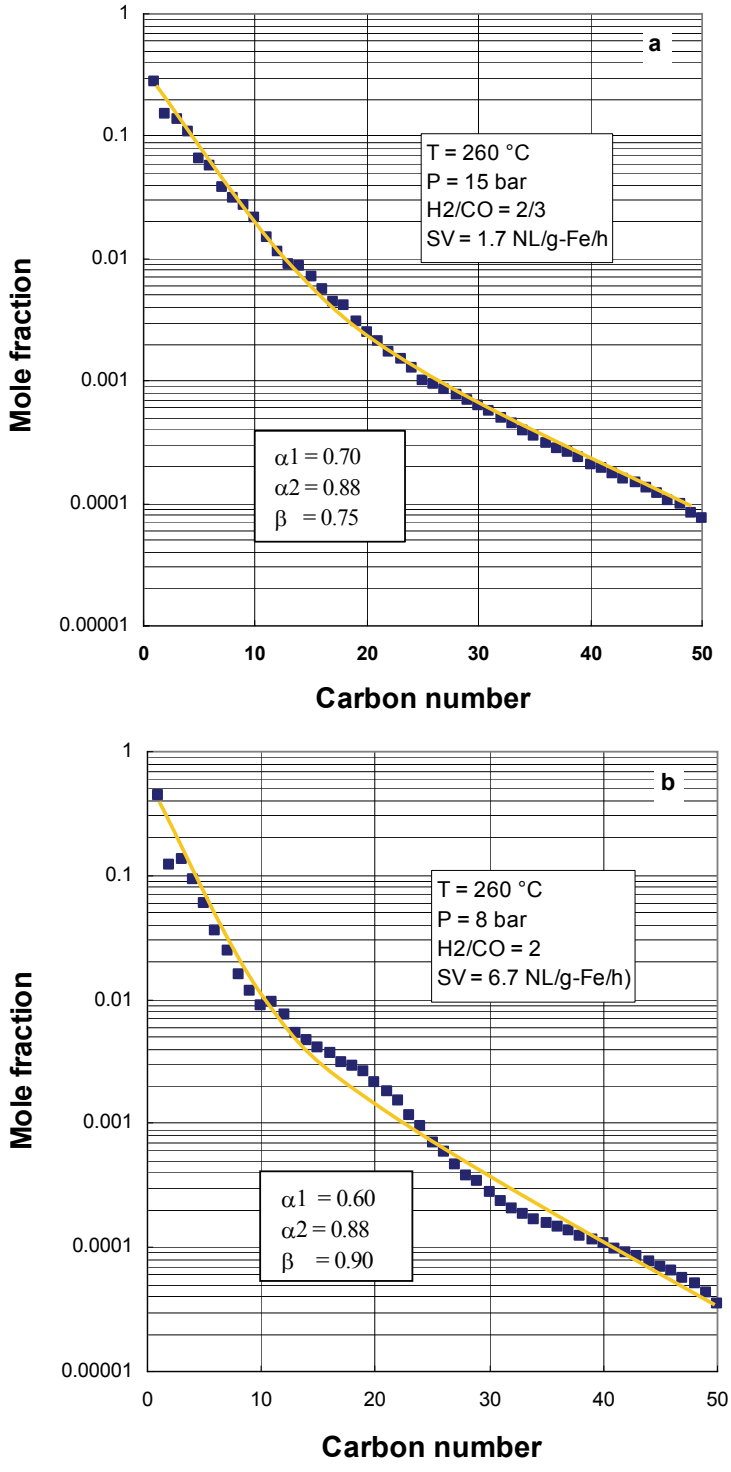

Figure 18. Carbon number product distribution according to extended Anderson Schulz-Flory model (T = 260°C).

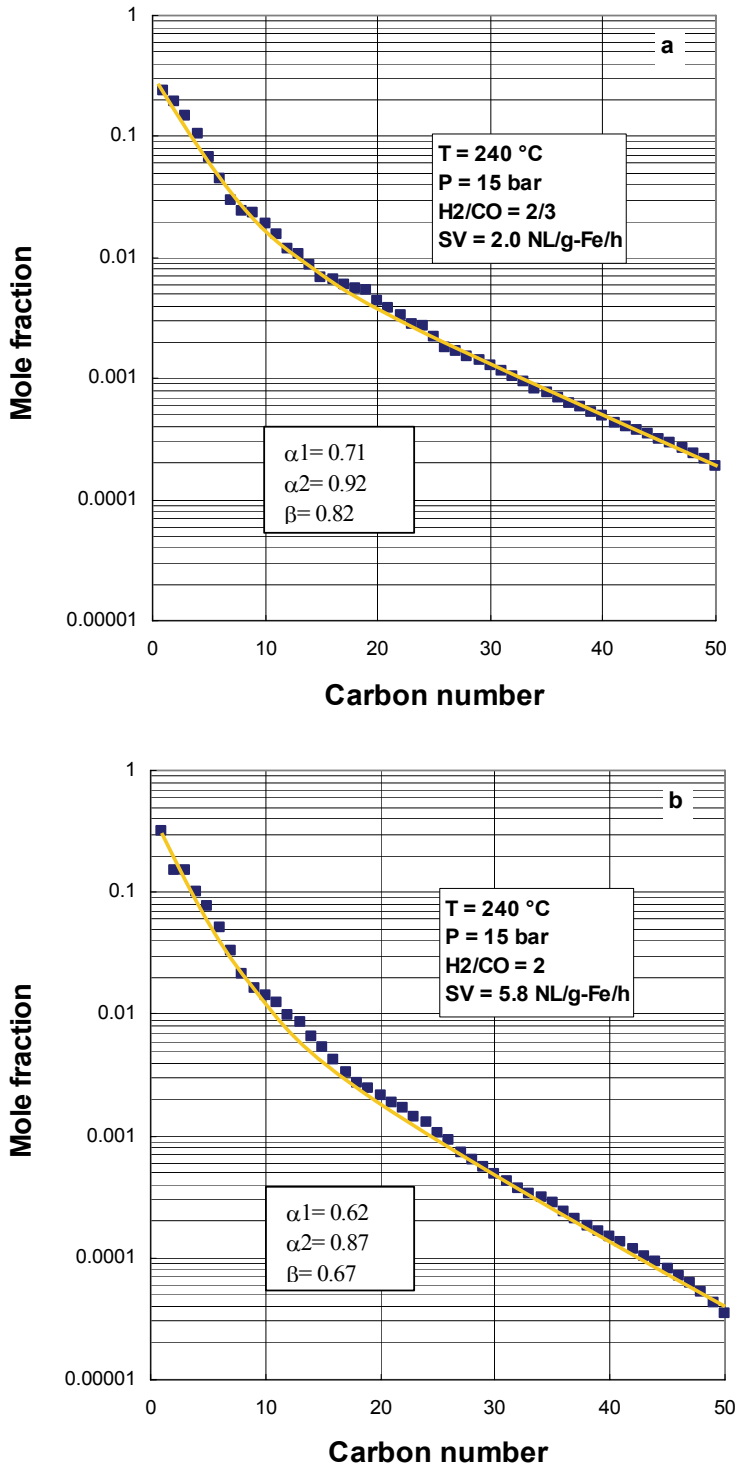

Figure 19. Carbon number product distribution according to extended Anderson-Schulz-Flory model (T = 240°C).

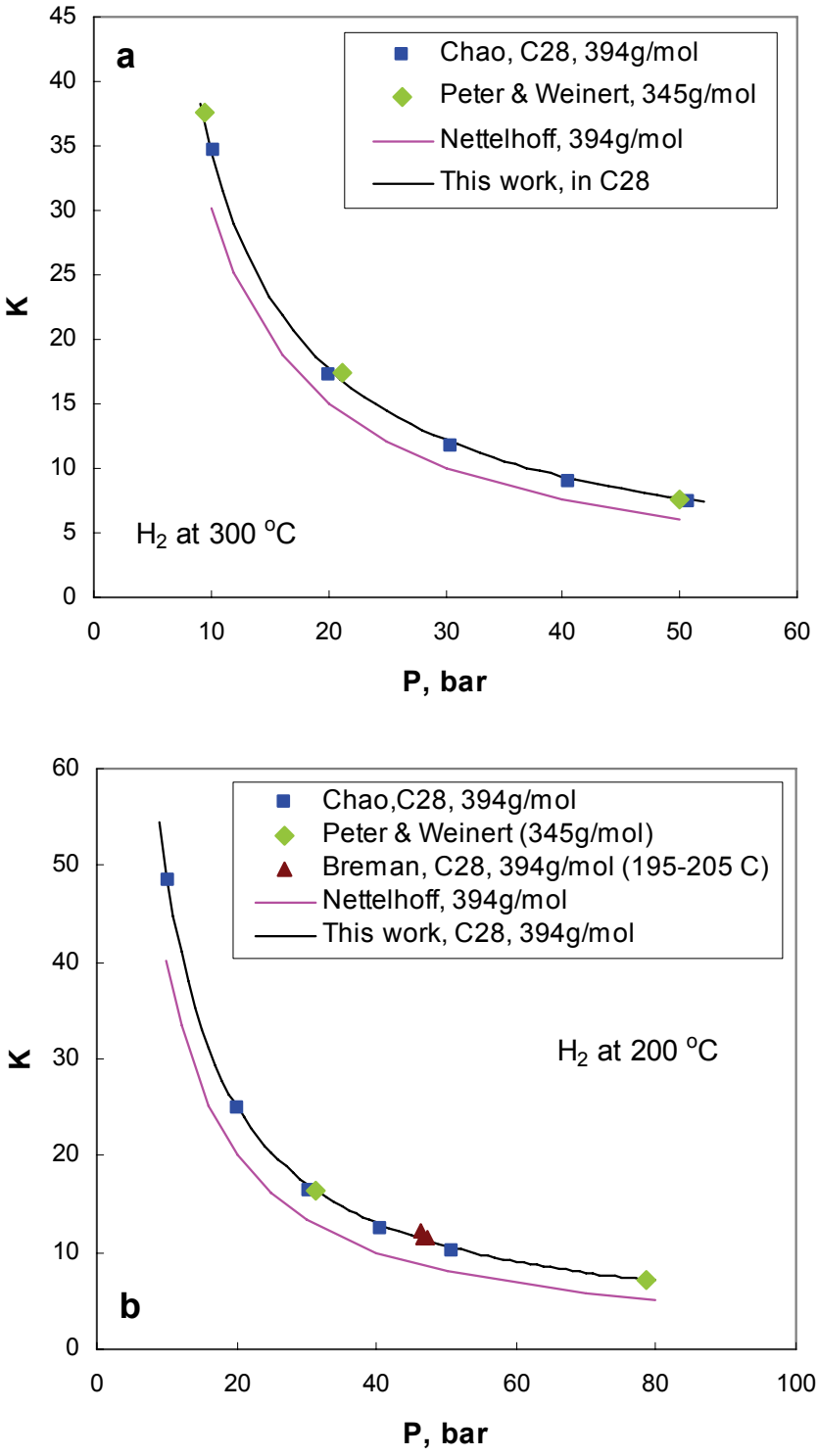

Figure 20. VLE calculations for binary system hydrogen in n-Octacosane ($C_{28}H_{58}$, MW = 394 g/mol).

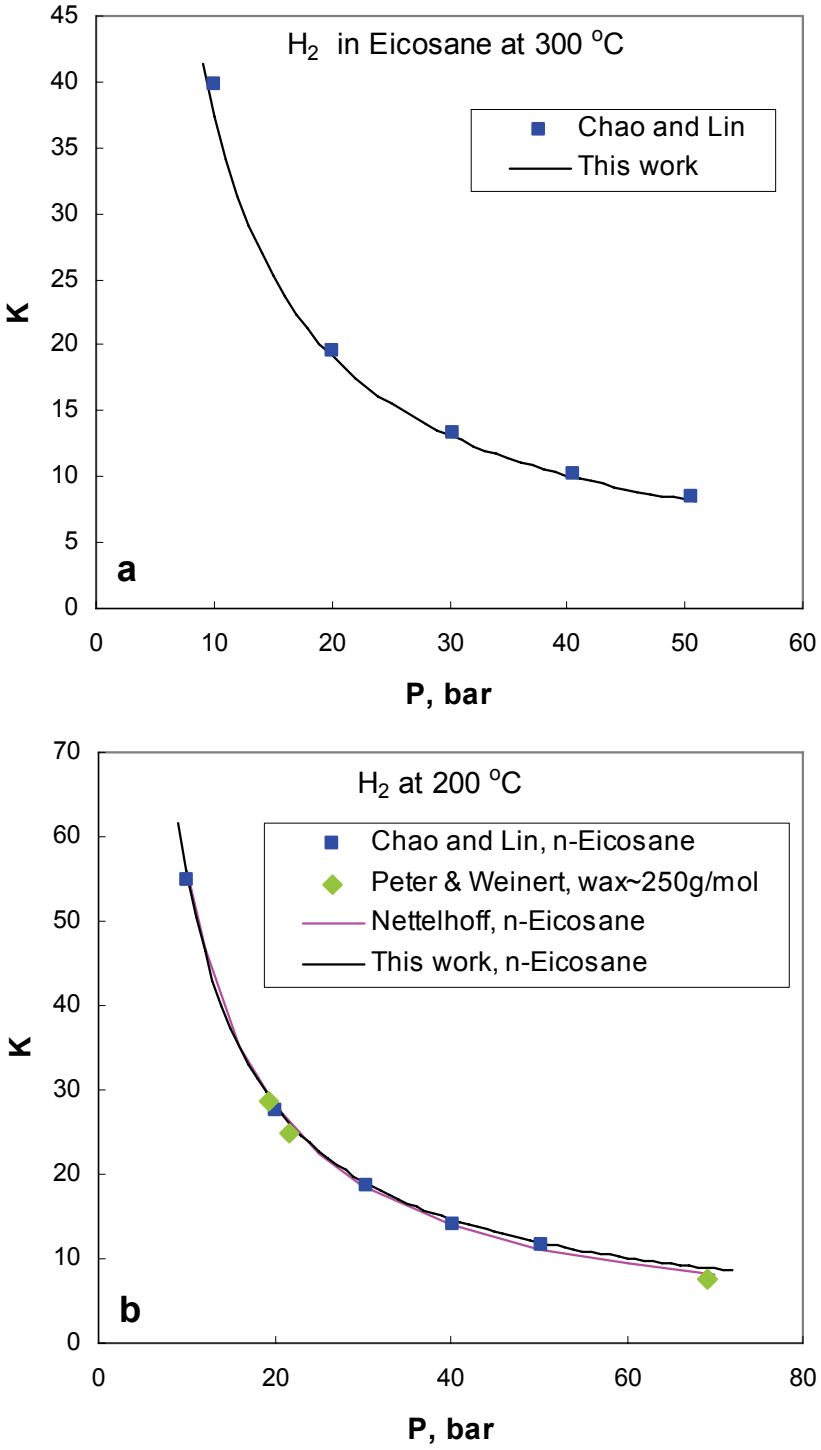

Figure 21. VLE calculations for binary system: hydrogen in n-Eicosane ($C_{20}H_{42}$, MW = 282 g/mol).

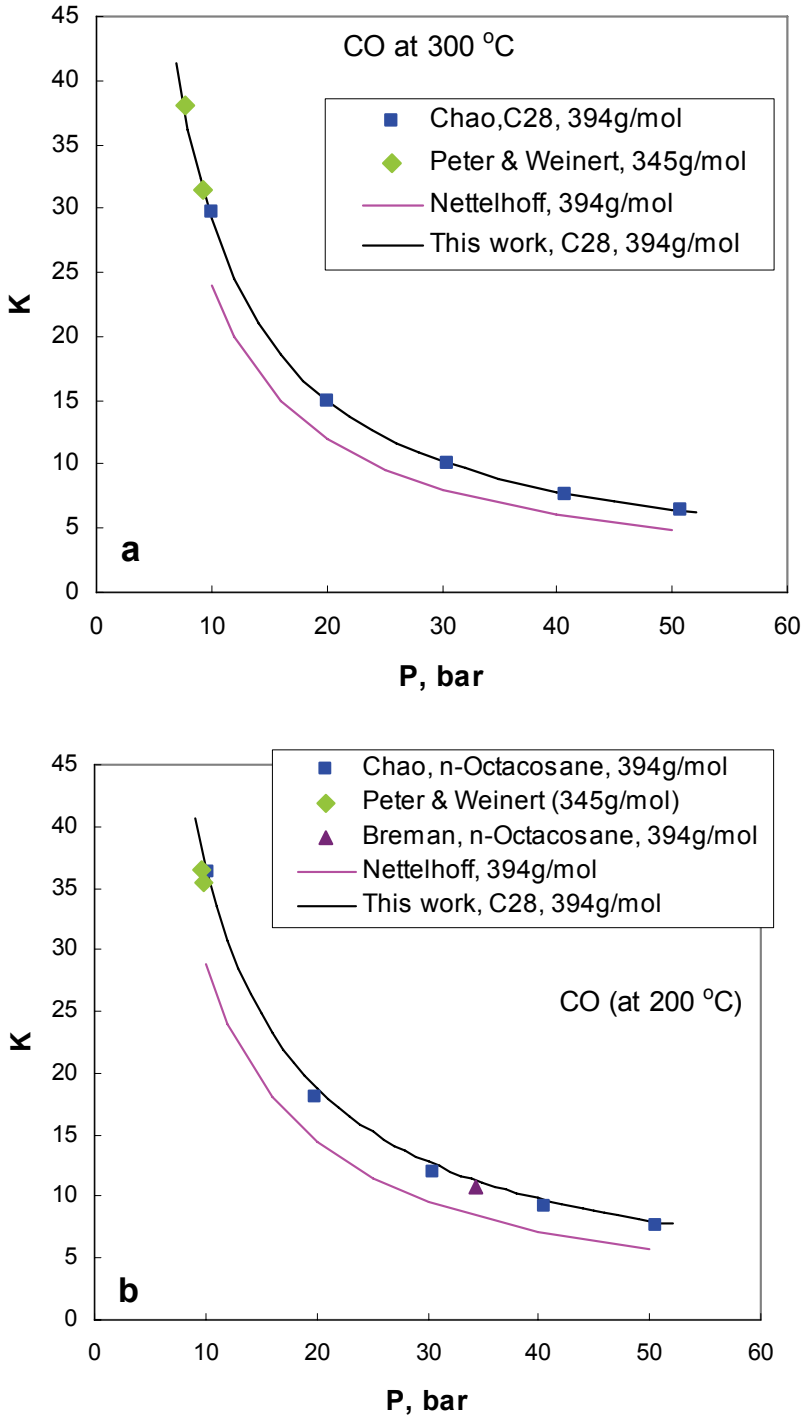

Figure 22. VLE calculations for binary system: carbon monoxide in n-Octacosane ($C_{28}H_{58}$, MW = 394 g/mol).

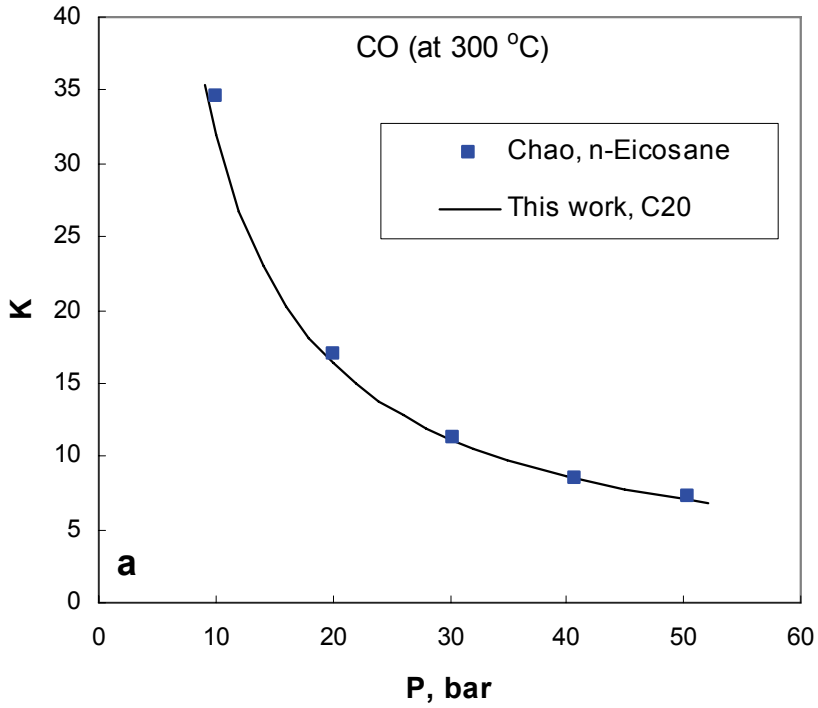

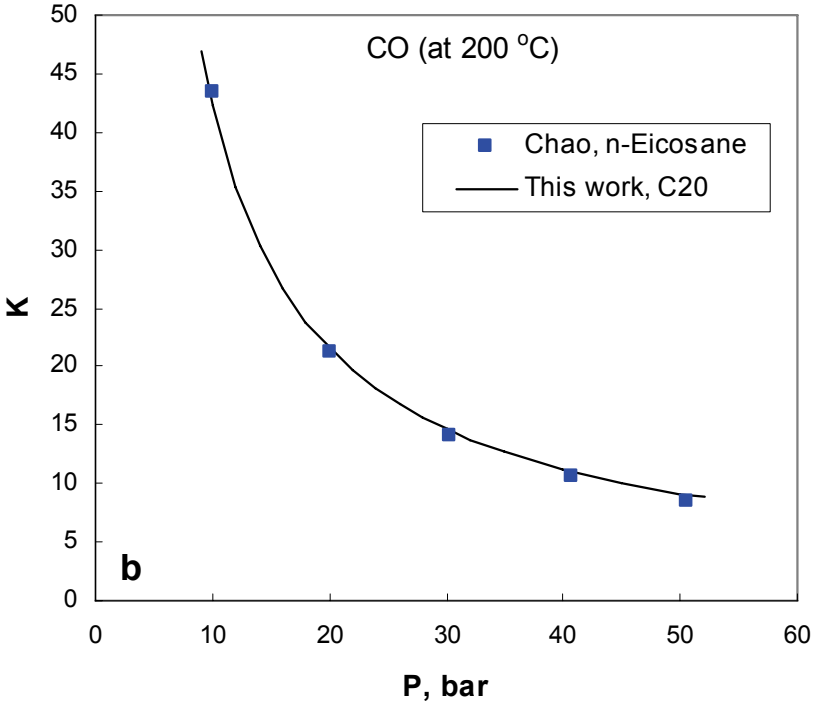

Figure 23. VLE calculations for binary system. carbon monoxide in n-Eicosane ($C_{20}H_{42}$, MW = 282 g/mol).

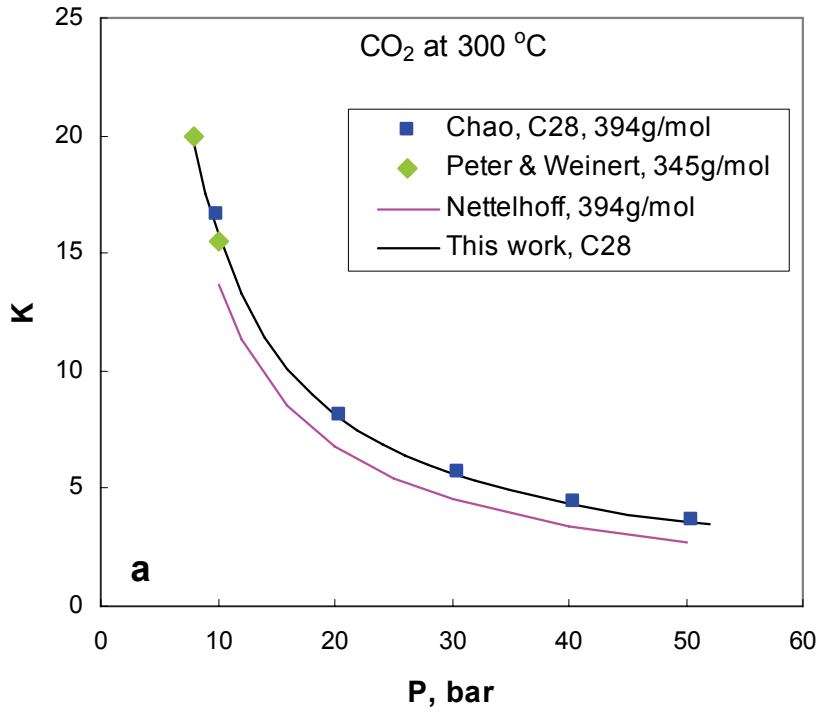

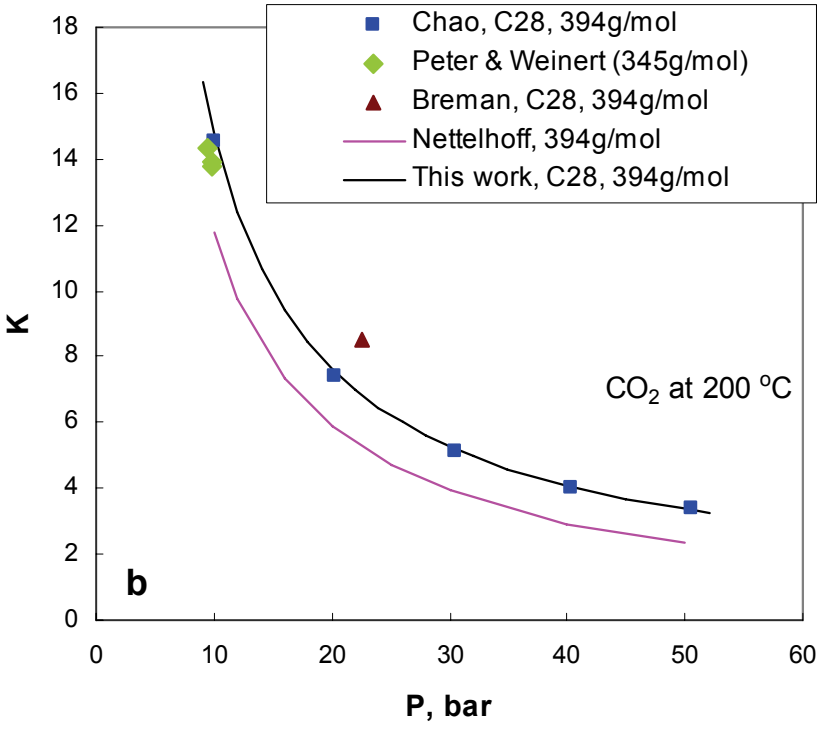

Figure 24. VLE calculations for binary system: carbon dioxide in n-Octacosane ($C_{28}H_{58}$, MW = 394 g/mol).

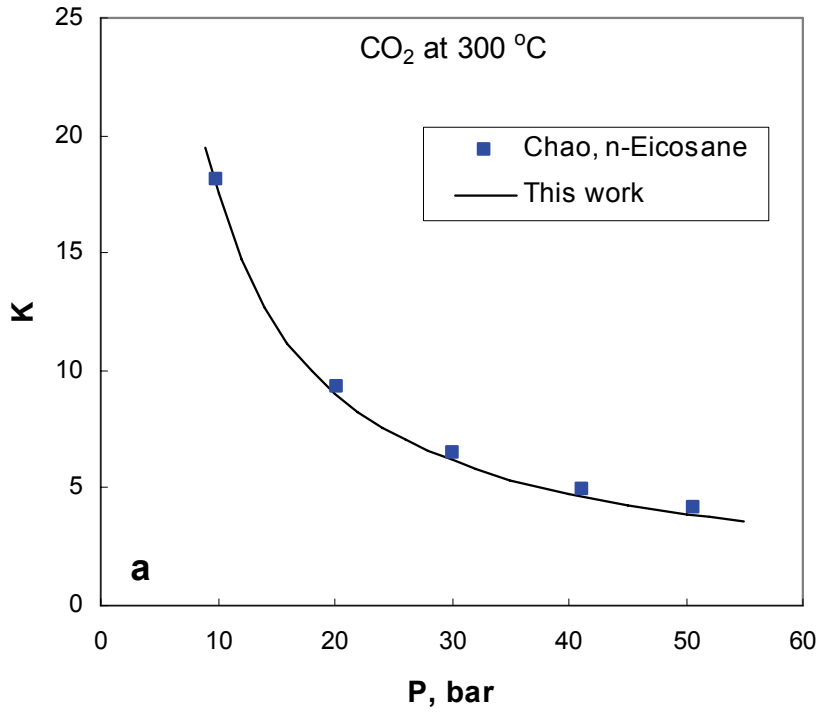

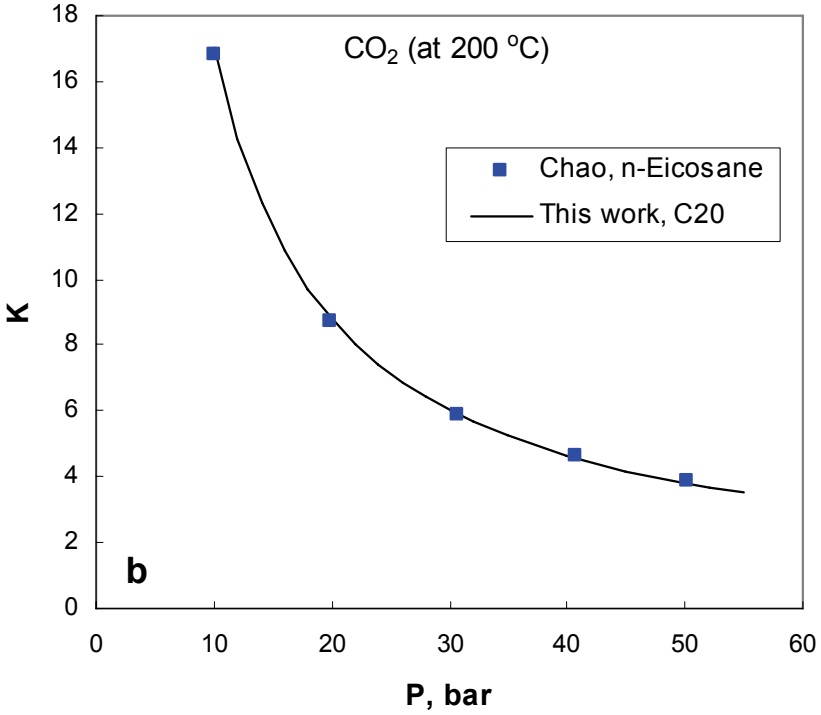

Figure 25. VLE calculations for binary system: carbon dioxide in n-Eicosane ($C_{20}H_{42}$, MW = 282 g/mol).

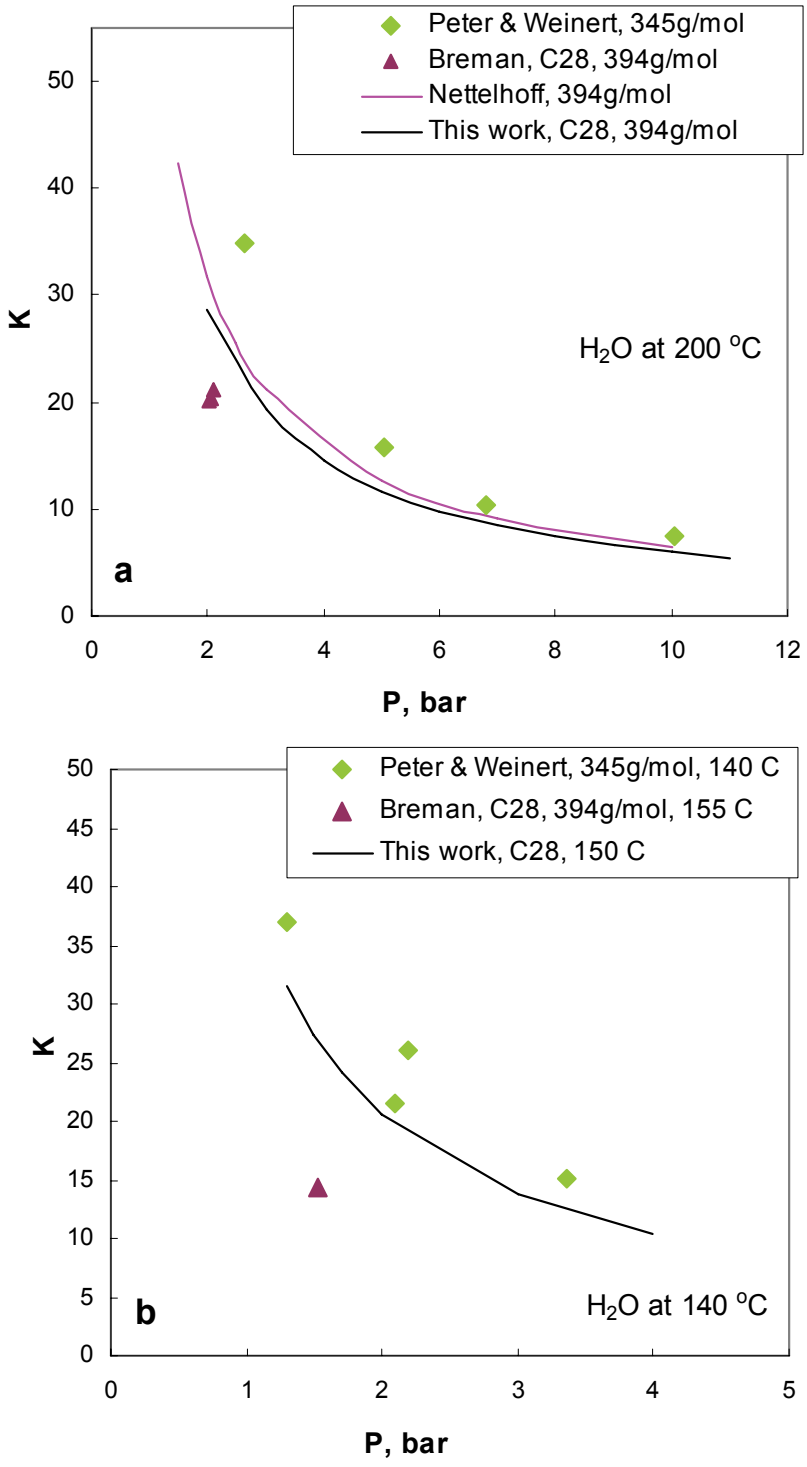

Figure 26. VLE calculations for binary system: water in n-Octacosane ($C_{28}H_{58}$, MW = 394 g/mol).

For hydrogen

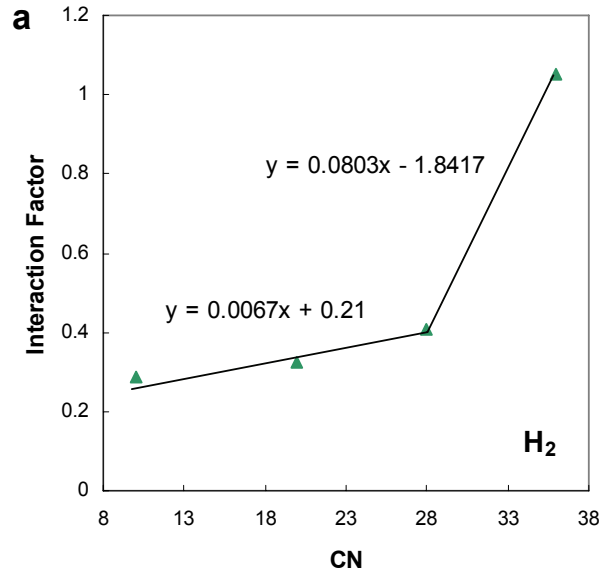

For carbon dioxide

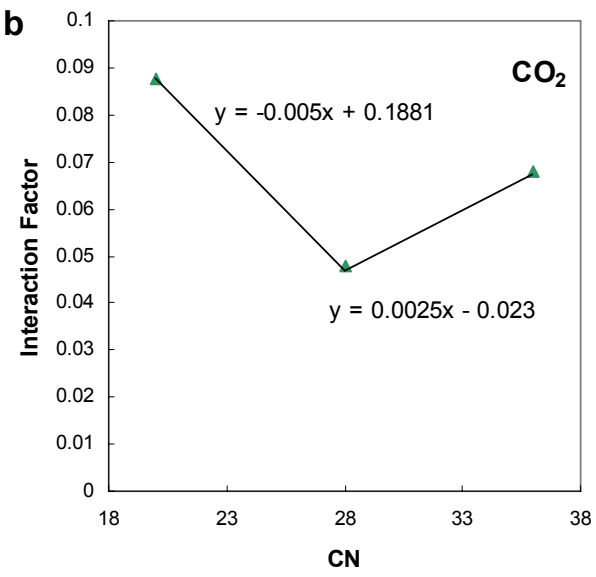

For carbon monoxide

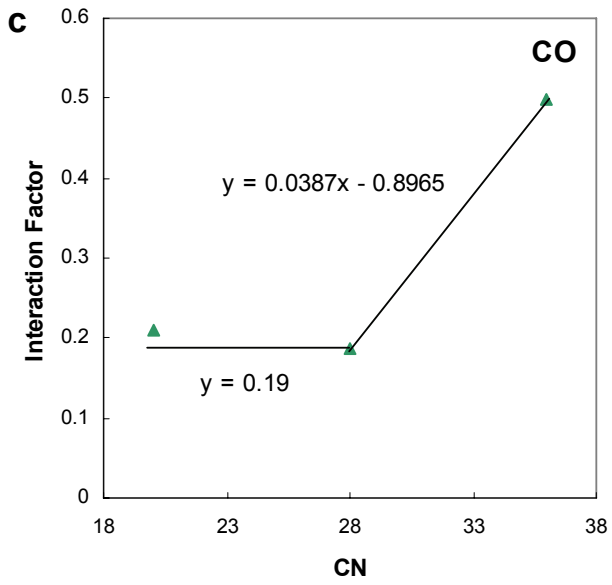

For water

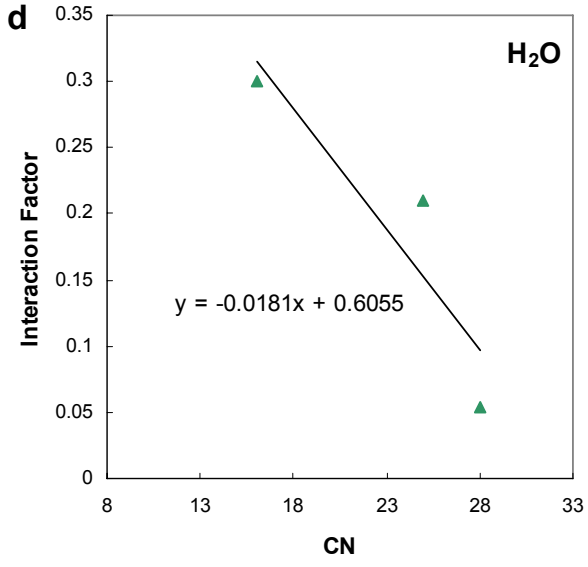

Figure 27. Estimated k_{ij} interaction factors as a function of carbon number.

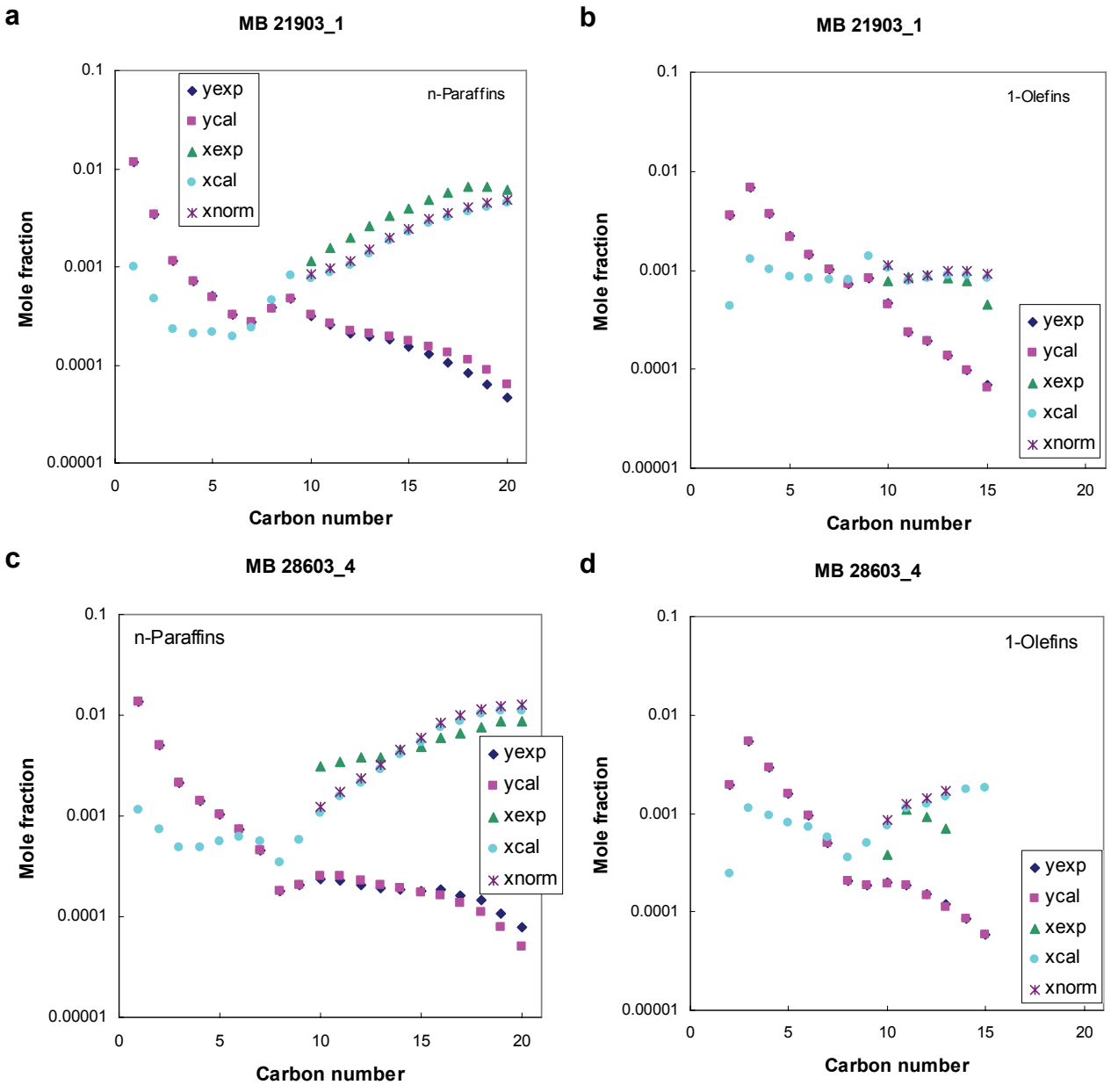

Figure 28. VLE calculations for FTS in the STSR. Reaction conditions: MB 21903_1 (a and b): 260°C, 2.17 bar, 0.68 H_2/CO and SV = 1.4 NL/g-Fe/h; MB 28603_4 (c and d): 220°C,1.48 bar, 2 H_2/CO and SV = 0.55 NL/g-Fe/h.

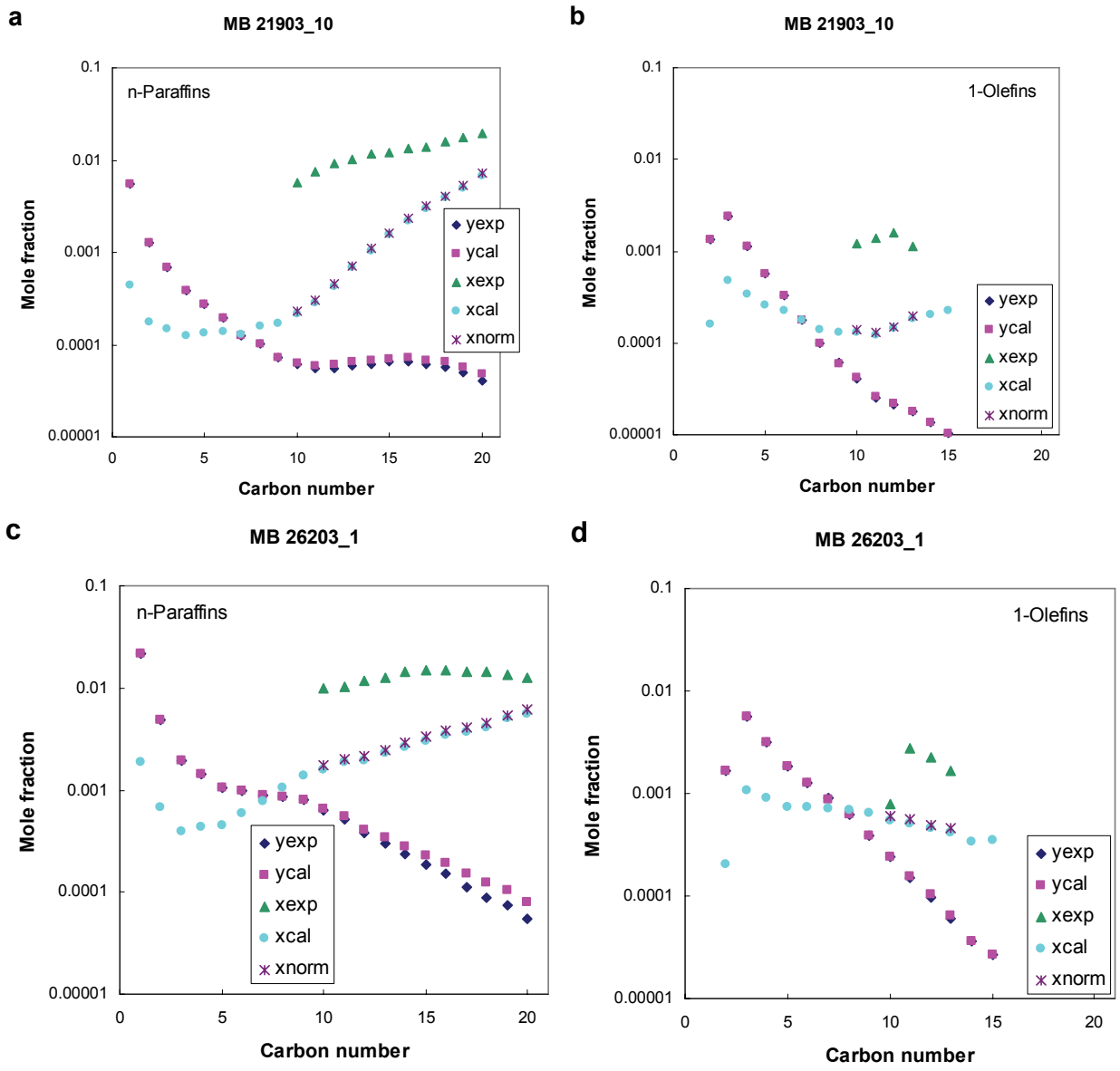

Figure 29. VLE calculations for FTS in the STSR. Reaction conditions: MB 21903_10 (a and b): 240°C, 1.48 bar, 2 H_2/CO and SV = 10.8 NL/g-Fe/h; MB 26203_1 (c and d): 260°C, 1.48 bar, 2 H_2/CO and SV = 7.1 NL/g-Fe/h.

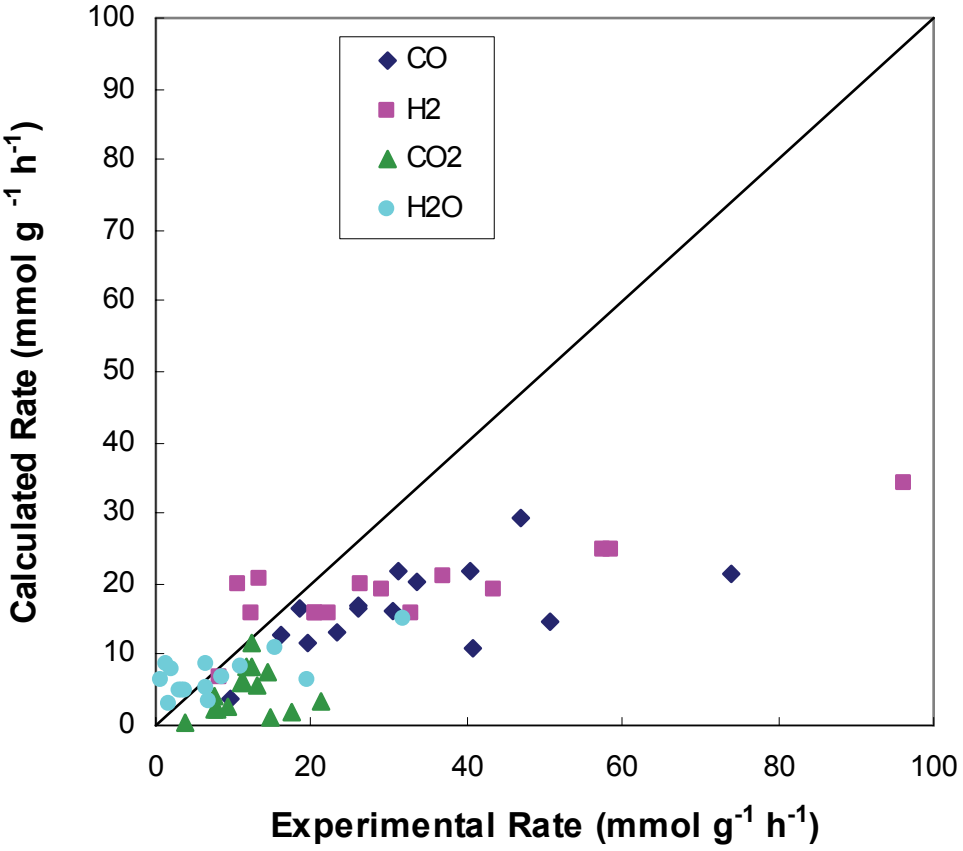

Figure 30. Parity graph of experimental and calculated reaction rates at *260 ℃* for H_2, CO, CO_2 and H_2O (Lox and Froment Model).

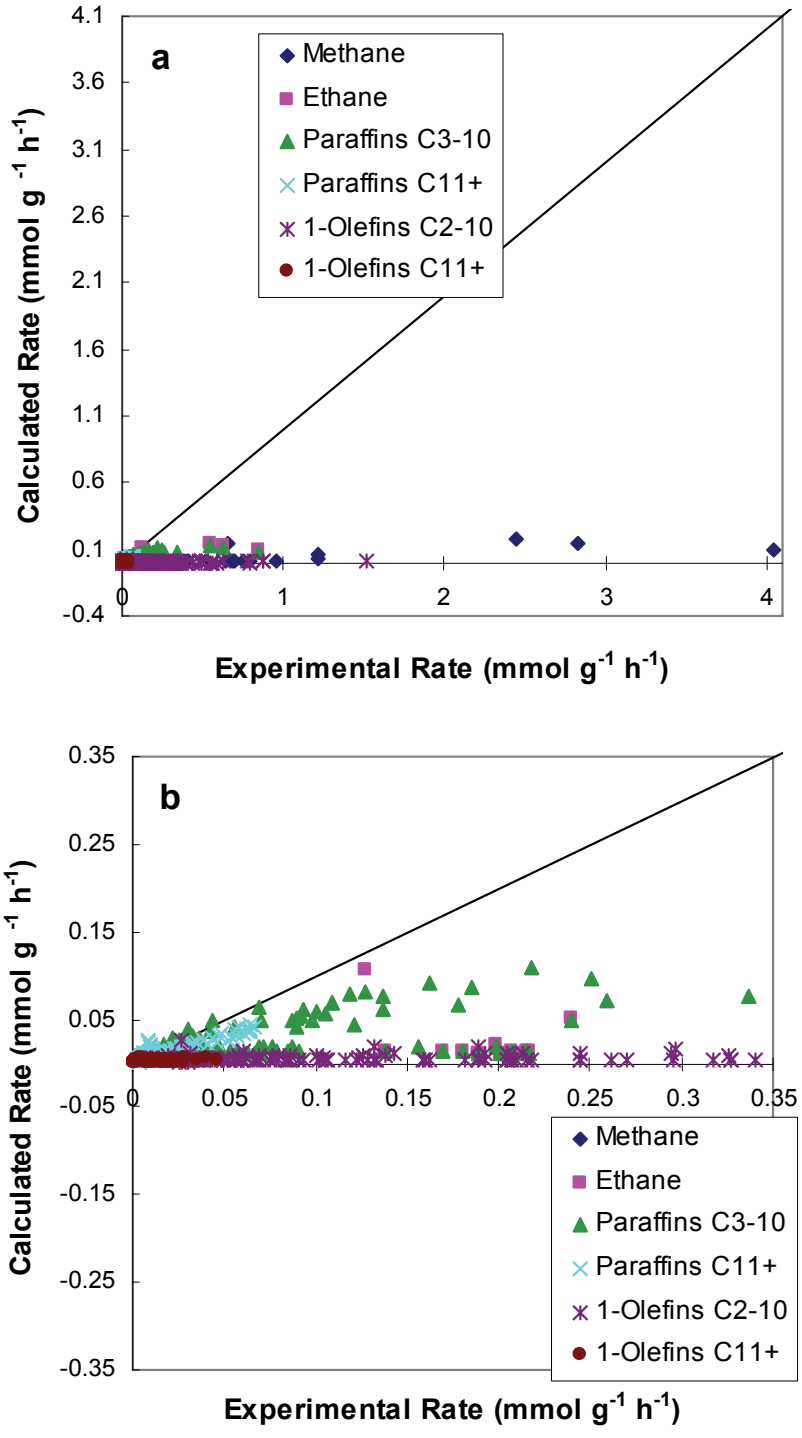

Figure 31. Parity graph of experimental and calculated reaction rates at *260 ℃* for hydrocarbons (Lox and Froment Model).

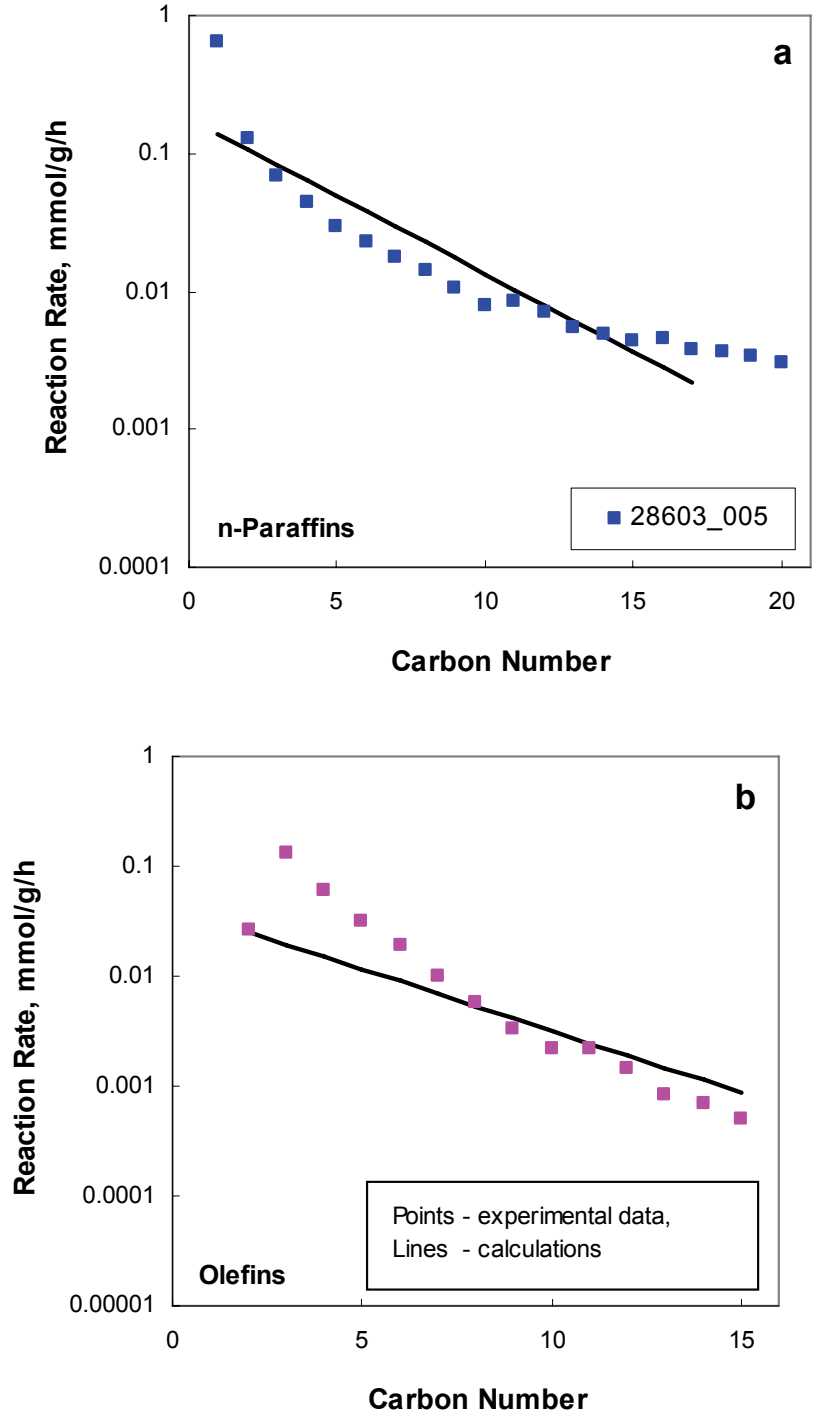

Figure 32. Comparison of experimental data and model predictions for n-paraffins and total olefins at T = 260°C, 8 bar, H_2/CO = 2, SV = 1.45 NL/g-Fe/h).

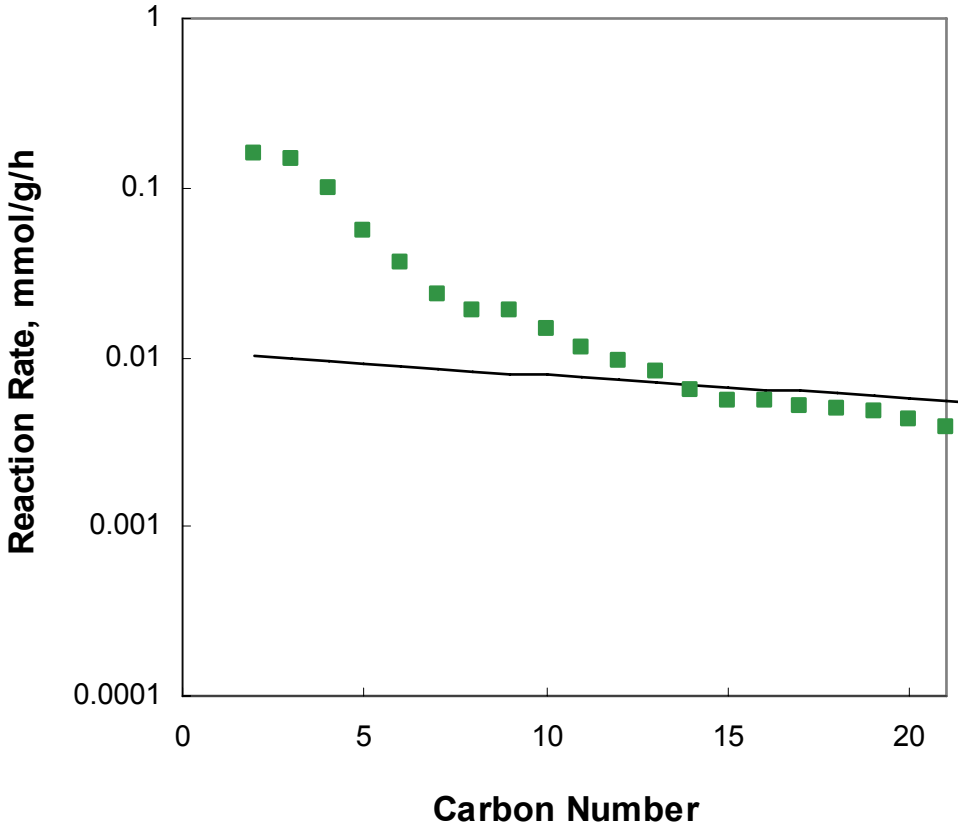

Figure 33. Carbon number distribution of hydrocarbon products - Comparison of model predictions with experimental data (Reaction conditions:T = 240°C, 15 bar, H_2/CO = 2/3, SV = 2.0 NL/g-Fe/h).

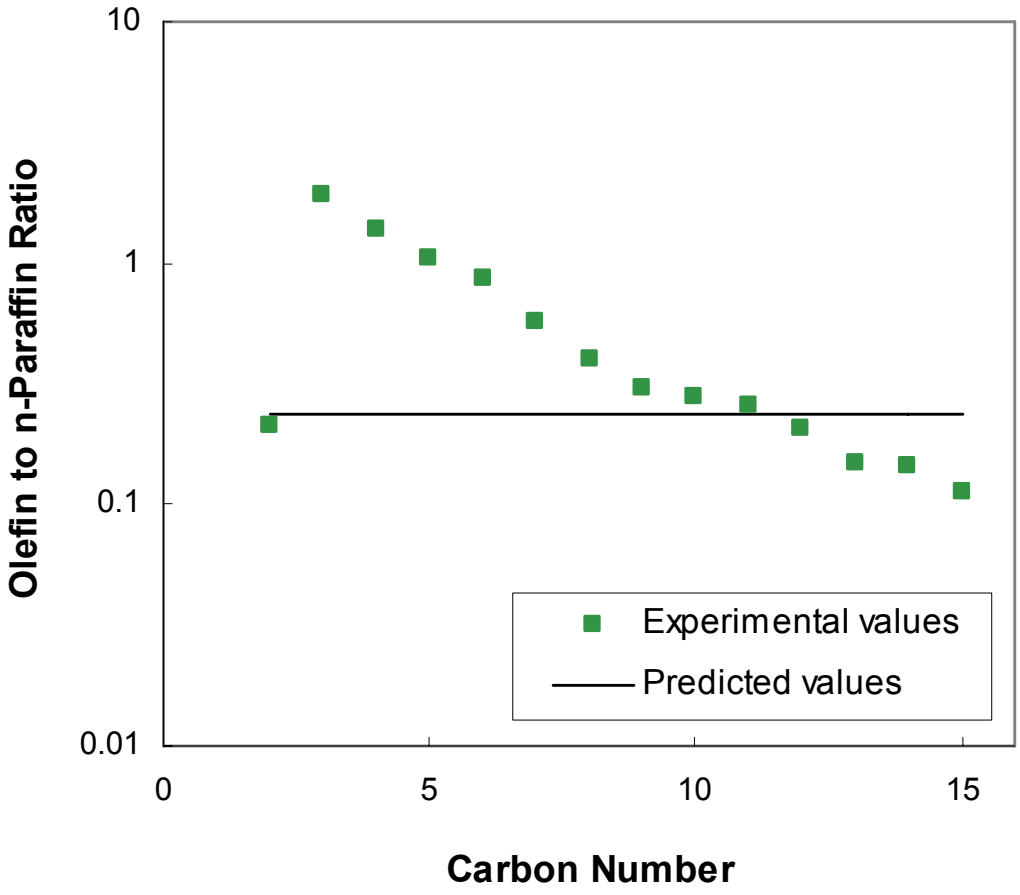

Figure 34. Olefin to paraffin ratio change with carbon number – Comparison of model predictions with experimental data (Reaction conditions: T = 260°C, 8 bar, $H_2/CO = 2$, SV = 1.45 NL/g-Fe/h).

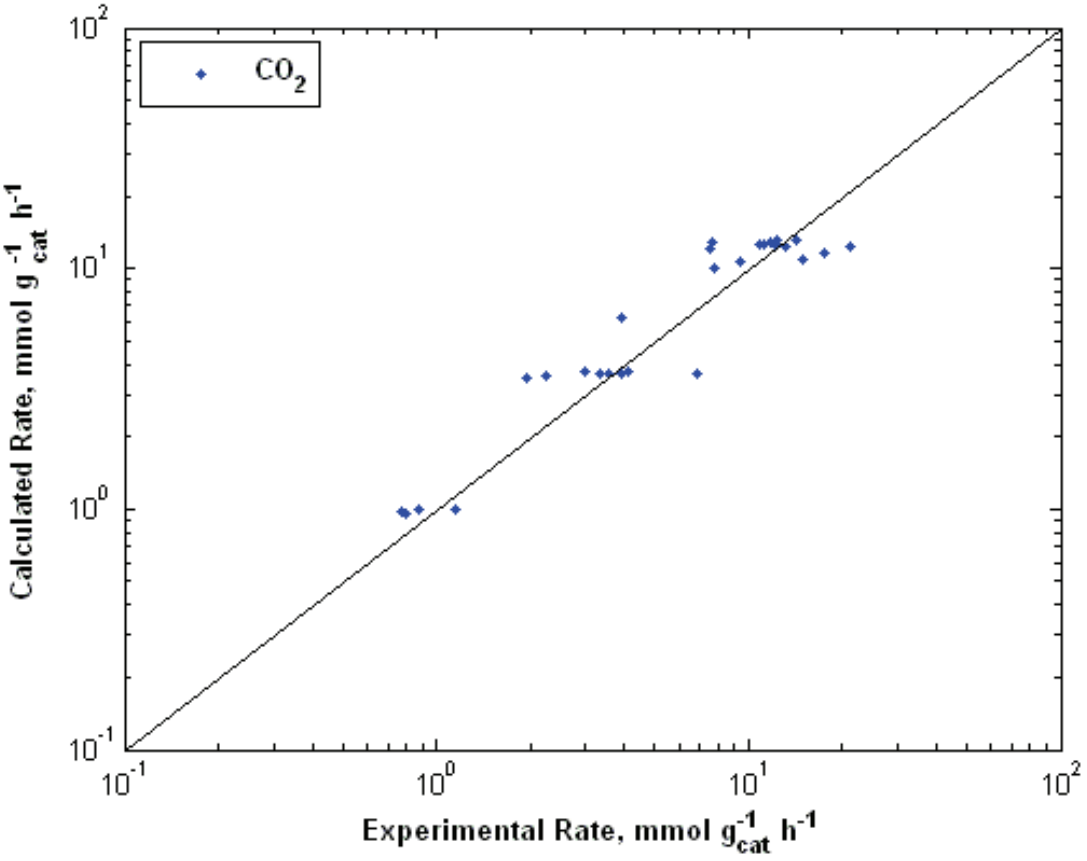

Figure 35. Parity plot for carbon dioxide formation rate (LS Method).

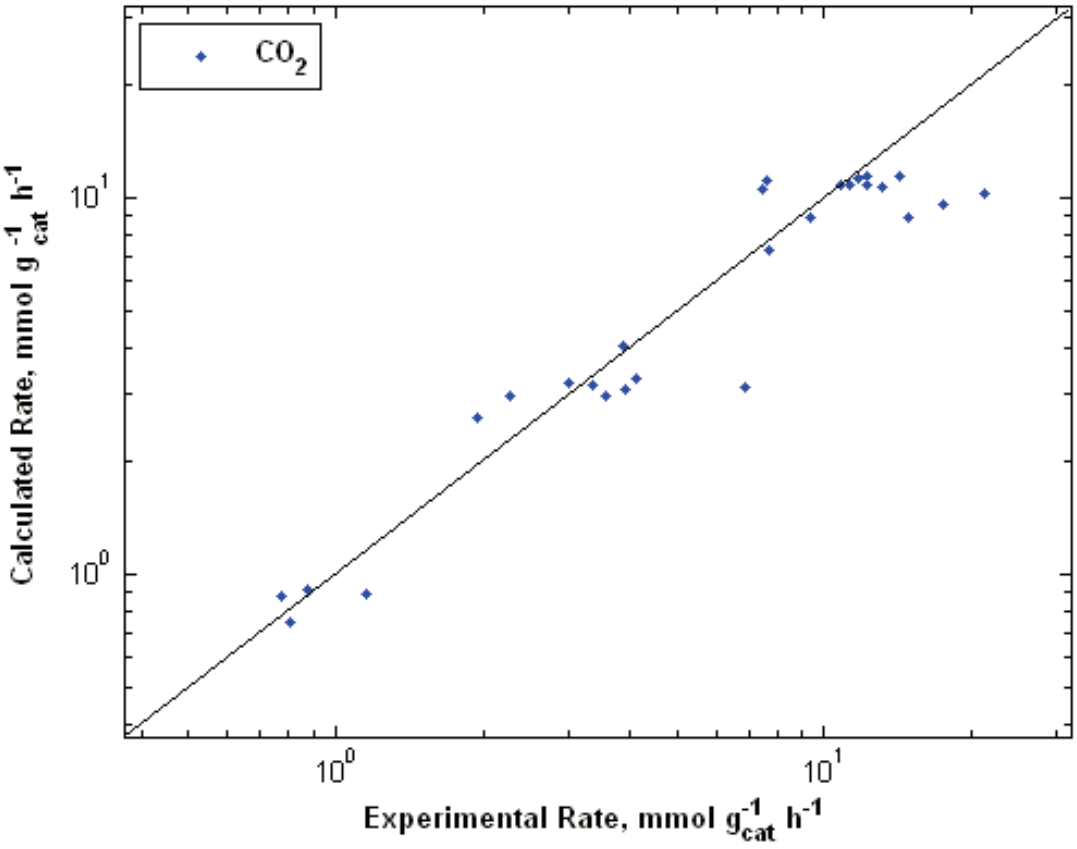

Figure 36. Parity plot for carbon dioxide (GA method followed by LM method).

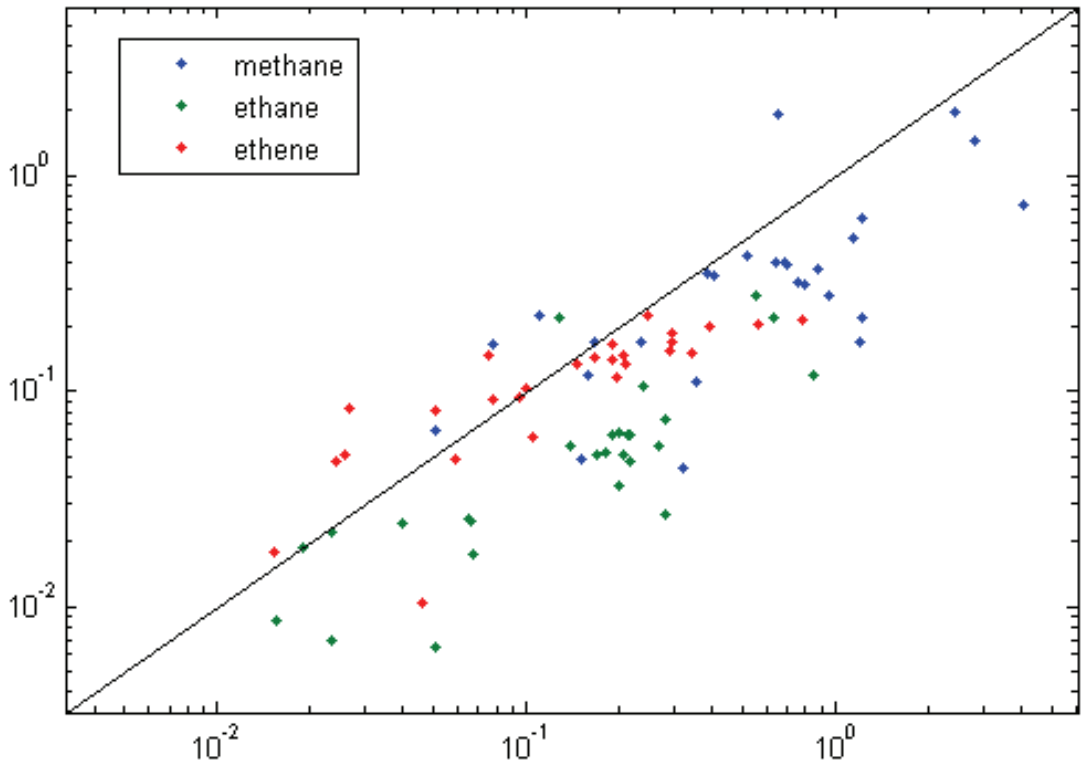

Figure 37. Parity plot for low molecular weight hydrocarbons (Yang et al. Model).

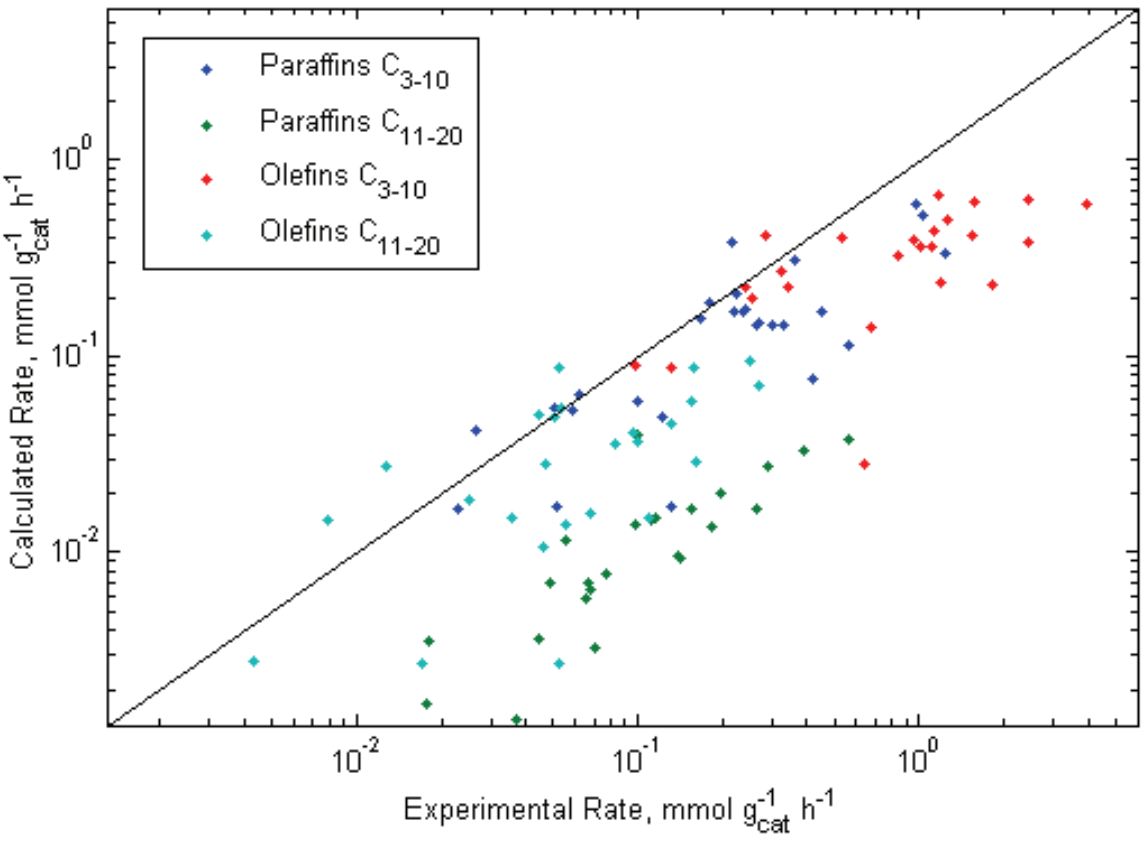

Figure 38. Parity plot for higher molecular weight hydrocarbons (Yang et al. Model).

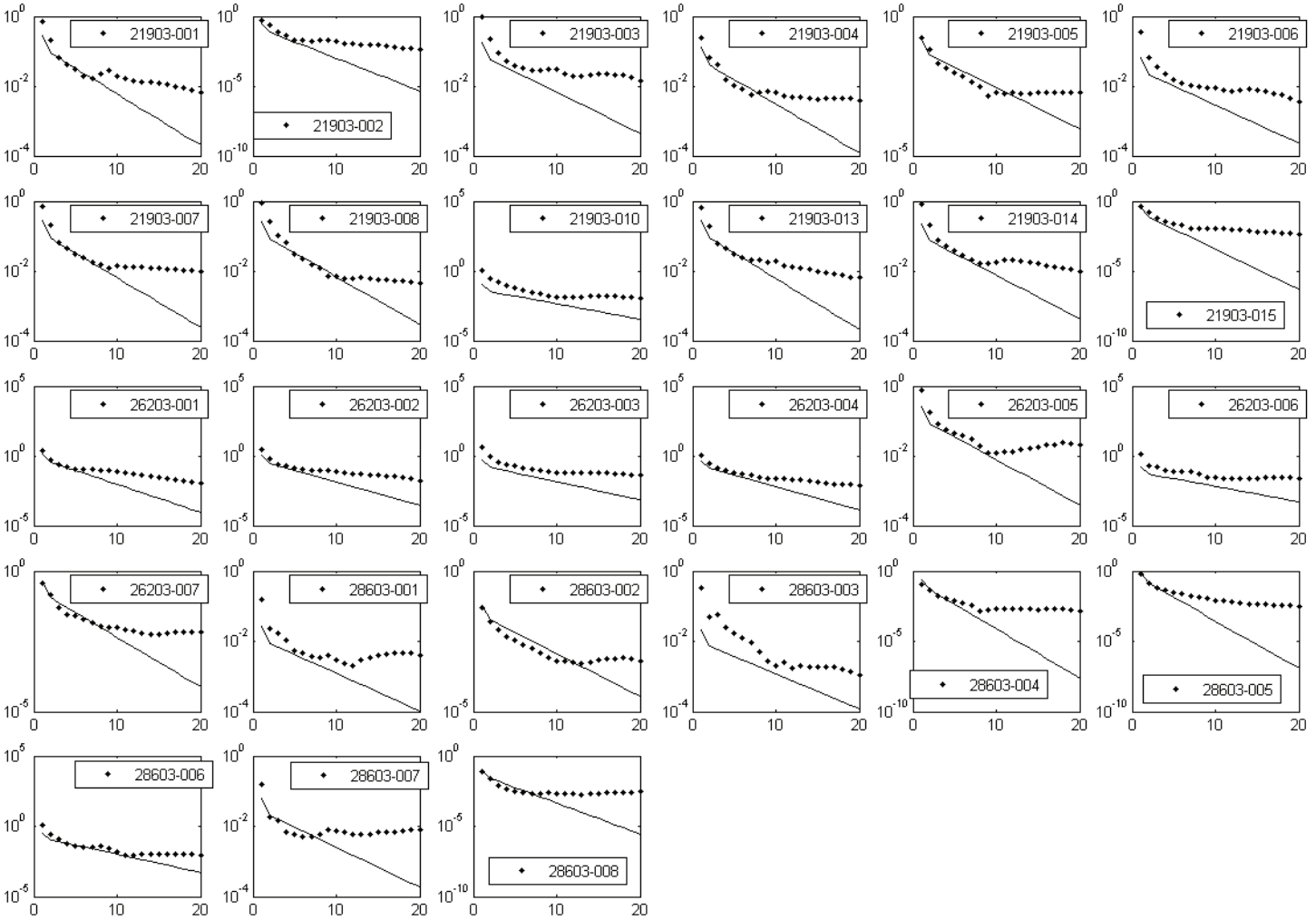

Figure 39. Comparison of experimental data and model predictions for n-paraffins (Yang et al. Model).

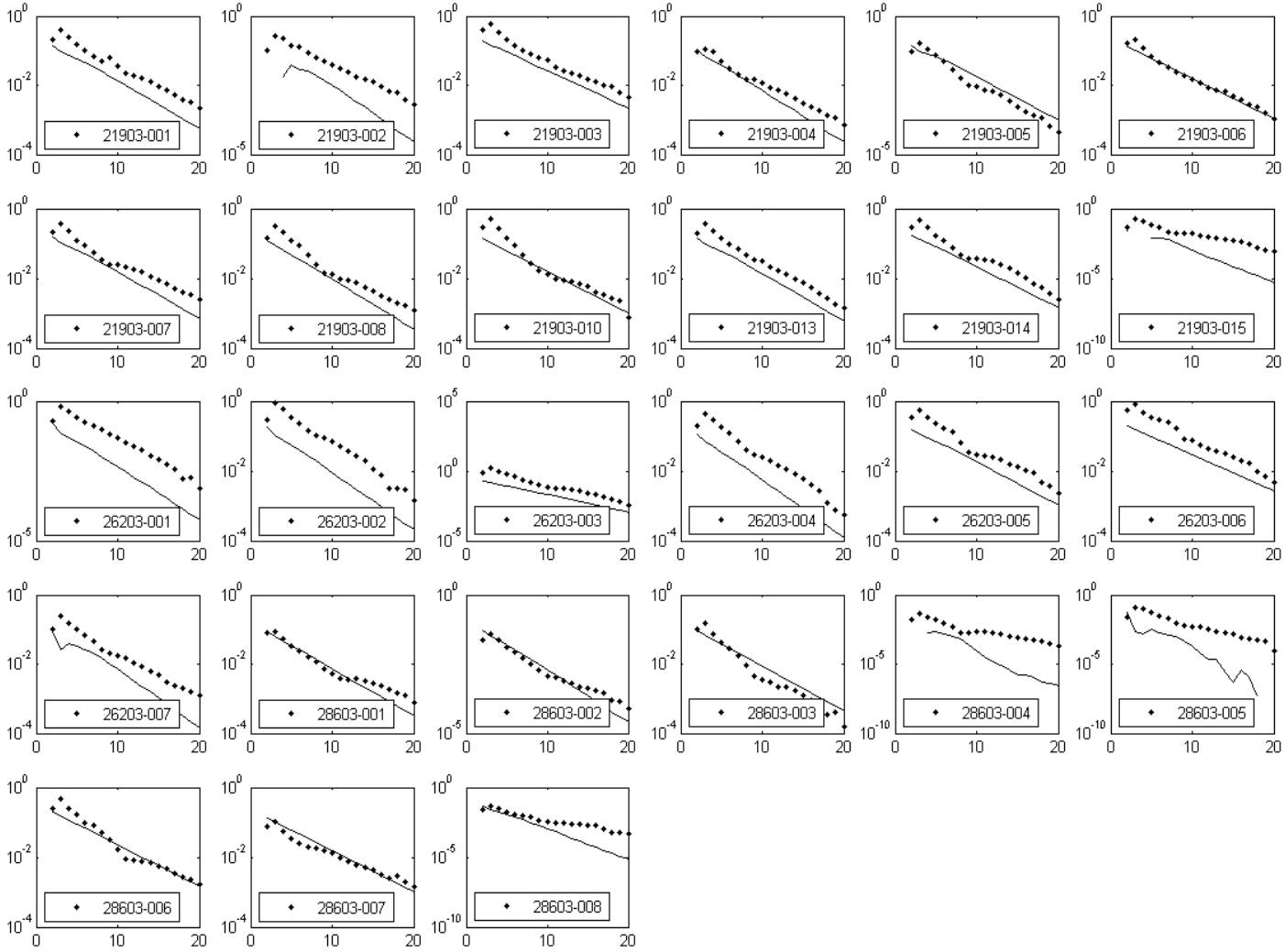

Figure 40. Comparison of experimental data and model predictions for linear olefins (Yang et al. Model).

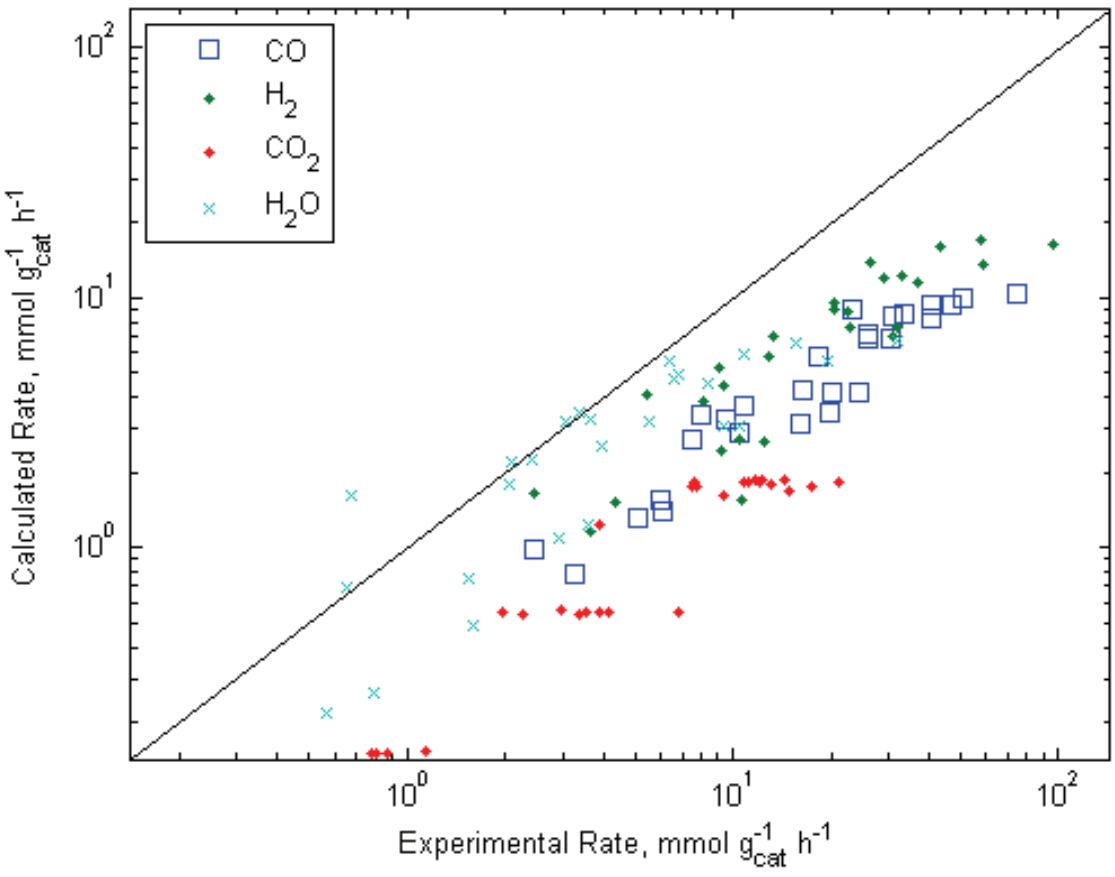

Figure 41. Parity plot for inorganic species (Yang et al. Model).

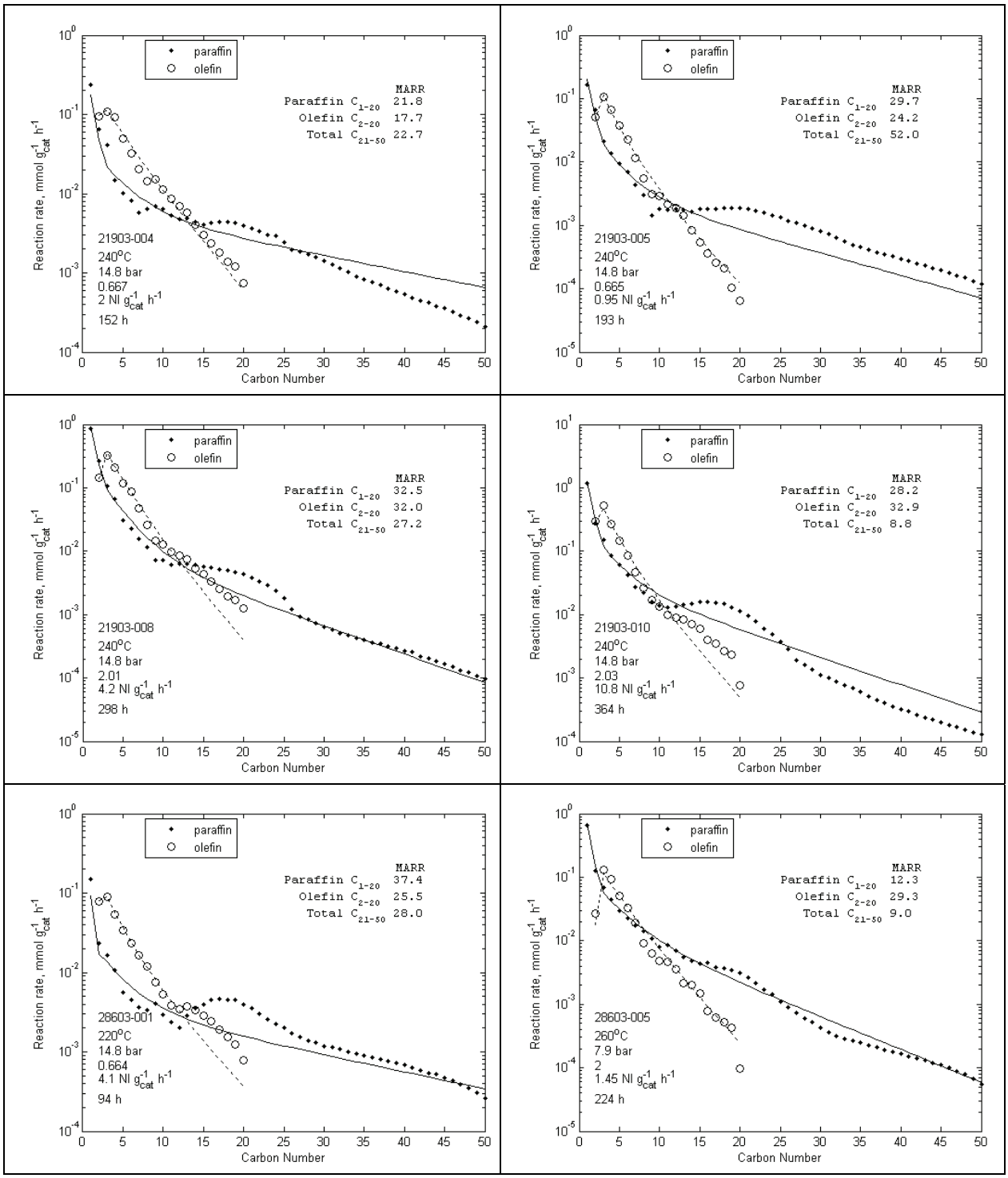

Figure 42. Comparison of predicted and experimental product distributions (Van der Laan and Beenackers Model).

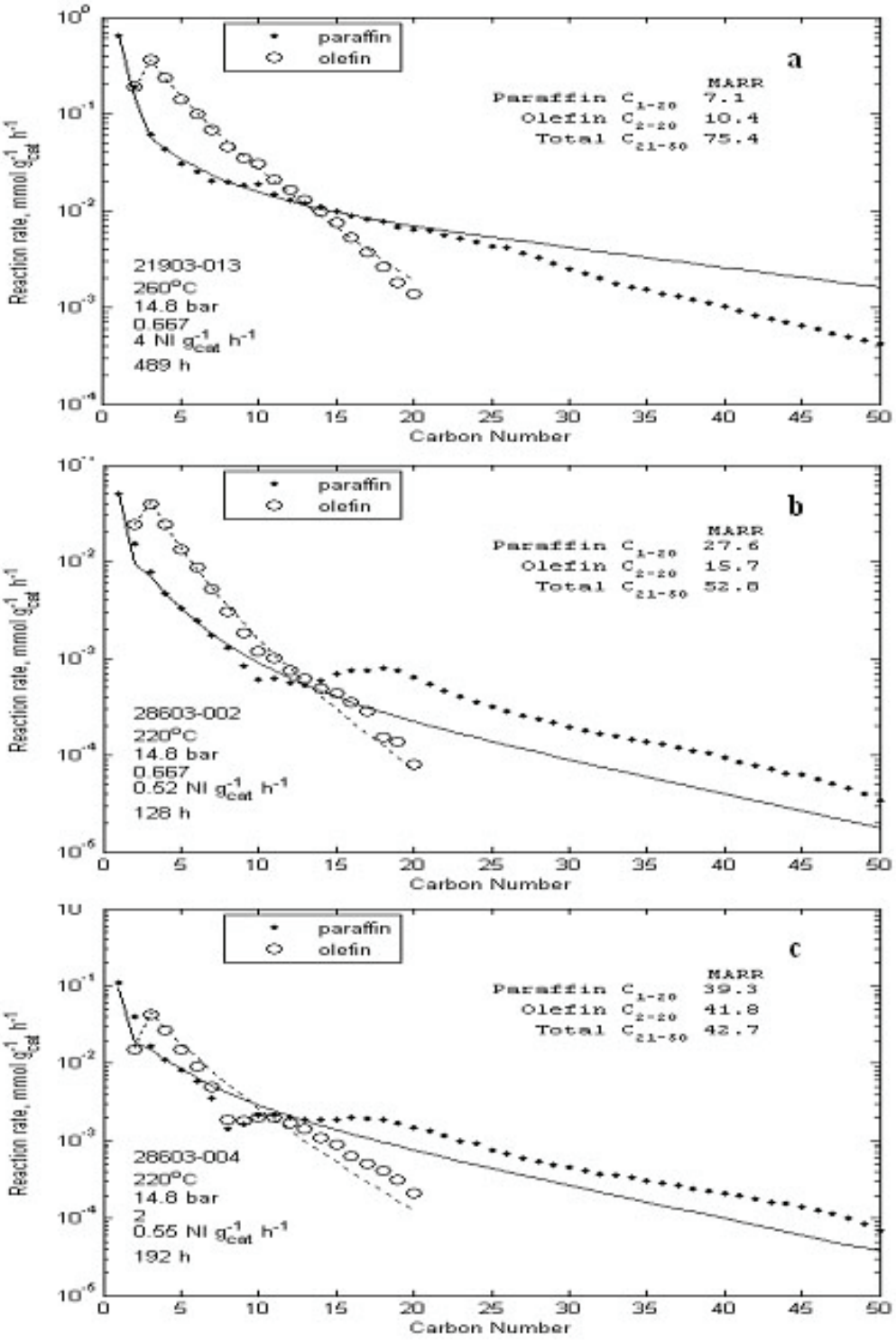

Figure 43. Comparison of predicted and experimental product distributions 9: a) best, (b) median and (c) worst total MARR.

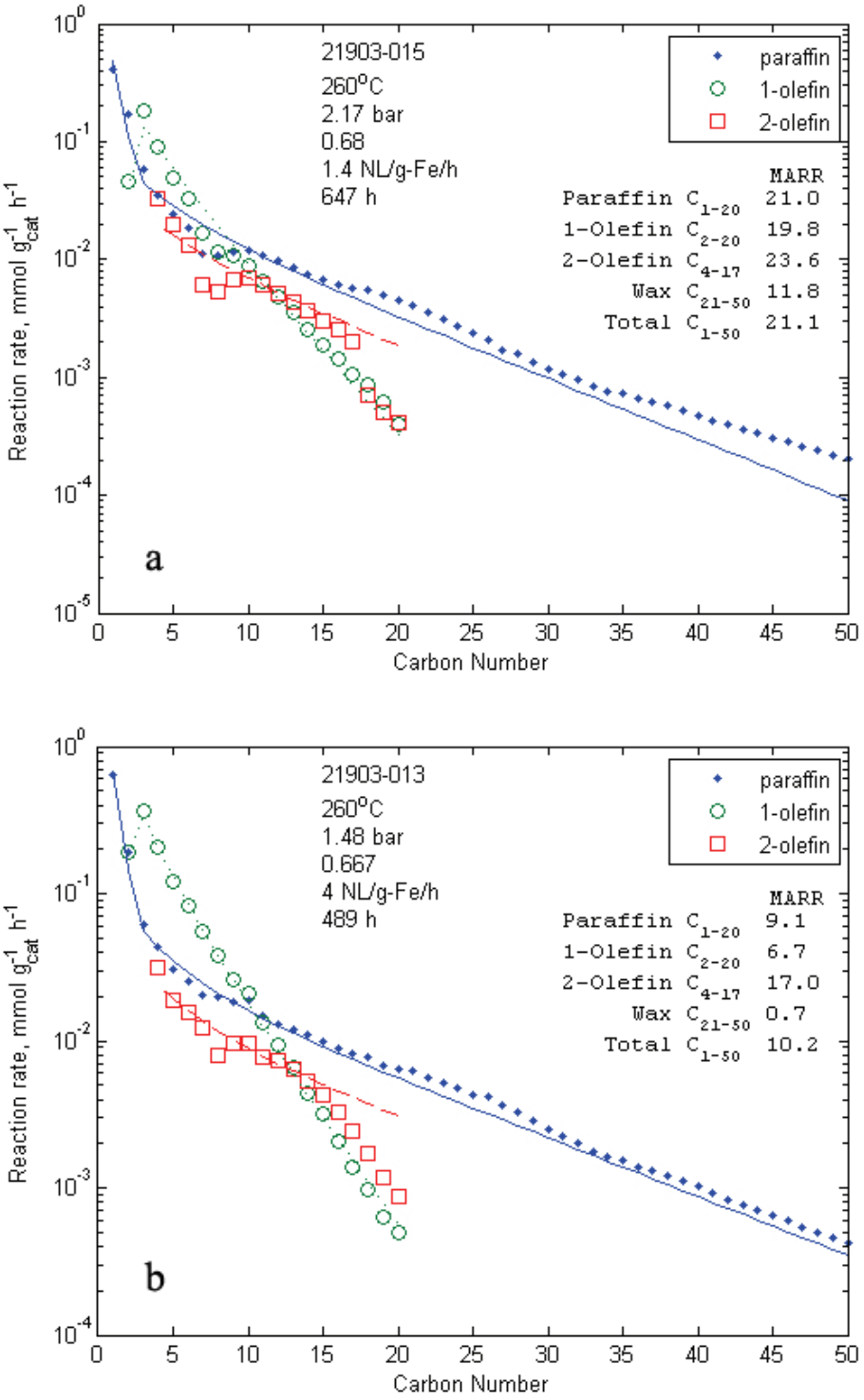

Figure 44. Comparison of predicted and experimental product distributions (extended Van der Laan and Beeenackers Model).

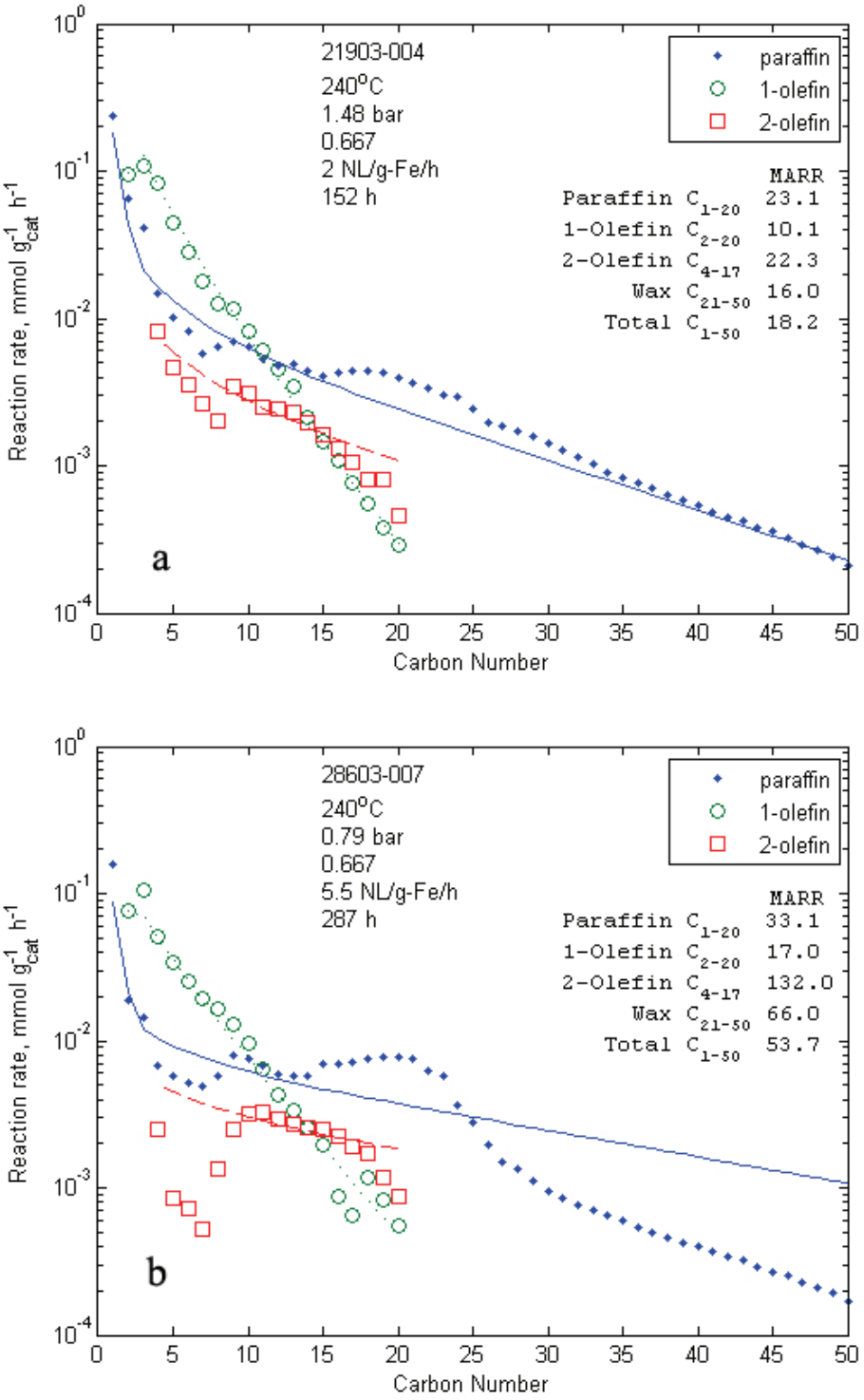

Figure 45. Comparison of predicted and experimental product distributions (extended Van der Laan and Beeenackers Model).

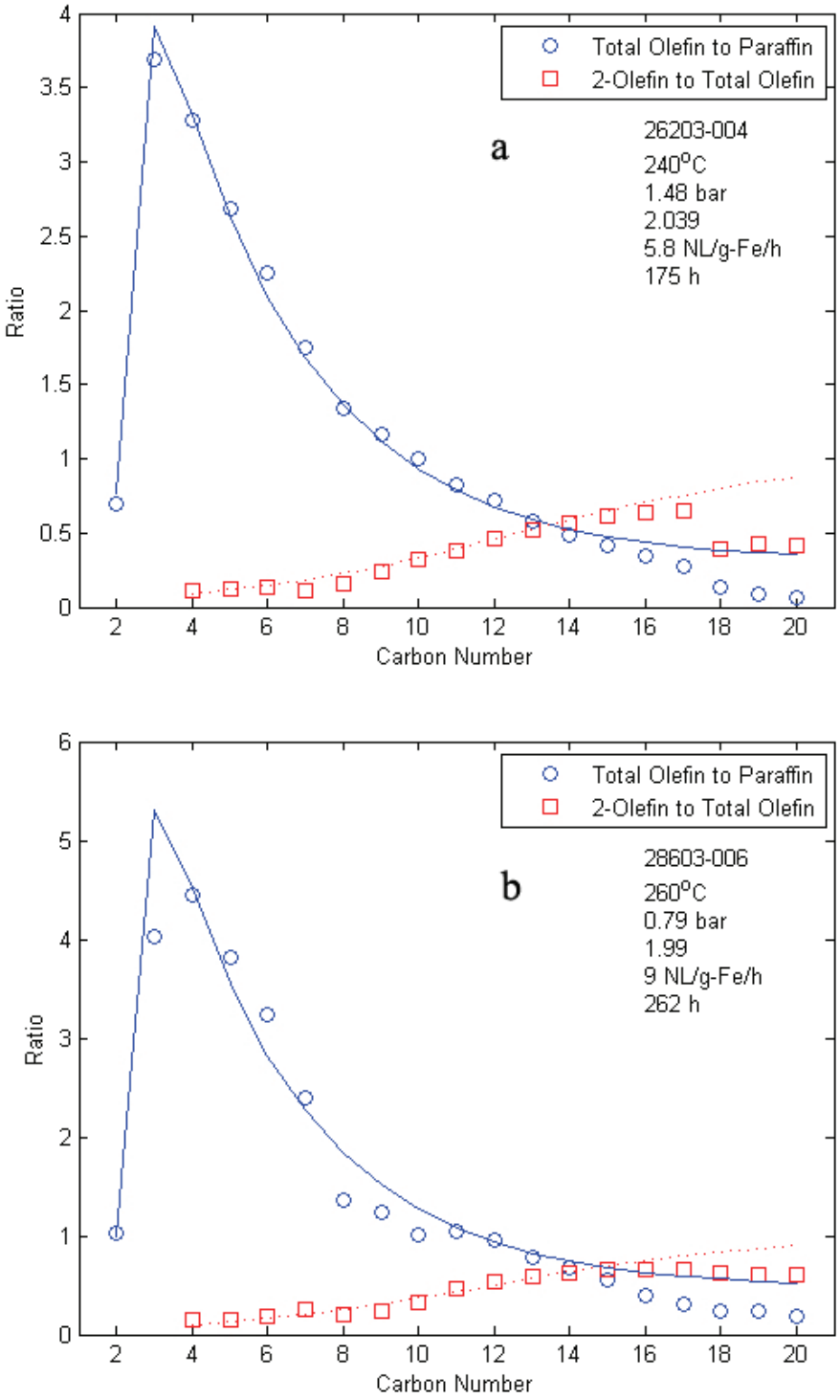

Figure 46. Total olefin to paraffin and 2-olefin to total olefin ratio (extended Van der Laan and Beeenackers Model).

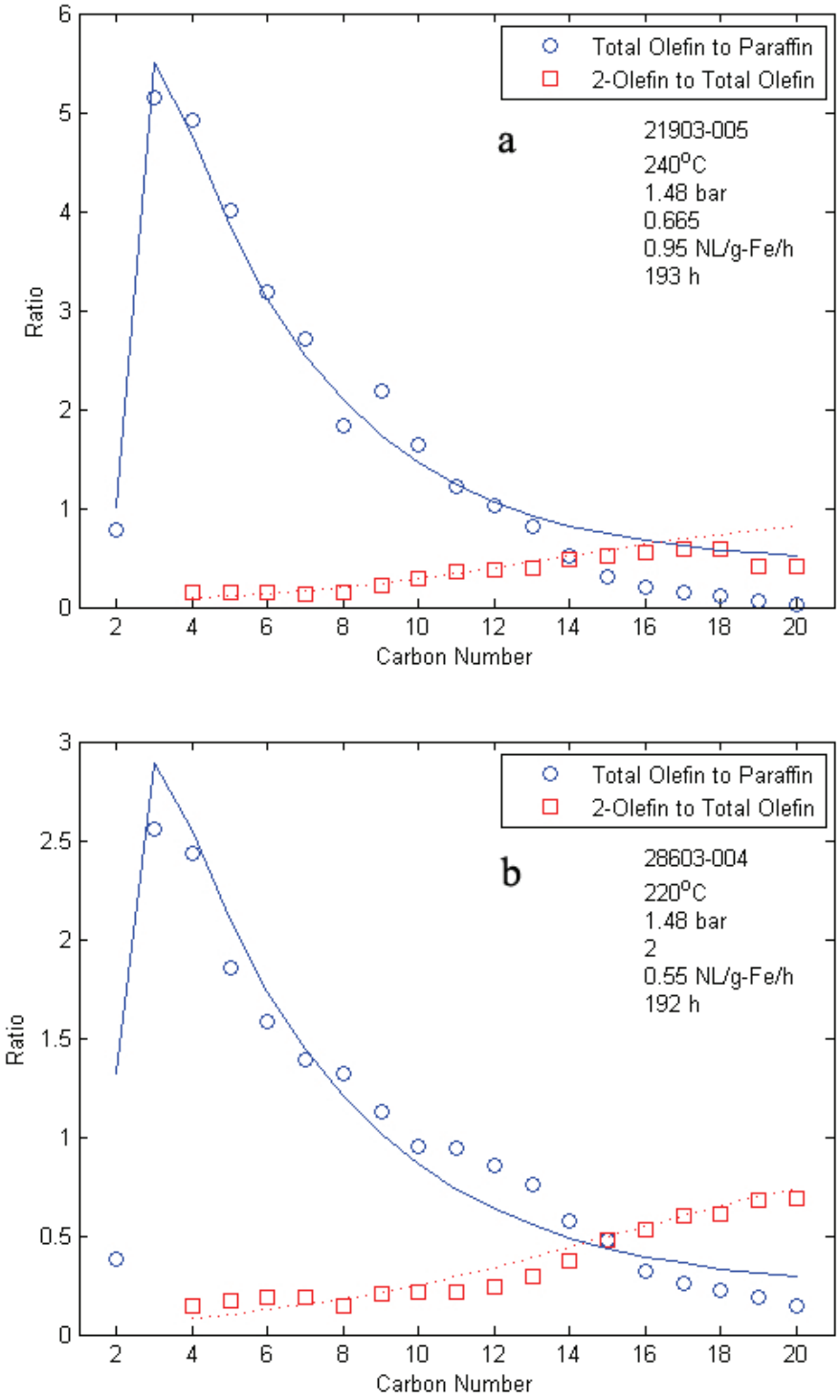

Figure 47. Total olefin to paraffin and 2-olefin to total olefin ratio (extended Van der Laan and Beeenackers Model).

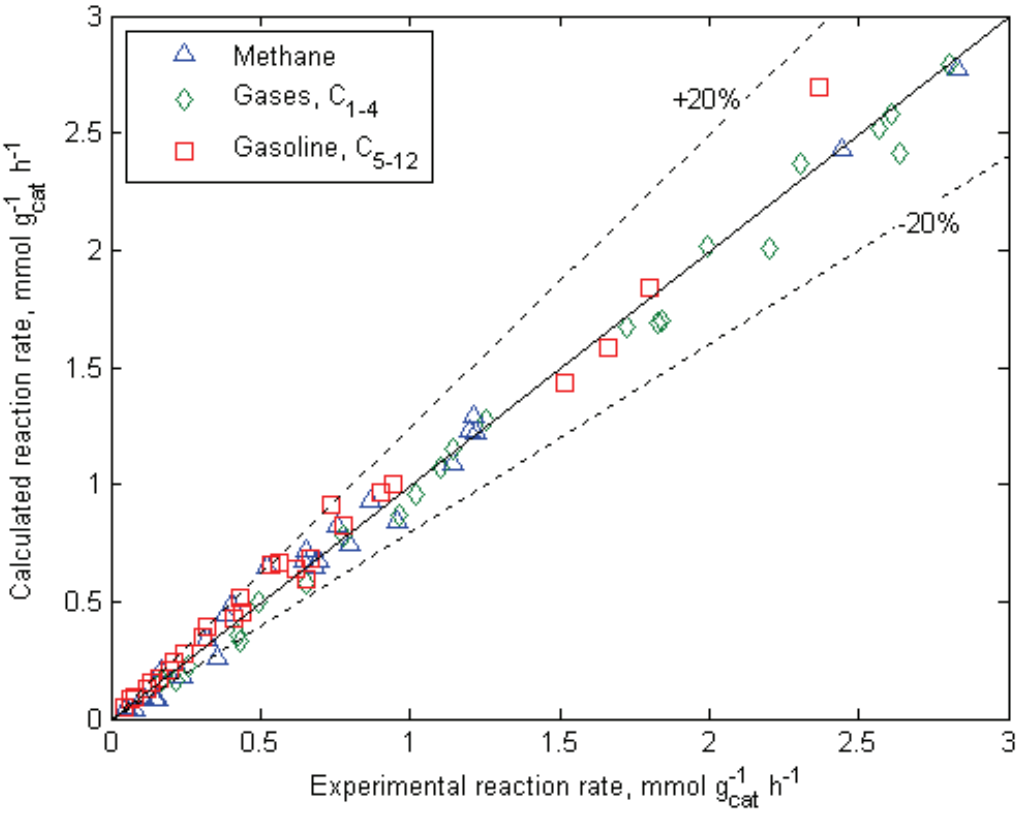

Figure 48. Parity plot for light components (extended Van der Laan and Beenackers Model).

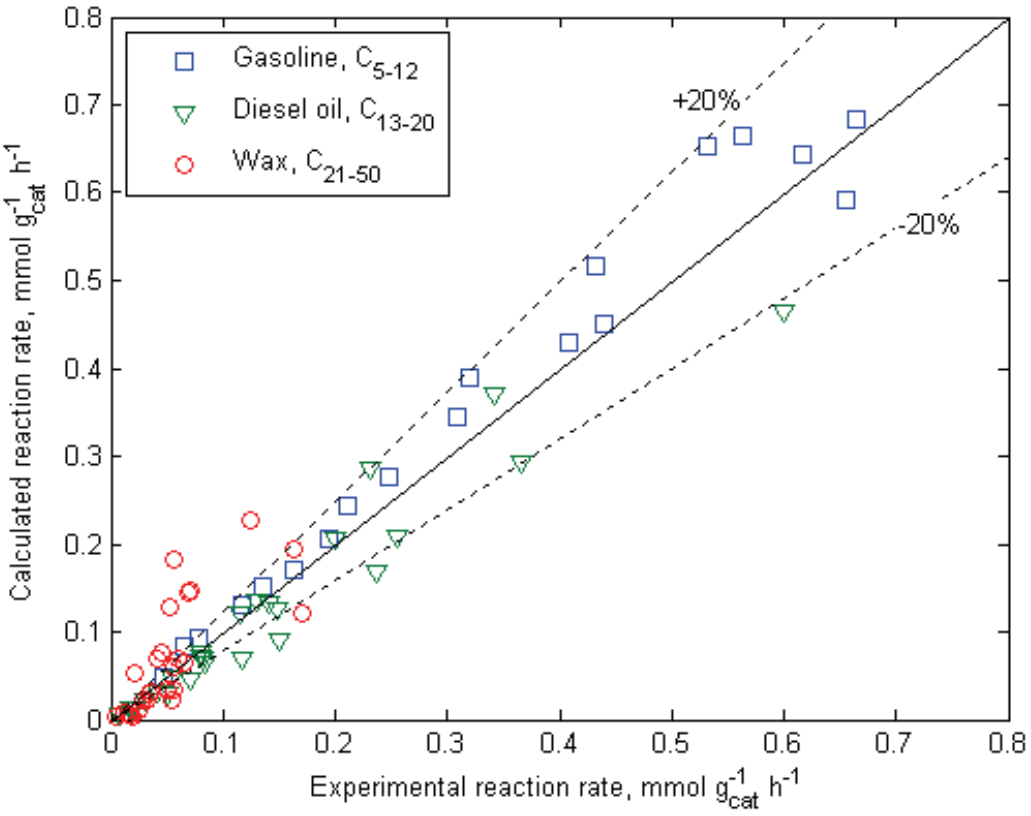

Figure 49. Parity plot for heavier components (extended Van der Laan and Beenackers Model).

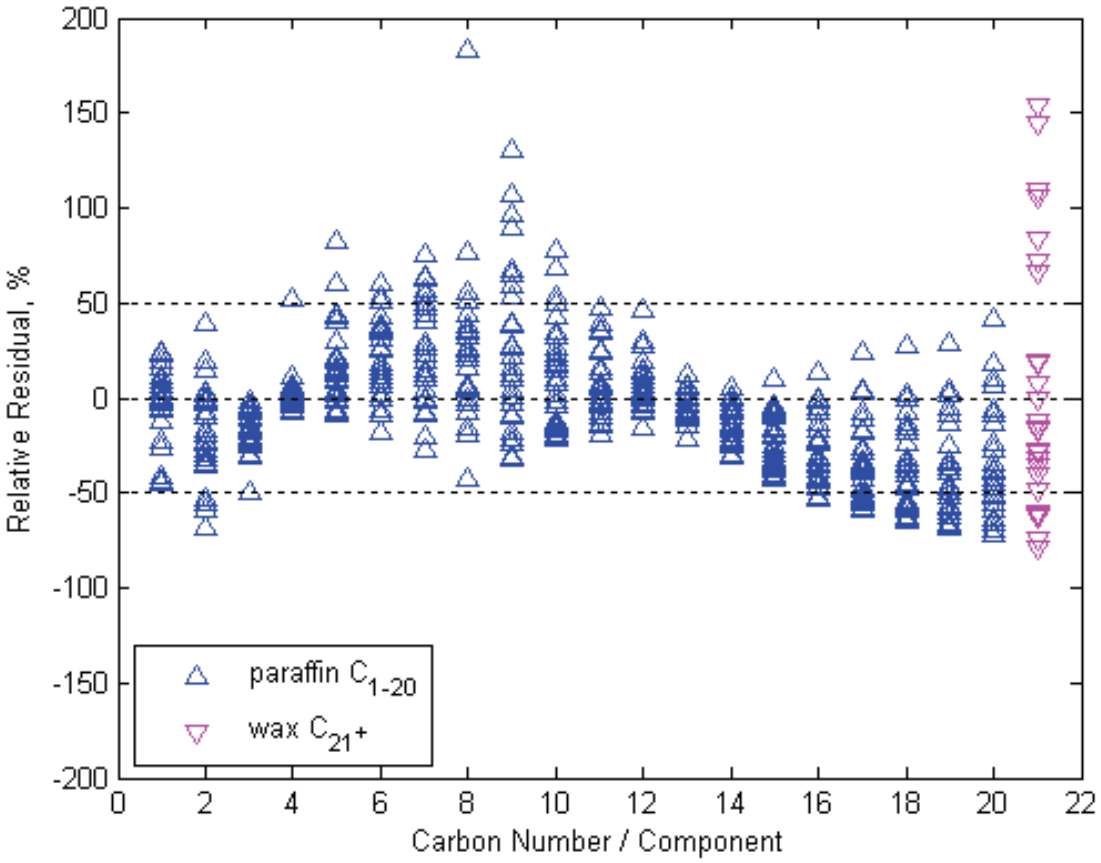

Figure 50. Relative residuals for n-paraffins (extended Van der Laan and Beenackers Model).

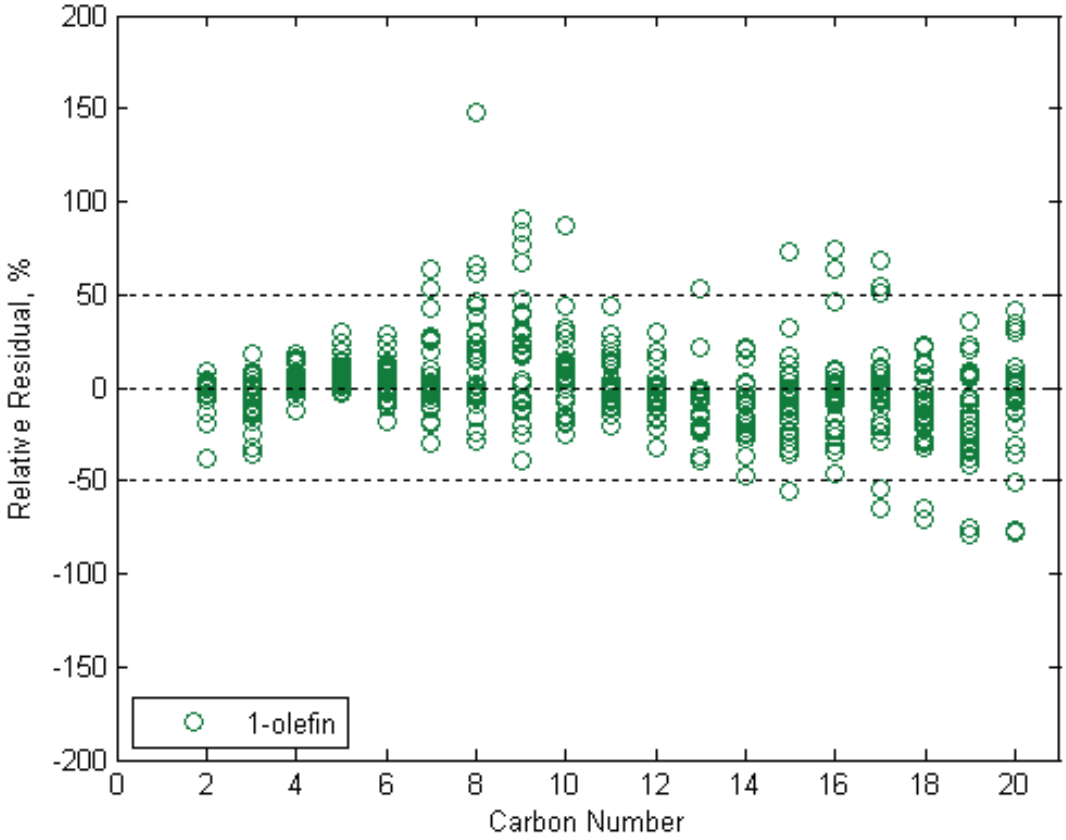

Figure 51. Relative residuals for 1-olefins (extended Van der Laan and Beenackers Model).

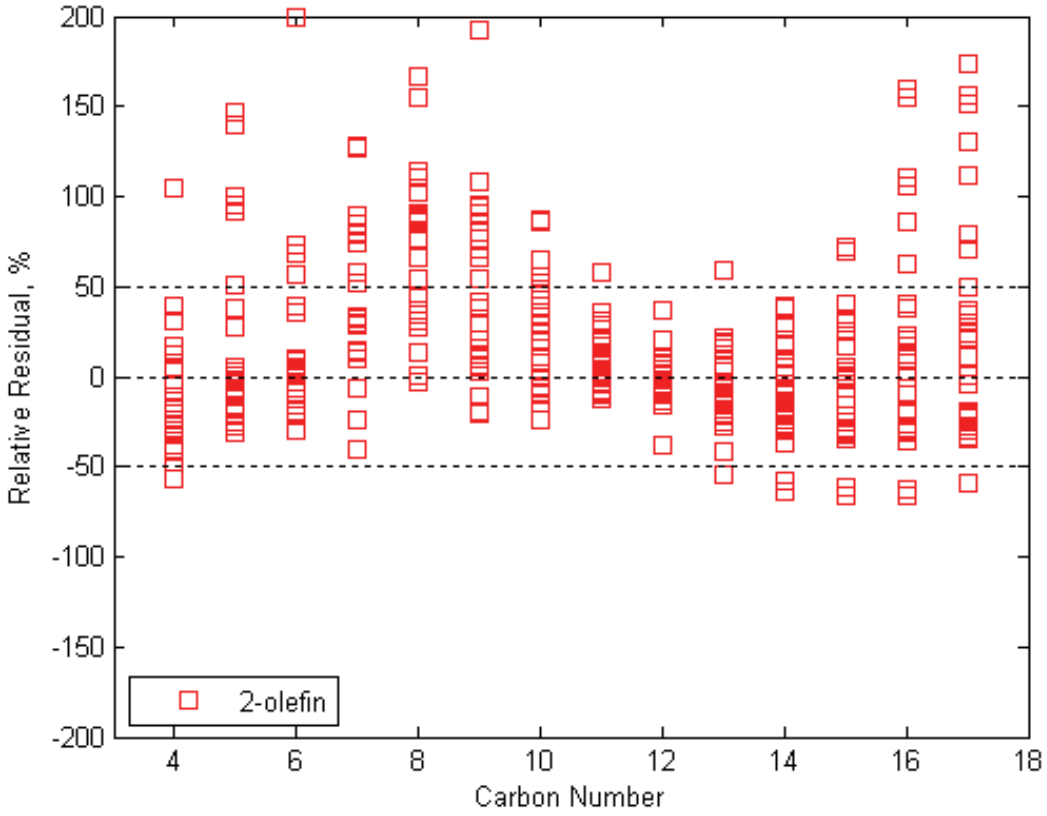

Figure 52. Relative residuals for 2-olefins (extended Van der Laan and Beenackers Model).

List of Acronyms and Abbreviations

ASF	Anderson-Schulz-Flory
EOS	Equation of state
FTS	Fischer-Tropsch synthesis
GA	Genetic algorithm
LHHW	Langmuir-Hinshelwood-Hougen-Watson
LM	Levenberg-Marquardt
LS	Large-scale (Newton large-scale method)
MARR	Mean absolute relative residual
MW	Molecular weight
ORPDM	Olefin readsorption product distribution model
PR	Peng-Robinson (equation of state)
RDS	Rate determining step
RR	Relative residual
STSR	Stirred-tank slurry reactor
SV	Space velocity (gas space velocity)
TAMU	Texas A&M University
UR	Usage ratio
VLE	Vapor-Liquid Equilibrium
WGS	Water-gas-shift (reaction)

Appendix A

Modified Peng-Robinson Equation of State

Peng and Robinson (1976) proposed the EOS of following form:

$$p = \frac{RT}{\upsilon - b} - \frac{a}{\upsilon(\upsilon + b) + b(\upsilon - b)} \tag{A.1}$$

where: p = pressure; T = temperature, υ = molar volume. Parameters *a* and *b* are correlated with critical properties of components and follow the mixing rules. The mixing rules are

$$a = \sum_{i=1}^{v} \sum_{j=1}^{v} z_i \cdot z_j \cdot a_{i,j} \tag{A.2}$$

$$a_{i,j} = \left(a_i \cdot a_j\right)^{0.5} \cdot \left(1 - k_{i,j}\right) \tag{A.3}$$

$$a_i = a_{c,i} \cdot \alpha_i(T) \tag{A.4}$$

$$a_{c,i} = \frac{0.45724 \cdot R^2 {T_{c,i}}^2}{P_{c,i}} \tag{A.5}$$

$$b = \sum z_i \cdot b_i \tag{A.6}$$

$$b_i = \frac{0.0778 \cdot R \cdot T_{c,i}}{P_{c,i}} \tag{A.7}$$

where: z is a mole fraction of species in the liquid x or in the gas y, T_c and P_c are the critical temperature and pressure for pure component, $k_{i,j}$ is a binary interaction factor between two species and temperature dependent coefficient α is:

$$\alpha_i(T) = \left(1 + f_i(\varpi) \cdot \left(1 - T_{r,i}^{0.5}\right)\right)^2 \tag{A.8}$$

where: $T_{r,i}$ is reduced temperature, $T_{r,i} = T/T_{c,i}$ (T and T_c are in *K*) and $f_i(\varpi)$ is a function of acentric factor ω,

$$f_i(\varpi) = 0.37464 + 1.54226 \cdot \omega_i - 0.26992 \cdot {\omega_i}^2 \tag{A.9}$$

Li and Froment (1996) proposed the following modification of $f_i(\varpi)$ function (for permanent gases and water only):

$$f_i(\varpi) = 0.3608281 + 1.14748 \cdot \omega_i - 0.5005316 \cdot {\omega_i}^2 - 0.04187888 \cdot {\omega_i}^3 \quad \text{(A.10)}$$

The Equation (A.1) can be expressed in dimensionless form by introducing a compressibility Z as follows:

$$Z^3 - (1 - B) \cdot Z^2 + \left(A - 2A - 3B^2\right) \cdot Z - \left(AB - B^2 - B^3\right) = 0 \quad \text{(A.11)}$$

where the dimensionless parameters A and B are

$$A = \frac{a \cdot P}{R^2 T^2} \quad \text{(A.12)}$$

$$B = \frac{b \cdot P}{R \cdot T} \quad \text{(A.13)}$$

and the compressibility factor is:

$$Z = \frac{P \cdot \upsilon}{R \cdot T} \quad \text{(A.14)}$$

Equation A.11 yields one root for a one-phase system or three roots for a two-phase mixture system. In case of the two-phase region, the largest root gives the compressibility factor Z of the vapor, whereas the smallest positive one gives the compressibility factor Z of the liquid.

Appendix B

Critical Properties of Durasyn 164 Oil

Durasyn 164 oil was used as a start-up fluid in the STSR tests of the Ruhrchemie catalyst, and it is present in the liquid withdrawn from the reactor during Fischer-Tropsch synthesis. Its critical properties and acentric factor are needed for the VLE calculations. The following information was obtained from the Amoco (BP group) Co. (manufacturer of Durasyn):

- Durasyn is a mixture of polyalfaolefins; i.e. mixture of 1-decene dimers, trimers, tetramers and higher oligomers.
- Its boiling point is 375 °C to 505 °C
- Average molecular weight is ~ 420 g/mol

In order to estimate the properties needed for the VLE calculations it was assumed that Durasyn is 1-decene trimer (416.8 g/mol). The structure of 1-decene trimer is shown in Figure B.1.

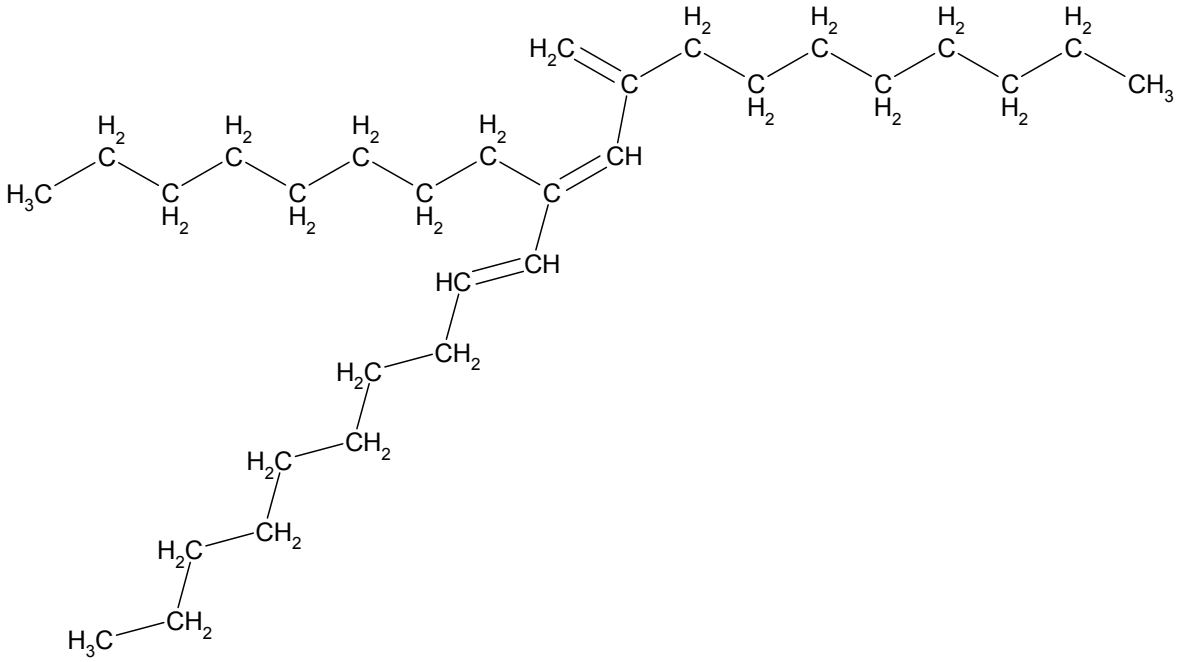

Figure B.1. 1-Decene trimer structure

Critical pressure

We have used Joback's group contribution method to calculate the critical pressure of Durasyn (Joback, 1984; Joback and Reid 1987). The Joback's method is modification of the Lydersen's method (Poling *et al*., 2001). According to this method the critical pressure is calculated as:

$$P_c(bar) = \left[0.113 + 0.0032 \cdot N_{atoms} - \sum_k N_k \cdot (pck) \right]^{-2} \quad \text{(B.1)}$$

where: N_k and pck are group number and group contribution, respectively; N_{atoms} is a total number of atoms in molecule. The *pck*-values are provided contributors and they are characteristic for particular molecule group. Parameter values as well as groups and atom numbers needed for calculation of critical properties of Durasyn are provided in Table B.1.

Table B.1. Parameters needed for Joback's Method (Poling et al., 2001).

Groups	N_k	*tck*	*pck*	N_{atoms}
-CH3	3	0.0141	-0.0012	12
=CH2	1	0.0113	-0.0028	3
=CH-	3	0.0129	-0.0006	6
=C<	2	0.0117	0.0011	2
-CH2-	21	0.0189	0	63
Total	30			86

Average error for compounds with 3 or more carbon atoms is less then 5% (Poling *et al*., 2001). The critical pressure predicted by this method for n-paraffins is in very good agreement with experimental data reported in the literature (Reid *et al*., 1977; Ambrose and Tsonopoulos, 1995; Passut and Danner, 1973; Poling *et al*., 2001; Nikitin *et al*., 1997; Gao *et al*., 1999, 2001) as shown in Figure B.2. Comparison of Joback's method with other methods for n-paraffin critical pressure is also shown in this figure. Experimental data in Figure B.2 are indicated by triangular points. Lydersen (1955), Marano and Holder (1997), Gao *et al*. (2001) and Joback's (Joback, 1984; Joback and Reid 1987) methods (lines in Fig. B.2) are predictions. Lydersen and Joback's methods are group contribution methods and can be used for a wide range of species

(like branched hydrocarbons), whereas Marano and Holder and Gao *et al.* predictions are valid only for n-paraffins (they are the asymptotic behavior correlation (ABC) methods).

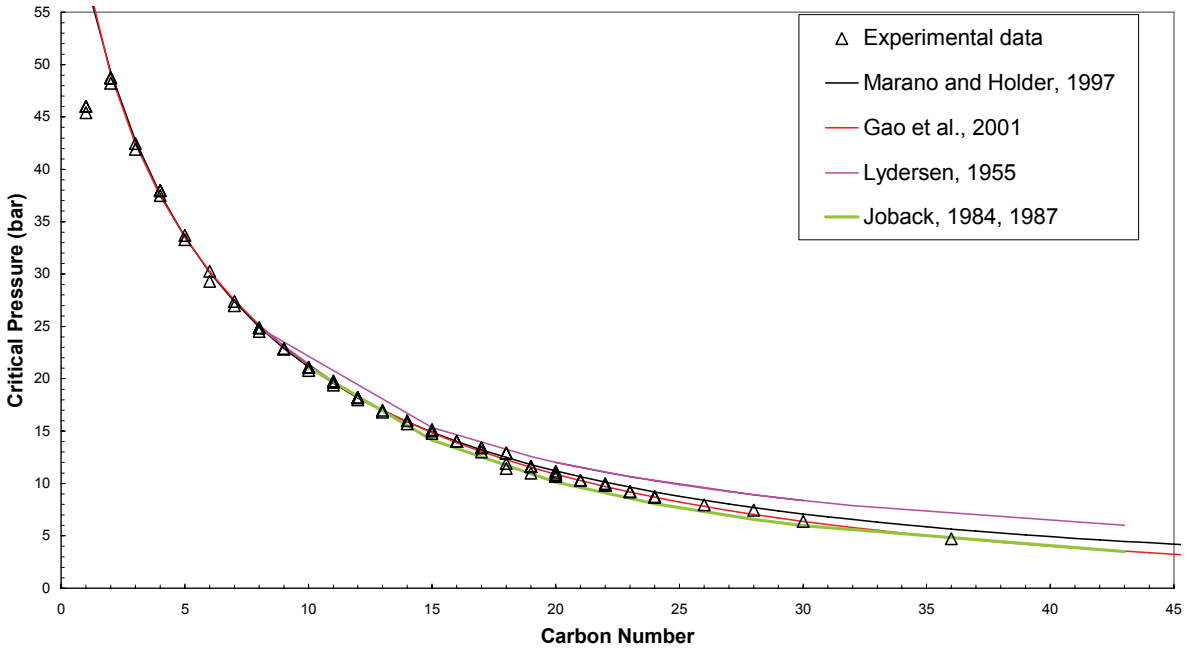

Figure B.2. Predictions of the critical pressure of n-paraffins.

Critical temperature

We have used two group contribution methods to calculate the critical temperature: Joback (Joback, 1984; Joback and Reid, 1987) and Klincewicz's method (Klincewicz and Reid, 1984).

Joback's method requires a boiling point and structure of a molecule to predict the critical temperature of a compound:

$$T_c(K) = T_b(K) \cdot \left[0.584 + 0.965 \cdot \left\{ \sum_k N_k \cdot (tck) \right\} - \left\{ \sum_k N_k \cdot (tck) \right\}^2 \right]^{-1} \qquad \text{(B.2)}$$

where: N_k and tck are group number and group contribution, respectively; T_b is a boiling point. Average error for compounds with 3 or more carbon atoms is 1.1% (Poling *et al.*, 2001). The critical temperature predicted by this method for n-paraffins is in good agreement with

experimental data up to C_{24}, but beyond C_{28} the error is greater then 5%. Therefore, we also used the Klincewicz's method to calculate the critical temperature of Durasyn, since it is more accurate for n-paraffins around C_{30}, but is less accurate for paraffins up to C_{24} (Figure B.3). Besides the boiling point and the structure of molecule, this method requires a molecular weight of the compound:

$$T_c(K) = 45.40 - 0.77 \cdot MW(g/mol) + 1.55 \cdot T_b(K) + \left\{ \sum_k N_k \cdot (tck) \right\} \tag{B.3}$$

where: N_k and tck are group number and group contribution, respectively; T_b is a boiling point; MW is a molecular weight of compound. The N_k and *tck*-values for Durasyn are shown in Table B.1.

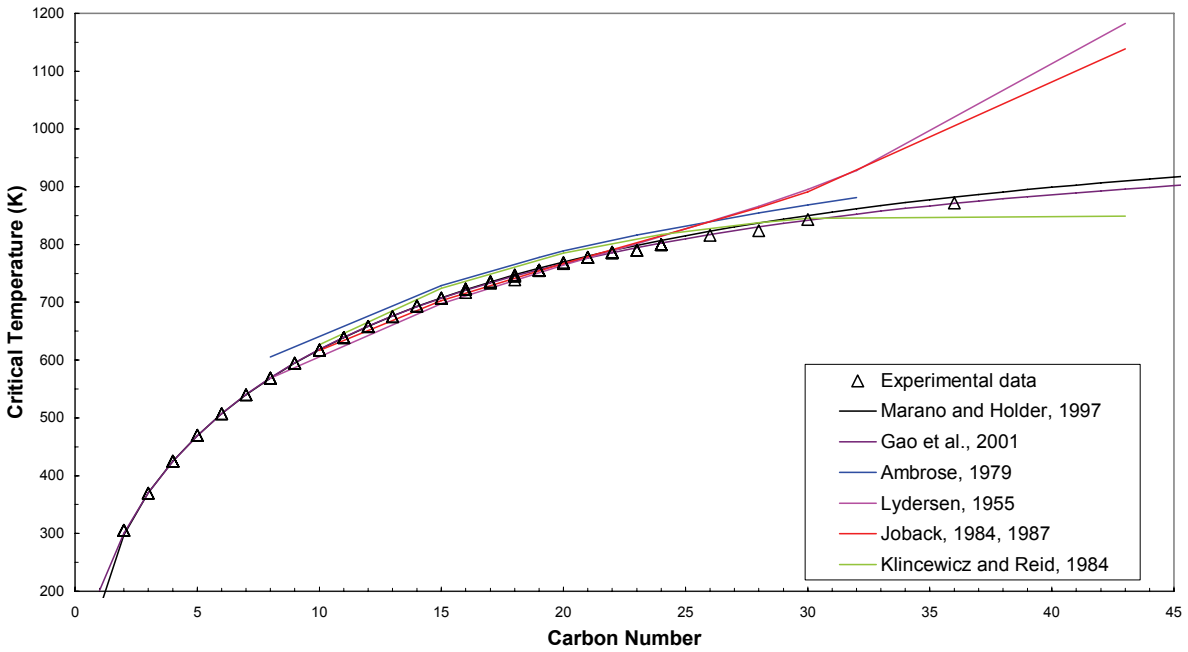

Figure B.3. Predictions of the critical temperature for n-paraffins.

A comparison of these two (Joback's and Klincewicz's) and other prediction methods with experimental data is shown in the Figure B.3 for n-paraffins. Experimental data are designated with triangular points, whereas solid lines are predictions. Ambrose (1979), Lydersen (1995), Joback (Joback, 1984; Joback and Reid 1987) and Klincewicz's (Klincewicz and Reid,

1984) are group contribution methods and can be used for prediction of properties of different types of hydrocarbons. Marano and Holder (1997) and Gao *et al*. (2001) are ABC (asymptotic behavior correlation) methods that can be used only for n-paraffins. As can be seen the ABC methods provide more accurate predictions for n-paraffins but can't be used for predictions of critical properties of branched hydrocarbons.

Both of these methods (Joback's and Klincewicz's) give almost the same result for the maximum value of the critical point and similar values for the minimum T_c. However, the critical temperature range calculated by the Joback's method is more narrow than the one calculated from the Klincewicz's method (Table B.2). We used the average critical temperature calculated from the Joback's method for the VLE calculations.

Table B.2. Predicted critical properties for Durasyn.

	P_c, bar	T_c, K		T_c^{avg}
Joback	6.44	794.4	953.7	874.1
Klincewicz	-	751.5	953.0	852.2

where T_c^{avg} is the average critical temperature; $T_c^{avg} = \left(T_c^{\min} + T_c^{\max}\right)/2$.

Acentric Factor (ω)

Several methods are available for prediction of an acentric factor. Comparison of predicted values with experimental data for n-paraffins is shown in Figure B.4. Experimental data are represented by triangular points, and predictions by solid lines. Gao *et al*. (2001) and Marano and Holder (1997) methods can predict acentric factor for n-paraffins only. Gao *et al*.'s model has the best accuracy for n-paraffins experimental data. Edmister (1958), Ambrose and Walton (1989) and Lee and Kesler (1975) methods require the critical pressure, critical temperature and boiling point temperature for prediction of the acentric factor, but they can be used to predict acentric factors for different types of organic species. Ambrose and Walton's and Lee and Kesler's method have similar accuracy and are more accurate than Edmister's method for n-paraffins up to C_{20} (Fig. B.4). These two methods were used for calculation of the acentric factor of Durasyn.

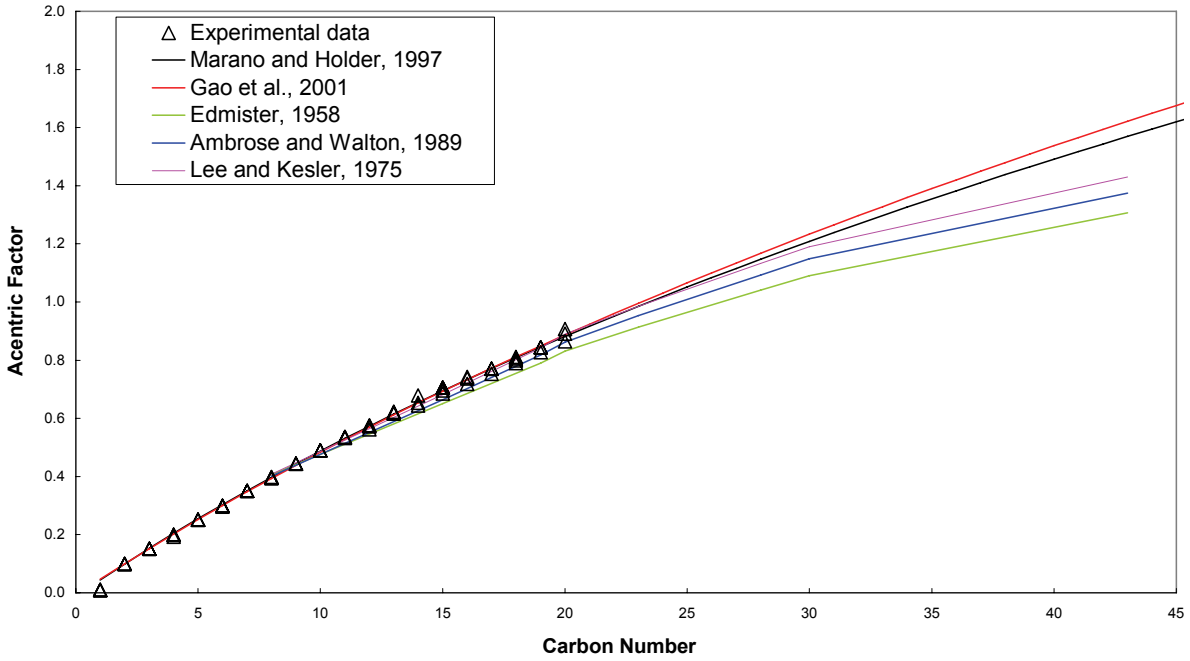

Figure B.4. Predictions of the acentric factor for n-paraffins.

The critical pressure and the critical pressure, and ratio of the boiling point to the critical temperature (T_b/T_c) of Durasyn were calculated by Joback's method. The ratio of T_b/T_c is equal to 0.816. Calculated acentric factors are shown in Table B.3.

Table B.3. Predicted values of the acentric factor for Durasyn.

Acentric factor (ω)	
Ambrose and Walton	0.546
Lee and Kesler	0.569

For the VLE calculations we used the critical pressure and the average critical temperature from the Joback's method, and the acentric factor from the Lee and Kesler's method (Table B.4).

Table B.4. Properties of Durasyn for the VLE calculations.

P_c, bar	T_c, K	ω
6.44	874.1	0.569

The corresponding experimental values of critical properties for C_{30} n-paraffin are: T_c = 843 K, Pc = 6.36 bar, whereas the calculated value of the acentric factor is ω =1.233.

Appendix C
Calculation of the Vapor-Liquid Equilibrium

There are two phases in the reactor under the reaction conditions: the gas phase and the liquid phase (Figure C.1). The gas phase in the reactor consists of components that are measured at the exit of the reactor in one of the three phases: tail gas, aqueous phase and organic phase (see Figure 2). The gas phase components are: inorganic species (H_2, CO, CO_2, H_2O) and hydrocarbons (up to ~ C_{30}). The liquid phase in the reactor consists of wax (high molecular weight products produced during F-T synthesis) and the start-up fluid (Durasyn).

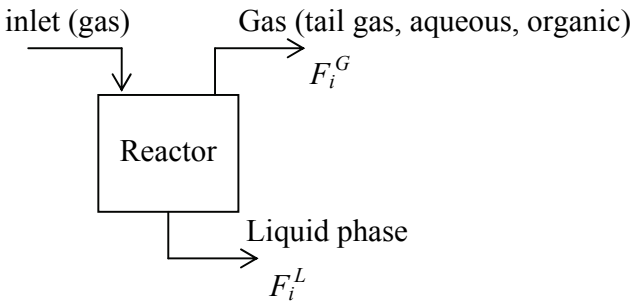

Figure C.1. Reactor schematics for the VLE calculations

Molar flow rate of *i* component in the gas phase F_i^G (*mol/h*), is calculated as follows

$$F_i^G = F_i^{tail} + F_i^{aqu} + \cdot F_i^{org} \tag{C.1}$$

whereas for the liquid phase F_i^L (*mol/h*) is

$$F_i^L = F_i^{wax} \tag{C.2}$$

where "wax" refers to analyzed hydrocarbons ($C_{10\text{-}50}$), unanalyzed wax and Durasyn.

The following species were taken into account in the VLE calculations: inorganic species (H_2, CO, CO_2, H_2O), n-paraffins (C_1-C_{20}), 1-olefins (C_2-C_{15}), Durasyn (C_{30}) and two pseudo-components: C_{21}^+ paraffins and unanalyzed wax (with critical properties and acentric factor of

C_{30} n-paraffin). Thus, the VLE calculations were done for a two-phase mixture of 41 components (species).

The pseudo-component C_{21}^{+} represents lumped hydrocarbons (up to C_{50}) and its molar flow rate is calculated as a sum of molar flow rates of paraffins from C_{21} to C_{50} (some of these are present in both the gas and the liquid phase):

$$F_{C_{21}+}^{G,L} = \sum_{i=21}^{50} F_i^{G,L} \tag{C.3}$$

where superscripts *G* and *L* denote vapor and liquid phases, respectively.

The unanalyzed wax was treated like n-paraffin with 30 carbon atoms, whereas critical properties of Durasyn were calculated as described in Appendix B.

Experimental values of mole fractions in the gas and liquid phases were calculated as follows:

$$y_i^{\exp} = \frac{F_i^G}{\sum_{i\in\Omega} F_i^G} \tag{C.4}$$

$$x_i^{\exp} = \frac{F_i^L}{\sum_{i\in\Omega} F_i^L} \tag{C.5}$$

where F^G and F^L represent molar flow rates of species in the gas and liquid phase, respectively; Ω represents the set of species that were included in VLE calculation (H_2, CO, CO_2, water, paraffins $C_{1\text{-}20}$, 1-olefins $C_{2\text{-}15}$, lumped pseudo-component C_{21}^{+}, pseudo-component unanalyzed wax and Durasyn).

However, experimental molar flow rates are not available for all components in both phases present in the reactor. For example inorganic species and lower molecular weight hydrocarbons (~C_1-C_9) were not analyzed in the liquid phase, whereas high molecular weight hydrocarbons (>C_{30}) are not detected in the products leaving the reactor as the gas phase (Figure C.1). Therefore, we need to apply some method to calculate molar flow rates of all species in the liquid and the gas phase. This is accomplished through VLE calculations.

VLE Calculations Procedure

Figure C.2 illustrates the input and output variables in VLE calculations.

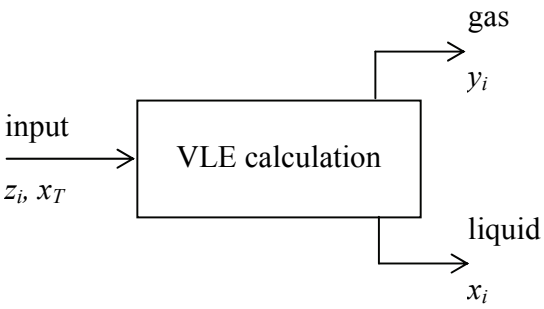

Figure C.2. VLE calculations schematic

Total mole fraction of component *i* (z_i) at the reactor exit is calculated as follows:

$$z_i = \frac{F_i^G + F_i^L}{\sum_i \left(F_i^G + F_i^L\right)} \tag{C.6}$$

Mole fraction of the liquid phase (x_T) is given by:

$$x_T = \frac{\sum_i F_i^L}{\sum_i \left(F_i^G + F_i^L\right)} = \frac{F_T^L}{F_T} \tag{C.7}$$

whereas the total mole fraction of the gas phase is:

$$y_T = 1 - x_T \tag{C.8}$$

Assuming that the gas and the liquid phase are in thermodynamic equilibrium one has to solve the following set of equations:

$$\frac{y_i}{x_i} = \frac{\hat{\phi}_i^L(x_i)}{\hat{\phi}_i^G(y_i)} \tag{C.9}$$

$$x_i \cdot x_T + y_i \cdot (1 - x_T) = z_i \tag{C.10}$$

This is the nonlinear set of equations where fugacity coefficients $\hat{\phi}_i^L(x_i), \hat{\phi}_i^G(y_i)$ are functions of P, T and composition. The total mole fraction of species z_i and total mole fraction of liquid phase x_T are known from the product analysis, whereas mole fractions of species in the liquid (x_i) and gas (y_i) are unknown.

Algorithm for calculation of vapor-liquid equilibrium

1. Guess initial values of the mole fractions of all species in the liquid and the gas phase

$$x_i, y_i$$

2. Solve the modified Peng –Robinson EOS and calculate fugacity coefficients in the gas $\hat{\phi}_i^V$ and liquid phase $\hat{\phi}_i^L$ corresponding to the current values of x_i and y_i.

Inputs into this subroutine are: composition of the liquid and gas phase; the system temperature and pressure, as well as critical properties (temperature, pressure, acentric factor) of all species.

3. Calculation of *K*-values:

$$K_i = \frac{\hat{\phi}_i^L}{\hat{\phi}_i^V}. \tag{C.11}$$

4. Calculation of "new" x_i and y_i values:

$$x_i = \frac{z_i}{x_T + K_i \cdot (1 - x_T)} \tag{C.12}$$

$$y_i = K_i \cdot x_i \tag{C.13}$$

Equation (C.12) is obtained from mass balance on species *i* at the exit as follows:

Molar flow rate of *i* in the liquid + Molar flow rate of *i* in the gas = Molar flow rate of *i* in the overall flux at the reactor exit, i.e.:

$$x_i \cdot F_T^L + y_i \cdot F_T^G = z_i \cdot \left(F_T^L + F_T^G\right) \tag{C.14}$$

where: F_T^L, F_T^G are the total molar flow rates of the liquid and the gas phase, respectively.

Divide (C.14) by the total molar flow rate at the reactor exit ($F_T = F_T^L + F_T^G$), to obtain:

$$x_i \cdot x_T + y_i \cdot y_T = z_i \tag{C.15}$$

Combining (C.6) and (C.13) we obtain:

$$x_i \cdot x_T + x_i \cdot K_i \cdot (1 - x_T) = z_i$$

which after rearrangement leads to (C.12).

Equation (C.11) follows from the definitions of the K-value and fugacity coefficients:

$$K_i \equiv \frac{y_i}{x_i} \tag{C.16}$$

$$y_i \cdot \hat{\phi}_i^V \cdot P = x_i \cdot \hat{\phi}_i^L \cdot P \tag{C.17}$$

In equilibrium: $\hat{f}_i^V = \hat{f}_i^L$, and combining the last two equations one obtains (C.11).

5. Checking of objective function for convergence. If the objective function is less or equal to criterion for convergence ε then finish.

$$if \left(S_{VLE} = \sum_i \left| \hat{f}_i^V - \hat{f}_i^L \right| \le \varepsilon \right) then\ finish \tag{C.18}$$

where $\hat{f}_i^V$ and $\hat{f}_i^L$ are fugacities of *i* species in the vapor and liquid phase, respectively.

6. If (C.18) is not satisfied go back to step 2 and keep on iterating until the criterion for convergence is satisfied.

As an illustration of the above procedure we show results from one set of calculations (Table C.1 and Figure C.3). Additional results (in graphical form) are shown in the Results and Discussion section of the report (Figures 28 and 29).

Table C.1. Example of VLE calculation

MB: 21903_001

xT: 0.0109369 - mole fraction of total liquid at the exit (Input to subroutine)

		Input	Experimental values		Output - calculated values			
Group	**Carbon #**	**z**	**yexp**	**xexp**	**y**	**x**	**K**	**xnorm**
Carbon Monoxide		0.4268405	0.43156	0	0.43068	0.024686	17.45	
Hydrogen		0.2495477	0.252307	0	0.251793	0.011932	21.10	
Carbon Dioxide		0.2200364	0.222469	0	0.222016	0.024698	8.99	
Water		0.051163	0.051729	0	0.051623	0.011289	4.57	
paraffin	1	0.0114569	0.011584	0	0.01156	0.00099	11.68	
	2	0.0033668	0.003404	0	0.003397	0.000471	7.22	
	3	0.0011265	0.001139	0	0.001137	0.000231	4.93	
	4	0.0006931	0.000701	0	0.000699	0.000207	3.37	
	5	0.0004922	0.000498	0	0.000497	0.000212	2.34	
	6	0.0003209	0.000324	0	0.000324	0.000197	1.64	
	7	0.000271	0.000274	0	0.000273	0.000236	1.16	
	8	0.0003744	0.000379	0	0.000378	0.000461	0.819	
	9	0.0004623	0.000467	0	0.000466	0.000801	0.582	
	10	0.0003244	0.000315	0.001151	0.000319	0.000772	0.414	0.000842
	11	0.0002698	0.000255	0.001579	0.000263	0.000882	0.298	0.000963
	12	0.0002293	0.00021	0.002009	0.00022	0.001045	0.211	0.00114
	13	0.0002199	0.000194	0.002605	0.000207	0.001382	0.150	0.001508
	14	0.0002136	0.00018	0.00326	0.000196	0.001841	0.106	0.002009
	15	0.0001954	0.000155	0.003852	0.000173	0.002249	0.0768	0.002454
	16	0.0001826	0.000131	0.004863	0.000154	0.002779	0.0554	0.003033
	17	0.0001652	0.000105	0.005644	0.000132	0.003201	0.0411	0.003494
	18	0.0001533	8.32E-05	0.006494	0.000114	0.003698	0.0309	0.004036
	19	0.0001325	6.25E-05	0.006457	8.85E-05	0.00411	0.0215	0.004487
	20	0.0001122	4.6E-05	0.006094	6.41E-05	0.004461	0.0144	0.004869
1-olefin	2	0.003509	0.003548	0	0.003541	0.000434	8.15	
	3	0.006693	0.006767	0	0.006753	0.001291	5.23	
	4	0.0036065	0.003646	0	0.003639	0.001009	3.61	
	5	0.0021617	0.002186	0	0.002181	0.00087	2.51	
	6	0.0014214	0.001437	0	0.001434	0.000827	1.73	
	7	0.0009928	0.001004	0	0.001002	0.000798	1.26	
	8	0.0007179	0.000726	0	0.000724	0.00081	0.894	
	9	0.0008199	0.000829	0	0.000827	0.001372	0.603	
	10	0.0004638	0.00046	0.000768	0.000457	0.001036	0.441	0.001131
	11	0.0002408	0.000234	0.000863	0.000235	0.000767	0.306	0.000837
	12	0.000197	0.000189	0.000881	0.00019	0.000825	0.230	0.000901
	13	0.0001451	0.000138	0.000829	0.000137	0.000887	0.154	0.000968
	14	0.0001064	9.91E-05	0.000768	9.76E-05	0.000896	0.109	0.000978
	15	7.362E-05	6.95E-05	0.000448	6.52E-05	0.000834	0.0782	0.00091
lumped C21+		0.0007026	9.65E-05	0.055512	5.47E-05	0.059292	0.0009	0.064717
unanalyzed wax		0.0013133	0	0.12008	7.49E-05	0.110604	0.0007	0.120723
Durasyn		0.0084854	0	0.775844	0.001813	0.714619	0.0025	0.78

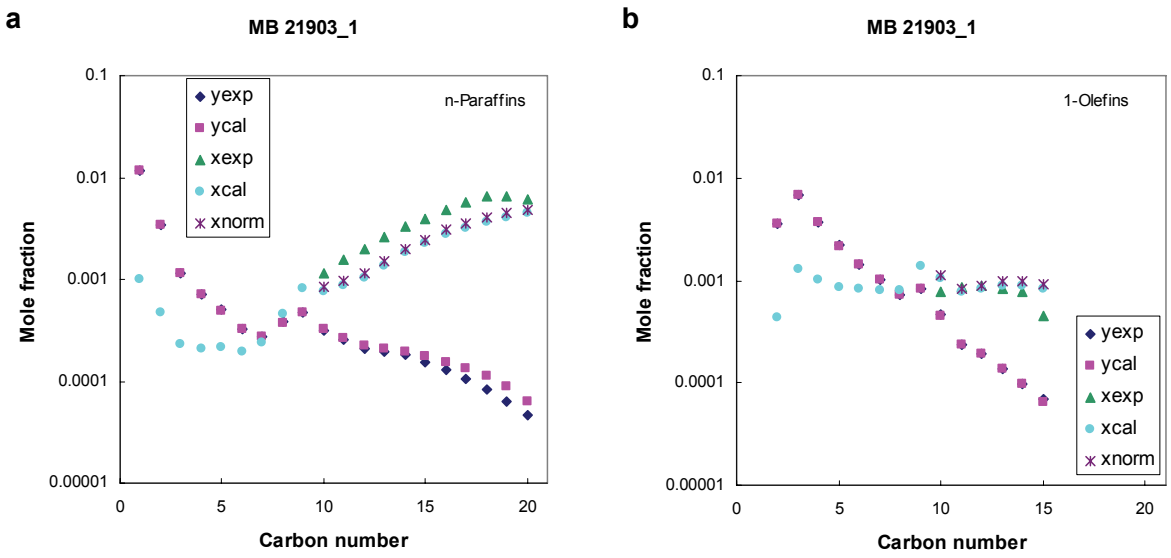

Figure C.3. Example of VLE calculations (MB 21903_1; Reaction conditions: 260°C, 1.48 bar, 0.667 H_2/CO and SV = 4 NL/g-Fe//h

Table C.1 shows all input values for the VLE calculations (xT and the overall mole fractions for all 41 components considered in the VLE calculations) and the results of the VLE calculations (mole fractions in the liquid phase and the vapor phase, and the corresponding K values). In columns 5 and 6 of this Table are experimental values in the gas phase and the liquid phase, respectively. The last column contains the normalized values of calculated mole fractions in the liquid phase defined by equation (5) in the Results and Discussion section of the report. It can be noted that the calculated values for the inorganic species in the gas phase are in excellent agreement with the corresponding experimental values.

Comparison of calculated and experimental values for hydrocarbons (except for C_{21}^+, unanalyzed wax and Durasyn) is shown in Figure C.3. There is very good agreement between the calculated and experimental values for the gas phase over a wide range of carbon numbers, whereas larger differences are observed for the liquid phase composition. We believe that the latter is caused by experimental errors in quantification of the liquid phase components (including Durasyn and wax).

Appendix D

Kinetic Model of Lox and Froment

ALII model of Lox and Froment (1993b) utilizes Langmuir-Hinshelwood-Hougen-Watson (LHHW) approach and concept of the rate-determining steps (RDS). Elementary steps (reactions) for Fischer-Tropsch synthesis (FTS) and Water-Gas-Shift (WGS) reaction are shown in Tables D.1 and D.2, respectively. Reactant molecules are adsorbed on two types of active sites, one for FTS and the second for WGS reaction, where the surface reactions take place. The model assumes two RDS in each path of formation of paraffins and olefins in the Fischer-Tropsch reaction:

- adsorption of carbon monoxide (HC1) and desorption of the paraffin (HC5) in the reaction path leading to the paraffins,
- adsorption of carbon monoxide (HC1) and desorption of the olefin (HC6) in the reaction path leading to the olefins,

Table D.1. Elementary reactions for FTS (ALII Model in Lox and Froment, 1993b).

No.	Elementary reactions	Expression of rates and equilibrium constants
HC1	$CO + C_{n-1}H_{2n-1}l_1 \rightarrow C_{n-1}H_{2n-1}\,l_1CO \quad (n \geq 1)$	$k_{HC1}\ (k_{CO})$
HC 2	$C_{n-1}H_{2n-1}\,l_1CO + H_2 = C_{n-1}H_{2n-1}\,l_1C + H_2O \ (n \geq 1)$	K_{HC2}
HC 3	$C_{n-1}H_{2n-1}\,l_1C + H_2 = C_{n-1}H_{2n-1}\,l_1CH_2 \ (n \geq 1)$	K_{HC3}
HC 4	$C_{n-1}H_{2n-1}\,l_1CH_2 = C_nH_{2n+1}l_1 \quad (n \geq 1)$	K_{HC4}
HC 5	$C_nH_{2n+1}\,l_1 + H_2 \rightarrow C_nH_{2n+2} + Hl_1 \quad (n \geq 1)$	$k_{\mathrm{HC5}}\ (k_{\mathrm{t,p}})$
HC 6	$C_nH_{2n+1}\,l_1 \rightarrow C_nH_{2n} + Hl_1 \quad (n \geq 2)$	$k_{\mathrm{HC6}}\ (k_{\mathrm{t,o}})$
HC 7	$H_2 + 2l_1 = 2Hl_1$	$K_{\mathrm{HC7}}\ (K_{\mathrm{H_2}})$

where l_1 means a vacant active site on the surface of catalyst.

Assumptions:

- Elementary reactions 2,3,4,7 are in pseudo equilibrium. Steps 1, 5 and 6 are not at equilibrium (irreversible steps).
- There is no single rate-determining step.
- Reactant molecules are absorbed at active sites onto the surface of the catalyst
- Reactant molecules are absorbed at active sites onto the surface of the catalyst

The above mechanism gives following rates for particular components (concentrations expressed in mol/m^3):

Paraffin rates:

$$R_{C_nH_{2n+2}} = \frac{k_{t,p} \cdot C_{H_2} \cdot \frac{k_{CO,HC} \cdot C_{CO}}{k_{CO,HC} \cdot C_{CO} + k_{t,p} \cdot C_{H_2}} \cdot (\alpha)^{n-1}}{1 + \frac{k_{CO,HC} \cdot C_{CO}}{k_{CO,HC} \cdot C_{CO} + k_{t,p} \cdot C_{H_2}} \cdot \frac{1}{1-\alpha}} \quad n \geq 1 \tag{D.1}$$

Olefin rates:

$$R_{C_nH_{2n}} = \frac{k_{t,o} \cdot \frac{k_{CO,HC} \cdot C_{CO}}{k_{CO,HC} \cdot C_{CO} + k_{t,p} \cdot C_{H_2}} \cdot (\alpha)^{n-1}}{1 + \frac{k_{CO,HC} \cdot C_{CO}}{k_{CO,HC} \cdot C_{CO} + k_{t,p} \cdot C_{H_2}} \cdot \frac{1}{1-\alpha}} \quad n \geq 2 \tag{D.2}$$

where

$$\alpha = \frac{k_{CO,HC} \cdot C_{CO}}{k_{CO,HC} \cdot C_{CO} + k_{t,p} \cdot C_{H_2} + k_{t,o}} \tag{D.3}$$

$$\langle k_{CO,HC} \rangle = \frac{1}{s \cdot g_{cat}} \cdot m^3 \qquad \langle k_{t,p} \rangle = \frac{1}{s \cdot g_{cat}} \cdot m^3 \qquad \langle k_{t,o} \rangle = \frac{1}{s \cdot g_{cat}} \cdot mol$$

These parameters correspond to k_1, k_5 and k_6, respectively, in Table IX (Lox and Froment, 1993b).

The following WGS mechanism was used. The RDS for the WGS reaction is a reaction between adsorbed carbon monoxide and adsorbed hydroxyl group (WGS2 in Table D.2).

Table D.2. Elementary reactions for WGS (ALII Model in Lox and Froment, 1993b).

No.	Elementary reactions	Expression of rates (small) and equilibrium constants (capital letter)
WGS1	$CO + l_2 = COl_2$	$K_{1,WGS}$
WGS2	$COl_2 + OHl_2 = COOHl_2 + l_2$	$k_{2,WGS}$, $K_{2,WGS}$
WGS3	$COOHl_2 = CO_2 + Hl_2$	$K_{3,WGS}$
WGS4	$H_2O + 2 \cdot l_2 = OHl_2 + Hl_2$	$K_{4,WGS}$
WGS5	$H_2 + 2 \cdot l_2 = 2 \cdot Hl_2$	$K_{5,WGS}$

where l_2 is a vacant active site on the surface of catalyst, but different type than l_1 (in Table D.1)

Rate of carbon dioxide formation is given by:

$$R_{CO_2} = \frac{k_v' \cdot \left(C_{H_2O} \cdot C_{CO} / {C_{H_2}}^{0.5} - \frac{1}{K_{WGS}} \cdot C_{CO_2} \cdot {C_{H_2}}^{0.5} \right)}{\left(1 + K_v \cdot C_{H_2O} / {C_{H_2}}^{0.5}\right)^2} \qquad \text{(D.4)}$$

where

$$k_v' = k_{2,WGS} \cdot \frac{K_{CO,WGS} \cdot K_{H_2O,WGS}}{{K_{H_2,WGS}}^{0.5}} \cdot {C_{l_2,tot}}^2 \qquad \left\langle k_v' \right\rangle = \frac{mol}{s \cdot g_{cat}} \cdot \left(\frac{m^3}{mol} \right)^{1.5}$$

$$K_v = \frac{K_{H_2O,WGS}}{{K_{H_2,WGS}}^{0.5}} \qquad \left\langle k_v' \right\rangle = \left(\frac{m^3}{mol} \right)^{-0.5}$$

These parameters correspond to k_v and K_v parameters in Table IX (Lox and Froment, 1993b).

The equilibrium constant of water gas shift reaction K_{WGS} is a function of temperature only (Lox and Froment, 1993b)

$$\ln(K_{WGS}) = 5078.0045 \cdot T^{-1} - 5.8972089 + 13.958689 \cdot 10^{-4} \cdot T + - 27.592844 \cdot 10^{-8} \cdot T^{2} \quad \text{(D.5)}$$

If one assumes that the only products are n-paraffins, linear olefins, carbon dioxide and water, then the rates of formation of CO, H_2, and water can be expressed from the reaction stoichiometry as:

Carbon monoxide

$$R_{CO} = \sum_{n=1}^{50}\left(\frac{-n}{1} \cdot R_{C_nH_{2n+2}}\right) + \sum_{n=2}^{50}\left(\frac{-n}{1} \cdot R_{C_nH_{2n}}\right) + \frac{-1}{1} R_{CO_2} \quad \text{(D.6)}$$

Hydrogen

$$R_{H_2} = \sum_{n=1}^{50}\left(\frac{-2n-1}{1} \cdot R_{C_nH_{2n+2}}\right) + \sum_{n=2}^{50}\left(\frac{-2n}{1} \cdot R_{C_nH_{2n}}\right) + \frac{1}{1} \cdot R_{CO_2} \quad \text{(D.7)}$$

Water

$$R_{H_2O} = \sum_{n=1}^{50}\left(\frac{n}{1} \cdot R_{C_nH_{2n+2}}\right) + \sum_{n=2}^{50}\left(\frac{n}{1} \cdot R_{C_nH_{2n}}\right) + \frac{-1}{1} R_{CO_2} \quad \text{(D.8)}$$

Note that rates of formation of H_2 and CO will be negative. Also, this model predicts that rates of formation of n-paraffins and olefins, as well as the chain growth probability factor, are independent of carbon number (Equations D.1-D.3). This model predicts that the olefin to paraffin ratio is independent of carbon number, and that the carbon number distribution follows the ideal Schulz-Flory distribution.

Appendix E

Kinetic Model of Yang et al.

Main features of the kinetic model of Yang et al. (2003) are:

- olefin readsorption,
- different kinetic rate constant for methane than for others paraffins,
- solution of hydrocarbon formation reaction rates requires numerical solution of a set of two non-linear algebraic equations,
- olefin to paraffin ratio is a function of carbon number.

Hydrocarbon Formation

Elementary reactions for this model are given in Table E.1.

Table E.1. Elementary steps of FTS (FTIII in Yang et al., 2003).

No.	Elementary reactions	Expression of rates (small) and equilibrium constants (capital letter)
HC1	$CO + l_1 \rightarrow COl_1$	$K_{HC1}\ (K_{CO})$
HC 2	$COl_1 + H_2 = H_2COl_1$	K_{HC2}
HC 3	$H_2COl_1 + H_2 = CH_2 l_1 + H_2O$	$K_{HC3}\ (K_{H_2O})$
HC 4	$H_2 + 2l_1 = 2Hl_1$	$K_{HC4}\ (K_{H_2})$
HC 5(n)	$CH_2 l_1 + CH_2\ l_1 = CH_2CH_2 l_1 + l_1$ $C_nH_{2n} l_1 + CH_2\ l_1 = C_nH_{2n}CH_2 l_1 + l_1$ $n \geq 1$	$k_{HC5}\ (k_p)$
HC 6(n)	$C_nH_{2n}\ l_1 + H\ l_1 = C_nH_{2n+1}\ l_1 + l_1$ $n \geq 1$	K_{HC6}
HC 7(n)	$C_nH_{2n+1}\ l_1 + H\ l_1 \rightarrow C_nH_{2n+2} + 2\ l_1$ $n \geq 1$	$k_{HC7M}\ (k_{t,CH_4})$ $k_{HC7}\ (k_{t,p})$
HC 8(n)	$C_nH_{2n}\ l_1 = C_nH_{2n} + l_1$ $n \geq 2$	$k^{+}_{HC8},\ k^{-}_{HC8},\ (K_{t,o})$

where l_1 means a vacant active site on the surface of catalyst.

Assumptions:

- Steps HC5, 7 and 8 are RDS. All other elementary reactions are in dynamic equilibrium;
- Steady-state conditions are reached for both the surface composition of catalyst and concentrations of all of surface intermediates involved;
- Rate constant of elementary steps for formation of hydrocarbons ($k_{t,p}$) is independent of carbon number of the intermediate involved in the elementary reaction except for methane (k_{t,CH_4});
- Reactant molecules are absorbed at active sites onto the surface of the catalyst.

Rates of formation of methane, other paraffins and olefins are given in Equations E.1, E.2 and E.3, respectively. Methane rate constant (k_{HC7M}) is different than rate constants for other paraffins (k_{HC7}).

$$R_{CH_4} = k_{HC7M} \cdot K_1 \cdot K_2 \cdot K_3 \cdot K_4 \cdot K_6 \cdot \frac{\hat{f}_{CO} \cdot \hat{f}_{H_2}^3}{\hat{f}_{H_2O}} \cdot \left(\frac{1}{DENOM} \right)^2 \tag{E.1}$$

$$R_{C_nH_{2n+2}} = k_{HC7} \cdot K_1 \cdot K_2 \cdot K_3 \cdot K_4 \cdot K_6 \cdot \frac{\hat{f}_{CO} \cdot \hat{f}_{H_2}^3}{\hat{f}_{H_2O}} \cdot \prod_{i=2}^{n} \alpha_i \cdot \left(\frac{1}{DENOM} \right)^2 \tag{E.2}$$

$$n \geq 2$$

$$R_{C_nH_{2n}} = k_{HC8}^{+} \cdot (1 - \beta_n) \cdot K_1 \cdot K_2 \cdot K_3 \cdot \frac{\hat{f}_{CO} \cdot \hat{f}_{H_2}^2}{\hat{f}_{H_2O}} \cdot \frac{1}{DENOM} \cdot \prod_{i=2}^{n} \alpha_i \tag{E.3}$$

$$n \geq 2$$

where

$$\alpha_n = \frac{k_{HC5} \cdot A_1}{k_{HC5} \cdot A_1 + k_{HC7} \cdot A_2 + k_{HC8}^{+} \cdot (1 - \beta_n) \cdot DENOM} \tag{E.4}$$

$$n \geq 2$$

$$\beta_n = \frac{k_{HC8}^{-}}{k_{HC8}^{+}} \cdot \frac{\hat{f}_{C_nH_{2n}}}{A_1 \cdot A^{n-1} + B \cdot \sum_{i=2}^{n} A^{i-2} \cdot \hat{f}_{C_{n-i+2}H_{2(n-i+2)}}} \tag{E.5}$$

$$n \geq 2$$

$$A = \frac{k_{HC5} \cdot A_1}{k_{HC5} \cdot A_1 + k_{HC7} \cdot A_2 + k_{HC8}^{+} \cdot DENOM} \tag{E.6}$$

$$B = \frac{k_{HC8}^{-} \cdot DENOM}{B_1 + k_{HC8}^{+} \cdot DENOM} \tag{E.7}$$

$$B_1 = k_{HC5} \cdot A_1 + k_{HC7} \cdot A_2 \tag{E.8}$$

$$A_1 = K_1 K_2 K_3 \cdot \frac{\hat{f}_{CO} \cdot \hat{f}_{H_2}^2}{\hat{f}_{H_2O}} \tag{E.9}$$

$$A_2 = K_4 K_6 \cdot \hat{f}_{H_2} \tag{E.10}$$

and DENOM is

$$\begin{aligned} DENOM = {} & 1 + K_4^{0.5} \cdot \hat{f}_{H_2}^{0.5} + K_1 \cdot \hat{f}_{CO} + A_1 + K_1 K_2 \cdot \hat{f}_{CO} \cdot \hat{f}_{H_2} + \\ & + K_1 \cdot K_2 \cdot K_3 \cdot K_4^{0.5} \cdot K_6 \cdot \frac{\hat{f}_{CO} \cdot \hat{f}_{H_2}^{2.5}}{\hat{f}_{H_2O}} + \\ & + A_1 \cdot \left(1 + K_4^{0.5} K_6 \cdot \hat{f}_{H_2}^{0.5}\right) \cdot \sum_{j=2}^{n} \prod_{i=2}^{j} \alpha_i \end{aligned} \tag{E.11}$$

WGS Reaction

Assumptions:

- Elementary reactions 1 – 3 and 5 (Table E.2) are in dynamic equilibrium. The 4th step is the rate-determining step (RDS);
- Reactant molecules are absorbed at active sites onto the surface of the catalyst.
- Concentrations of the adsorbed species involved in RDS reaction(s) are much larger then those of the other adsorbed species.

Table E.2. Elementary steps for WGS reaction (WGS3 in Yang et al., 2003).

No.	Elementary reactions	Expression of rates (small) and equilibrium constants (capital letter)
WGS1	$CO + l_2 = COl_2$	K_{WGS1}
WGS2	$H_2O + 2 \cdot l_2 = OHl_2 + Hl_2$	K_{WGS2}
WGS3	$COl_2 + OHl_2 = COOHl_2 + l_2$	K_{WGS3}
WGS4	$COOHl_2 = CO_2 + Hl_2$	k_{WGS4} , K_{WGS4}
WGS5	$2 \cdot Hl_2 = H_2 + 2 \cdot l_2$	$1/K_{WGS5}$

where l_2 means a vacant active site on the surface of catalyst, but different type than l_C.

The above mechanism leads to the following rate of carbon dioxide formation:

$$R_{CO_2} = k_V \cdot \left(\frac{\hat{f}_{CO} \cdot \hat{f}_{H_2O} - \frac{1}{K_{WGS}} \cdot \hat{f}_{CO_2} \cdot \hat{f}_{H_2}}{\hat{f}_{H_2}^{0.5} + K_V \cdot \hat{f}_{CO} \cdot \hat{f}_{H_2O}} \right) \tag{E.12}$$

where K_{WGS} is given by Equation (D.5) and

$$K_V = K_{WGS} \frac{K_{WGS5}^{0.5}}{K_{WGS4}} \tag{E.13}$$

$$k_V = k_{WGS4} K_{WGS} \tag{E.14}$$

Appendix F

Hydrocarbon Selectivity Model of Van der Laan and Beenackers

Van der Laan and Beenackers (1998, 1999) developed olefin readsorption product distribution model (ORPDM) for formation of hydrocarbons in Fischer-Tropsch synthesis (FTS). Reaction network of hydrocarbon formation for this model is presented in Figure F.1. Chain growth is initiated by hydrogenation of adsorbed monomer ($^*CH_2$) to adsorbed methyl group ($^*CH_3$). Chain propagation occurs via insertion of adsorbed monomer into adsorbed alkyl species ($^*C_nH_{2n+1}$), which can terminate to paraffin (C_nH_{2n+2}) by hydrogenation or to olefin (C_nH_{2n}) by dehydrogenation (hydrogen abstraction). According to this reaction network olefin readsorbtion leads to adsorbed alkyl species, which can propagate or terminate. Detailed stoichiometry and kinetic equations of ORPDM model for its elementary reactions are presented in Table F.1.

ORPDM is selectivity model with pseudo-constants (λ), which include true kinetic constants (k) and concentrations of some intermediates. Van der Laan and Beenackers assumed that kinetic parameters (rate constant) for methane and ethylene formation are different than the corresponding rate constants for C_2^+ paraffins and C_3^+ olefins.

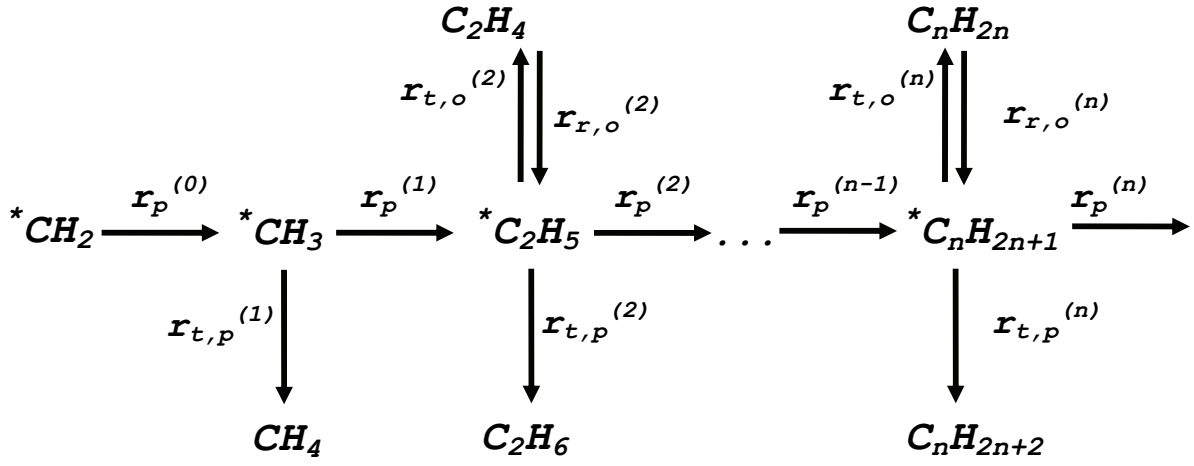

Figure F.1. Reaction network of hydrocarbon formation (FTS) with olefin readsorption.

Table F.1. Elementary steps of FTS (Van der Laan and Beenackers 1998)

No.	Stoichiometry equations	Kinetic equations
HC1	**formation of adsorbed methyl group C_1^*** $CH_2,s_1 + H,s_1 \xrightarrow{k_{p,1}} CH_3,s_1$	$r_p^{(0)} = k_{p,1} \cdot \theta_{CH_2,s_1} \cdot \theta_{H,s_1} = \lambda_1$
HC2	**propagation** $C_nH_{2n+1},s_1 + CH_2,s_1 \xrightarrow{k_p} C_{n+1}H_{2n+3},s_1$ $n = 1,2,...$	$r_p^{(n)} = k_p \cdot \theta_{CH_2,s_1} \cdot \theta_{C_nH_{2n+1},s_1}$ $r_p^{(n)} = \lambda_p \cdot \theta_{C_nH_{2n+1},s_1}$ *where* $\lambda_p = k_p \cdot \theta_{CH_2,s_1}$ $n = 1,2,...$
HC3	**termination to paraffin** $C_nH_{2n+1},s_1 + H,s_1 \xrightarrow{k_{t,p}} C_nH_{2n+2} + 2s_1$ $n = 1,2,...$	$r_{t,p}^{(n)} = k_{t,p} \cdot \theta_{H,s_1} \cdot \theta_{C_nH_{2n+1},s_1}$ $r_{t,p}^{(n)} = \lambda_{t,p} \cdot \theta_{C_nH_{2n+1},s_1}$ *where* $\lambda_{t,p} = k_{t,p} \cdot \theta_{H,s_1}$ $n = 1,2,...$
HC4	**termination to olefin** $C_nH_{2n+1},s_1 + s_1 \xrightarrow{k_{t,o}} C_nH_{2n} + H,s_1 + s_1$ $n = 2,3,...$	$r_{t,o}^{(n)} = k_{t,o} \cdot \theta_{s_1} \cdot \theta_{C_nH_{2n+1},s_1}$ $r_{t,o}^{(n)} = \lambda_{t,o} \cdot \theta_{C_nH_{2n+1},s_1}$ *where* $\lambda_{t,o} = k_{t,o} \cdot \theta_{s_1}$ $n = 2,3,...$
HC5	**olefin readsorption** $C_nH_{2n} + H,s_1 + s_1 \xrightarrow{k_{r,o}} C_nH_{2n+1},s_1 + s_1$ $n = 2,3,...$	$r_{r,o}^{(n)} = k_{r,o} \cdot \theta_{s_1} \cdot \theta_{H,s_1} \cdot C^s_{C_nH_{2n}}$ $r_{r,o}^{(n)} = \lambda^*_{r,o} \cdot C^s_{C_nH_{2n}}$ *where* $\lambda^*_{r,o} = k_{r,o} \cdot \theta_{s_1} \cdot \theta_{H,s_1}$ $n = 2,3,...$

s_1 means an active site on the surface of catalyst; θ is a surface coverage of adsorbed species;

C^S is a concentration of species at the surface.

Based on reaction network shown in Figure F.1 and kinetic equations in Table F.1 the reaction rates for paraffin and olefin formation are:

Methane

$$R_{CH_4} = r_{t,p}^{(1)} = \lambda_{t,p}^{(1)} \cdot \theta_{CH_3,s_1} \tag{F.1}$$

Paraffin C_2^+

$$R_{C_nH_{2n+2}} = r_{t,p}^{(n)} = \lambda_{t,p} \cdot \theta_{C_nH_{2n+1},s_1} \tag{F.2}$$

Ethene

$$R_{C_2H_4} = r_{t,o}^{(2)} - r_{r,o}^{(2)} = \lambda_{t,o}^{(2)} \cdot \theta_{C_2H_5,s_1} - \lambda_{r,o}^{*(2)} \cdot C_{C_2H_4}^{s} \tag{F.3}$$

Olefin C_3^+

$$R_{C_nH_{2n}} = r_{t,o}^{(n)} - r_{r,o}^{(n)} = \lambda_{t,o} \cdot \theta_{C_nH_{2n+1},s_1} - \lambda_{r,o}^{*} \cdot C_{C_nH_{2n}}^{s} \tag{F.4}$$

where θ is a surface coverage of adsorbed species whereas C^S is a concentration of species at the surface. Both of them are unknown.

The assumption was made that the reaction rate of an olefin $R_{C_nH_{2n}}$ is proportional to its partial pressure $p_{C_nH_{2n}}$ in the gas phase of perfectly mixed continuous reactor, i.e.

$$R_{C_nH_{2n}} = p_{C_nH_{2n}} \cdot \frac{SV}{R_g \cdot T} \quad n \geq 2 \tag{F.5}$$

where R_g is a universal gas constant, T is temperature and SV is a space velocity ($m^3\, g_{cat}\, h^{-1}$) at the reactor exit.

Partial pressure $p_{C_nH_{2n}}$ and concentration $C_{C_nH_{2n}}^{s}$ of species at the surface are related by vapor-liquid equilibrium constant called pseudo-Henry constant $He_{C_nH_{2n}}$

$$p_{C_nH_{2n}} = C_{C_nH_{2n}}^{s} \cdot He_{C_nH_{2n}} \tag{F.6}$$

Equilibrium constant $He_{C_nH_{2n}}$ is an exponential function which depends upon the carbon number of the olefin

$$He_{C_nH_{2n}} = He_0 \cdot \exp(-c \cdot n) \tag{F.7}$$

where *c* is a positive constant.

Surface coverage of the intermediate species $\theta_{\theta_{C_nH_{2n+1},s1}}$ can be calculated using the pseudo-steady state approximation:

$$\frac{d\theta_{\theta_{C_nH_{2n+1},s1}}}{dt} = 0 \tag{F.8}$$

All the above equations and assumptions lead to the following expressions for reaction rates of hydrocarbons:

Methane

$$R_{CH_4} = \lambda_{t,p}^{(1)} \cdot \frac{\lambda_1}{\lambda_p + \lambda_{t,p}^{(1)}} \tag{F.9}$$

Ethane

$$R_{C_2H_6} = \lambda_{t,p}^{(2)} \cdot \frac{\lambda_1}{\lambda_p + \lambda_{t,p}^{(1)}} \cdot \alpha_2 \tag{F.10}$$

Paraffin C_3^+

$$R_{C_nH_{2n+2}} = \lambda_{t,p} \cdot \frac{\lambda_1}{\lambda_p + \lambda_{t,p}^{(1)}} \cdot \prod_{i=2}^{n} \alpha_i \tag{F.11}$$

Ethene

$$R_{C_2H_4} = \frac{\lambda_{t,o}^{(2)}}{1 + \lambda_{r,p}^{(2)} \cdot \exp(2c)} \cdot \frac{\lambda_1}{\lambda_p + \lambda_{t,p}^{(1)}} \cdot \alpha_2 \tag{F.12}$$

Olefin C_3^+

$$R_{C_nH_{2n}} = \frac{\lambda_{t,o}}{1 + \lambda_{r,o} \cdot \exp(c \cdot n)} \cdot \frac{\lambda_1}{\lambda_p + \lambda_{t,p}^{(1)}} \cdot \prod_{i=2}^{n} \alpha_i \tag{F.13}$$

Olefin to Paraffin ratio, from Equations (F.13) and (F.11), is

$$\frac{R_{C_nH_{2n}}}{R_{C_nH_{2n+2}}} = \frac{\lambda_{t,o}}{\lambda_{t,p} \cdot \left(1 + \lambda_{r,o} \cdot \exp(c \cdot n)\right)} \qquad n \geq 3 \tag{F.14}$$

Equations F.9 to F.14 contain 10 parameters ($\lambda_1, \lambda_p, \lambda_{t,p}^{(1)}, \lambda_{t,p}^{(2)}, \lambda_{t,p}, \lambda_{t,o}^{(2)}, \lambda_{t,o}, \lambda_{r,o}^{(2)}, \lambda_{r,o}, c$).

In order to reduce number of parameters the pseudo-constants (λ) are re-parameterized with reference to termination of paraffin ($\lambda_{t,p}$). Additionally termination to ethene is related to ethane and olefin terminations. This leads to relative pseudo-constants (κ)

$$R_{CH_4} = \kappa_{t,p}^{(1)} \cdot \frac{\kappa_1}{\kappa_p + \kappa_{t,p}^{(1)}} \tag{F.15}$$

$$R_{C_2H_6} = \kappa_{t,p}^{(2)} \cdot \frac{\kappa_1}{\kappa_p + \kappa_{t,p}^{(1)}} \cdot \alpha_2 \tag{F.16}$$

$$R_{C_nH_{2n+2}} = \frac{\kappa_1}{\kappa_p + \kappa_{t,p}^{(1)}} \cdot \prod_{i=2}^{n} \alpha_i \quad ; n \geq 3 \tag{F.17}$$

$$R_{C_2H_4} = \frac{\kappa_{t,o}^{(2)}}{1 + \kappa_{r,o}^{(2)} \cdot \exp(2c)} \cdot \frac{\kappa_1}{\kappa_p + \kappa_{t,p}^{(1)}} \cdot \alpha_2 \tag{F.18}$$

$$R_{C_nH_{2n}} = \frac{\kappa_{t,o}}{1 + \kappa_{r,o} \cdot \exp(c \cdot n)} \cdot \frac{\kappa_1}{\kappa_p + \kappa_{t,p}^{(1)}} \cdot \prod_{i=2}^{n} \alpha_i \quad ; n \geq 3 \tag{F.19}$$

Chain growth probability factor α can be calculated as:

$$\alpha_n = \frac{\kappa_p}{1 + \kappa_p + \dfrac{\kappa_{t,o}}{1 + \kappa_{r,o} \cdot \exp(c \cdot n)}} \quad ; n \geq 3 \tag{F.20}$$

$$\alpha_2 = \frac{\kappa_p}{\kappa_{t,p}^{(2)} + \kappa_p + \dfrac{\kappa_{t,o}^{(2)}}{1 + \kappa_{r,o}^{(2)} \cdot \exp(2c)}} \tag{F.21}$$

where: $\kappa_1 = \lambda_1$,

$$\kappa_p = \lambda_p / \lambda_{t,p},$$

$$\kappa_{t,p}^{(1)} = \lambda_{t,p}^{(1)} / \lambda_{t,p},$$

$$\kappa_{t,p}^{(2)} = \lambda_{t,p}^{(2)} / \lambda_{t,p}, \tag{F.22}$$

$$\kappa_{t,o} = \lambda_{t,o} / \lambda_{t,p},$$

$$\kappa_{r,o} = \lambda_{r,o},$$

$$\kappa_{t,o}^{(2)} = \kappa_{t,p}^{(2)} \cdot \kappa_{t,o}$$

In addition, strong correlation between parameters $\kappa_{t,o}$ and $\kappa_{r,o}$ occurs at high olefin readsorption rate ($\kappa_{r,o} \cdot \exp(c \cdot n) >> 1$). In such a case, estimation of these parameters should not be done separately, and instead $\kappa_{t,o} / \kappa_{r,o}$ ratio needs to be estimated as one parameter (Van der Laan and Beenackers, 1999). This leads to the following equations:

$$R_{C_2H_4} = K_o^{(2)} \cdot \exp(-2c) \cdot \frac{\kappa_1}{\kappa_p + \kappa_{t,p}^{(1)}} \cdot \alpha_2 \tag{F.23}$$

$$R_{C_nH_{2n}} = K_o \cdot \exp(-c \cdot n) \cdot \frac{\kappa_1}{\kappa_p + \kappa_{t,p}^{(1)}} \cdot \prod_{i=2}^{n} \alpha_i \qquad n \geq 3 \tag{F.24}$$

$$\alpha_2 = \frac{\kappa_p}{\kappa_{t,p}^{(2)} + \kappa_p + K_o^{(2)} \cdot \exp(-2c)} \tag{F.25}$$

$$\alpha_n = \frac{\kappa_p}{1 + \kappa_p + K_o \cdot \exp(-c \cdot n)} \qquad n \geq 3 \tag{F.26}$$

where:

$$K_o^{(2)} = \frac{\kappa_{t,p}^{(2)} \cdot \kappa_{t,o}}{\kappa_{r,o}^{(2)}} \tag{F.26}$$

$$K_o = \frac{\kappa_{t,o}}{\kappa_{r,o}} \tag{F.27}$$

Then the meaning of parameters K_o is the following:

$$K_o^{(2)} = \frac{k_{t,p}^{(2)} \cdot k_{t,o}}{k_{r,o}^{(2)} \cdot \left(k_{t,p}\right)^2 \cdot \theta_{H,s_1}^2 \cdot \frac{R_g \cdot T}{SV \cdot He_o}} \tag{F.28}$$

$$K_o = \frac{k_{t,o}}{k_{r,o} \cdot k_{t,p} \cdot \theta_{H,s_1}^2 \cdot \frac{R_g \cdot T}{SV \cdot He_o}} \tag{F.29}$$

These parameters include reaction rate constants (k) as well as surface coverage of adsorbed hydrogen, so they may depend on the temperature as well as on the other process conditions (P, SV and/or H_2/CO feed ratio).

Appendix G

ORPDM with 2-olefin formation

The original ORPDM kinetic model of Van der Laan and Beenackers (1998, 1999) has been extended to account for formation of 2-olefins. The original model considers only the total olefin formation, whereas the extended model accounts separately for 1- and 2-olefins. Reaction network of hydrocarbon formation for this model is shown in Figure G.1. Elementary reactions are shown in Table G.1, and they are the same as for the original ORPDM model except that step HC6 (2-olefin formation) is added.

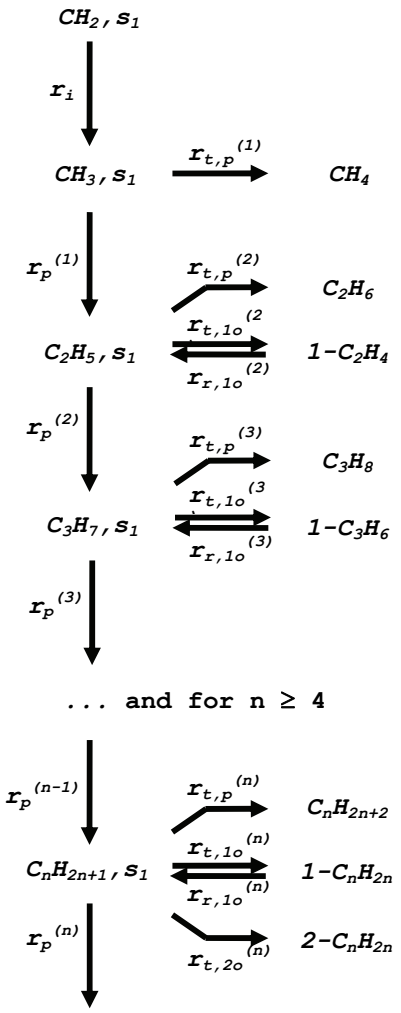

Figure G.1. Reaction network of hydrocarbon formation (FTS) for ORPDM with 2-olefin formation.

Table G.1. Elementary reaction steps for ORPDM with 2-olefin formation

No.	Stoichiometry equations	Kinetic equations
HC1	$CH_2,s_1 + H,s_1 \xrightarrow{k_i} CH_3,s_1$	$r_i = k_i \cdot \theta_{CH_2,s_1} \cdot \theta_{H,s_1} = \lambda_1$
HC2	**propagation** $C_nH_{2n+1},s_1 + CH_2,s_1 \xrightarrow{k_p} C_{n+1}H_{2n+3},s_1$ $n = 1,2,...$	$r_p^{(n)} = k_p \cdot \theta_{CH_2,s_1} \cdot \theta_{C_nH_{2n+1},s_1}$ $r_p^{(n)} = \lambda_p \cdot \theta_{C_nH_{2n+1},s_1}$ *where* $\lambda_p = k_p \cdot \theta_{CH_2,s_1}$
HC3	**termination to paraffin** $C_nH_{2n+1},s_1 + H,s_1 \xrightarrow{k_{t,p}} C_nH_{2n+2} + 2s_1$ $n = 1,2,...$	$r_{t,p}^{(n)} = k_{t,p} \cdot \theta_{H,s_1} \cdot \theta_{C_nH_{2n+1},s_1}$ $r_{t,p}^{(n)} = \lambda_{t,p} \cdot \theta_{C_nH_{2n+1},s_1}$ *where* $\lambda_{t,p} = k_{t,p} \cdot \theta_{H,s_1}$
HC4	**termination to 1-olefin** $C_nH_{2n+1},s_1 + s_1 \xrightarrow{k_{t,1o}} l\text{-}C_nH_{2n} + H,s_1 + s_1$ $n = 2,3,...$	$r_{t,1o}^{(n)} = k_{t,1o} \cdot \theta_{s_1} \cdot \theta_{C_nH_{2n+1},s_1}$ $r_{t,1o}^{(n)} = \lambda_{t,1o} \cdot \theta_{C_nH_{2n+1},s_1}$ *where* $\lambda_{t,1o} = k_{t,1o} \cdot \theta_{s_1}$
HC5	**1-olefin readsorption** $l\text{-}C_nH_{2n} + H,s_1 + s_1 \xrightarrow{k_{r,1o}} C_nH_{2n+1},s_1 + s_1$ $n = 2,3,...$	$r_{r,1o}^{(n)} = k_{r,1o} \cdot \theta_{s_1} \cdot \theta_{H,s_1} \cdot C^s_{l\text{-}C_nH_{2n}}$ $r_{r,1o}^{(n)} = \lambda^*_{r,1o} \cdot C^s_{l\text{-}C_nH_{2n}}$ *where* $\lambda^*_{r,1o} = k_{r,1o} \cdot \theta_{s_1} \cdot \theta_{H,s_1}$
HC6	**2-olefin formation** $C_nH_{2n+1},s_1 + s_1 \xrightarrow{k_{t,2o}} 2\text{-}C_nH_{2n} + H,s_1 + s_1$ $n = 4,5,...$	$r_{t,2o}^{(n)} = k_{t,2o} \cdot \theta_{s_1} \cdot \theta_{C_nH_{2n+1},s_1}$ $r_{t,2o}^{(n)} = \lambda_{t,2o} \cdot \theta_{C_nH_{2n+1},s_1}$ *where* $\lambda_{t,2o} = k_{t,2o} \cdot \theta_{s_1}$

s_1 means an active site on the surface of catalyst; θ is a surface coverage of adsorbed species;

C^S is a concentration of species at the surface.

Using the same assumptions and approximations as in the original ORPDM of Van der Laan and Beenackers, the following equations are obtained for prediction of all hydrocarbon products.

$$R_{CH_4} = \kappa_{t,p}^{(1)} \cdot \theta_{CH_3,s_1} \tag{G.1}$$

$$R_{C_2H_6} = \kappa_{t,p}^{(2)} \cdot \theta_{CH_3,s_1} \cdot \alpha_2 \tag{G.2}$$

$$R_{C_nH_{2n+2}} = \theta_{CH_3,s_1} \cdot \prod_{i=2}^{n} \alpha_i \quad ; n \geq 3 \tag{G.3}$$

$$R_{C_2H_4} = \frac{\kappa_{t,1o}^{(2)}}{1 + \kappa_{r,1o}^{(2)} \cdot \exp(2c)} \cdot \theta_{CH_3,s_1} \cdot \alpha_2 \tag{G.4}$$

$$R_{l\text{-}C_nH_{2n}} = \frac{\kappa_{t,1o}}{1 + \kappa_{r,1o} \cdot \exp(c \cdot n)} \cdot \theta_{CH_3,s_1} \cdot \prod_{i=2}^{n} \alpha_i \quad ; n \geq 3 \tag{G.5}$$

$$R_{2\text{-}C_nH_{2n}} = \kappa_{t,2o} \cdot \theta_{CH_3,s_1} \cdot \prod_{i=2}^{n} \alpha_i \quad ; n \geq 4 \tag{G.6}$$

where

$$\theta_{CH_3,s_1} = \frac{\kappa_1}{\kappa_p + \kappa_{t,p}^{(1)}} \tag{G.7}$$

$$\alpha_n = \begin{cases} \dfrac{\kappa_p}{\kappa_p + \kappa_{t,p}^{(2)} + \dfrac{\kappa_{t,1o}^{(2)}}{1 + \kappa_{r,1o}^{(2)} \cdot \exp(2c)}} & for \quad n = 2 \\ \dfrac{\kappa_p}{\kappa_p + \kappa_{t,p} + \dfrac{\kappa_{t,1o}}{1 + \kappa_{r,1o} \cdot \exp(3c)}} & for \quad n = 3 \\ \dfrac{\kappa_p}{\kappa_p + \kappa_{t,p} + \kappa_{t,2o} + \dfrac{\kappa_{t,1o}}{1 + \kappa_{r,1o} \cdot \exp(c \cdot n)}} & for \quad n \geq 4 \end{cases} \tag{G.8}$$

where: $\kappa_1 = \lambda_1$,

$\kappa_p = \lambda_p / \lambda_{t,p}$,

$$\kappa_{t,p}^{(1)} = \lambda_{t,p}^{(1)} / \lambda_{t,p} ,$$

$$\kappa_{t,p}^{(2)} = \lambda_{t,p}^{(2)} / \lambda_{t,p} ,$$

$$\kappa_{t,1o} = \lambda_{t,1o} / \lambda_{t,p} , \tag{G.9}$$

$$\kappa_{t,2o} = \lambda_{t,2o} / \lambda_{t,p} ,$$

$$\kappa_{r,1o}^{(2)} = \lambda_{r,1o}^{(2)}$$

$$\kappa_{r,1o} = \lambda_{r,1o}$$

$$\kappa_{t,1o}^{(2)} = \kappa_{t,p}^{(2)} \cdot \kappa_{t,1o}$$

A strong correlation between parameter $\kappa_{t,1o}$ and $\kappa_{r,1o}$ occurs at high olefin readsorption rate resulting in $\kappa_{r,1o} \cdot \exp(c \cdot n) >> 1$. In such a case, parameters $\kappa_{t,1o}^{(2)}$, $\kappa_{t,1o}^{(2)}$, $\kappa_{t,1o}$ and $\kappa_{r,1o}$ cannot be estimated separately. Instead, their ratios need to be estimated (Van der Laan and Beenackers, 1999). Thus, the olefin rates become

$$R_{C_2H_4} = K_{1o}^{(2)} \cdot \exp(-2c) \cdot \frac{\kappa_1}{\kappa_p + \kappa_{t,p}^{(1)}} \cdot \alpha_2 \tag{G.10}$$

$$R_{C_nH_{2n}} = K_{1o} \cdot \exp(-c \cdot n) \cdot \frac{\kappa_1}{\kappa_p + \kappa_{t,p}^{(1)}} \cdot \prod_{i=2}^{n} \alpha_i \quad ; n \geq 3 \tag{G.11}$$

$$\alpha_2 = \frac{\kappa_p}{\kappa_{t,p}^{(2)} + \kappa_p + K_{1o}^{(2)} \cdot \exp(-2c)} \tag{G.12}$$

$$\alpha_n = \frac{\kappa_p}{1 + \kappa_p + K_{1o} \cdot \exp(-c \cdot n)} \quad ; \; n \geq 3 \tag{G.13}$$

where:

$$K_{1o}^{(2)} = \frac{\kappa_{t,p}^{(2)} \cdot \kappa_{t,1o}}{\kappa_{r,1o}^{(2)}} \tag{G.14}$$

$$K_{1o} = \frac{\kappa_{t,1o}}{\kappa_{r,1o}} \tag{G.15}$$

Then the meaning of parameters *K* is the following

$$K_{1o}^{(2)} = \frac{k_{t,p}^{(2)} \cdot k_{t,1o}}{k_{r,1o}^{(2)} \cdot \left(k_{t,p}\right)^2 \cdot \theta_{H,s_1}^2 \cdot \frac{R_g \cdot T}{He_0 \cdot SV}} \tag{G.16}$$

$$K_{1o} = \frac{k_{t,1o}}{k_{r,1o} \cdot k_{t,p} \cdot \theta_{H,s_1}^2 \cdot \frac{R_g \cdot T}{He_0 \cdot SV}} \tag{G.17}$$

These two parameters include reaction constants (*k*) as well as the surface coverage of hydrogen, so they depend not only on temperature but other process condition as well. Final model has 8 parameters: $\kappa_1, \kappa_p, \kappa_{t,p}^{(1)}, \kappa_{t,p}^{(2)}, K_{1o}^{(2)}, K_{1o}, \kappa_{t,2o}$ *and* c.